NAVAL AIR WARFARE CENTER AIRCRAFT DIVISION
PATUXENT RIVER, MARYLAND

TECHNICAL REPORT

REPORT NO: NAWCADPAX/TR-2008/227

CALCULATION OF IMPEDANCE MATRIX INNER INTEGRAL TO PRESCRIBED PRECISION

by

John S. Asvestas
Stephen Yankovich
Oliver E. Allen

18 December 2008

NAVAIR Public Release 08-1123
Approved for public release; distribution is unlimited.

DEPARTMENT OF THE NAVY
NAVAL AIR WARFARE CENTER AIRCRAFT DIVISION
PATUXENT RIVER, MARYLAND

NAWCADPAX/TR-2008/227
18 December 2008

CALCULATION OF IMPEDANCE MATRIX INNER INTEGRAL TO PRESCRIBED PRECISION

by

John S. Asvestas
Stephen Yankovich
Oliver E. Allen

RELEASED BY:

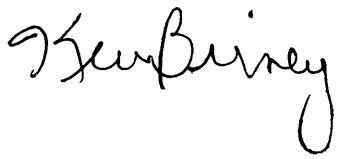

18 Dec 2008
KEVIN BIRNEY / 4.5.5 / DATE
Head, Radar and Antenna Systems Division
Naval Air Warfare Center Aircraft Division

REPORT DOCUMENTATION PAGE

Form Approved
OMB No. 0704-0188

1. REPORT DATE: 12/10/2008 18 December 2008	2. REPORT TYPE Technical Report	3. DATES COVERED 1 October 2006 to 30 September 2008

4. TITLE AND SUBTITLE:

Calculation of Impedance Matrix Inner Integral to Prescribed Precision

5a. CONTRACT NUMBER

5b. GRANT NUMBER

5c. PROGRAM ELEMENT NUMBER

6. AUTHOR(S)

John S. Asvestas
Stephen Yankovich
Oliver E. Allen

5d. PROJECT NUMBER

5e. TASK NUMBER

5f. WORK UNIT NUMBER

7. PERFORMING ORGANIZATION NAME(S) AND ADDRESS(ES)

Naval Air Warfare Center Aircraft Division
22347 Cedar Point Road, Unit #6
Patuxent River, Maryland 20670-1161

8. PERFORMING ORGANIZATION REPORT NUMBER

NAWCADPAX/TR-2008/227

9. SPONSORING/MONITORING AGENCY NAME(S) AND ADDRESS(ES)

Naval Air Systems Command
47123 Buse Road Unit IPT
Patuxent River, Maryland 20670-1547

10. SPONSOR/MONITOR'S ACRONYM(S)
ILIR

11. SPONSOR/MONITOR'S REPORT NUMBER(S): N/A

12. DISTRIBUTION/AVAILABILITY STATEMENT

NAVAIR Public Release 08-1123. Approved for public release; distribution is unlimited.

13. SUPPLEMENTARY NOTES

14. ABSTRACT

We present a new method for evaluating the inner integral of the impedance matrix element in the traditional Rao-Wilton-Glisson formulation of the method of moments for perfect conductors. In this method we replace the original integrand (modified by a constant phase factor) by its Taylor series and keep enough terms to guarantee a number of significant digits in the integration outcome. We develop criteria that relate the number of Taylor terms to the number of required significant digits. We integrate the leading Taylor terms analytically and the rest through iteration formulas. We show that the iteration formulas converge for all observation points within a sphere with a radius of half-a-wavelength and center the triangle's centroid. We compare results of our method with existing ones and find them in excellent agreement. Outside this sphere, we employ a set of triangle cubatures of increasing size together with a convergence criterion to determine the integration outcome to a prescribed number of significant digits. By designing appropriate numerical experiments using a set of 25 triangles and about 10,000 observation points, we define spherical regions of space where a cubature of minimum size will provide a desired number of significant digits. The approach is quite general but we demonstrate it explicitly by using seven significant digits as the required accuracy.

15. SUBJECT TERMS

Boundary-integral equations, method of moments, impedance-matrix, Taylor's theorem with a remainder, numerical integration, Gordon-Bilow transformation, cubatures, significant digits

16. SECURITY CLASSIFICATION OF:			17. LIMITATION OF ABSTRACT	18. NUMBER OF PAGES	19a. NAME OF RESPONSIBLE PERSON John S. Asvestas
a. REPORT	b. ABSTRACT	c. THIS PAGE			19b. TELEPHONE NUMBER (include area code)
Unclassified	Unclassified	Unclassified	SAR	91	631-673-8176

Standard Form 298 (Rev. 8-98)
Prescribed by ANSI Std. Z39-18

SUMMARY

We present a new method for evaluating the inner integral of the impedance matrix element in the traditional Rao-Wilton-Glisson formulation of the method of moments for perfect conductors. In this method we replace the original integrand (modified by a constant phase factor) by its Taylor series and keep enough terms to guarantee a number of significant digits in the integration outcome. We develop criteria that relate the number of Taylor terms to the number of required significant digits. We integrate the leading Taylor terms analytically and the rest through iteration formulas. We show that the iteration formulas converge for all observation points within a sphere with a radius of half-a-wavelength and center the triangle's centroid. We compare results of our method with existing ones and find them in excellent agreement. Outside this sphere, we employ a set of triangle cubatures of increasing size together with a convergence criterion to determine the integration outcome to a prescribed number of significant digits. By designing appropriate numerical experiments using a set of 25 triangles and about 10,000 observation points, we define spherical regions of space where a cubature of minimum size will provide a desired number of significant digits. The approach is quite general but we demonstrate it explicitly by using seven significant digits as the required accuracy.

Contents

List of Tables

Page No.

Part 1.

Part 2.

List of Figures

Page No.

Part 1.

Part 2.

INTRODUCTION

The Method of Moments (MoM) is one of the principal methods for electromagnetic simulations in the frequency domain. In this method, we express an unknown current density as a linear combination of known functions and the objective of the MoM is to determine the coefficients in this expansion by minimizing the square of the modulus of the residual error. It ultimately leads to a system of linear algebraic equations, the solution of which yields the values of the coefficients of the current density expansion. The elements of the matrix (known as the *impedance matrix* (IM)) are expressed as double surface integrals over flat, triangular regions of space. The purpose of this study is to compute the inner of these integrals to a prescribed precision when the object under consideration is a perfect conductor.

Until recently, the quantities of interest in electromagnetic simulations were the far-field electric and magnetic fields. From these, we could compute the radar cross section of a target or the radiation patterns of an antenna. This allowed for a considerable degree of error in computing the elements of the IM in the MoM because of the error smoothing effect of the near- to far-field transformation (integration). Moreover, due to computer hardware limitations, the size of the IM was small enough so that the round-off error did not have a severe effect on the accuracy of the solution.

In recent years, the MoM is being applied to problems where near-field information is required (e.g., antennas and antenna arrays). This requires a more accurate computation of the elements of the IM than when only the far fields are of interest. Additionally, advances in computer hardware allow us to address problems that result in an IM system with millions of unknowns. Thus, the effect of the round-off error becomes more pronounced. Both of these reasons lead us to the conclusion that the more accurate the representation of the IM is, the better the quality of the solution. This is the central theme of the present study: the computation of the inner surface integral of an IM element to prescribed precision when the platform of interest is perfectly conducting.

The calculation of the inner surface integral comprises two parts. In the first part we present an approximation method based on Taylor's Theorem with a Remainder. This theorem allows us to approximate the integrand (that we do not know how to integrate analytically) by a polynomial that we can integrate analytically. The degree of approximation, *i.e.*, the number of significant digits to which the approximation is accurate is known and, hence, so is that of the integration. The answer to this evaluation is given in terms of elementary transcendental functions for which there exist robust computational algorithms. Where these algorithms might fail, we have replaced them by approximations that yield the required number of significant digits.

The drawback in using this method to compute the inner integral of the IM element is that the process that involves the analytical evaluation of the approximated surface integral is based on two iteration formulas that do not converge for all values of the observation point. This point is the integration variable of the outer surface integral of the IM element. We have shown,

however, that the iteration formulas do converge for all values of the observation point within a distance of half a wavelength from the centroid of the triangle. Outside this region, we show in the second part of this report that we can use existing cubatures[1] to introduce spherical regions in the observation-point space where a cubature of a minimum size will produce the required number of significant digits. These spherical regions have their center at the triangle's centroid.

In conclusion, we have developed a procedure whereby we divide the entire space around a triangle into spherical regions with center the triangle's centroid. In the innermost region, we use approximation theory to determine the value of the inner integral of the IM element to a prescribed number of significant digits. In this region, there is no cubature that can yield the same precision in a shorter time. In the rest of the spherical regions, we use the limit of a (finite) sequence of cubatures to determine the value of the inner integral to the prescribed number of significant digits. Subsequently, in each spherical region, we use the smallest cubature that will yield this accuracy. We have found that three spherical regions are sufficient to cover the entire observation space.

We know of no other method that calculates the inner integral of the IM element to a prescribed precision.

[1] By *cubature* we mean a numerical algorithm that evaluates a *surface* integral. We reserve the term *quadrature* for an algorithm that evaluates a *line* integral.

PART 1. ANALYTICAL EVALUATION OF INTEGRALS

1. STATEMENT OF PROBLEM AND APPROACH

In the Rao-Wilton-Glisson [1] formulation of the method of moments (MoM), we need evaluate the integrals

$$\mathbf{I}^{(l)}(\mathbf{r}') = \int_T \frac{\mathbf{f}^{(l)}(\mathbf{r})\mathrm{e}^{-ikR}}{R} dS\,, \quad \mathbf{f}^{(l)}(\mathbf{r}) = \mathbf{r} - \mathbf{r}_l\,, \quad l = 1,2,3 \tag{1.1}$$

where

$$R = \sqrt{r'^2 - 2\mathbf{r}'\cdot\mathbf{r} + r^2} = \sqrt{\left(x - x'\right)^2 + \left(y - y'\right)^2 + h^2} \tag{1.2}$$

with

$$\mathbf{r} = x\hat{x} + y\hat{y}\,, \quad \mathbf{r}' = x'\hat{x} + y'\hat{y} + h\hat{z} \tag{1.3}$$

and the region of integration T being the triangle in figure 1.1. The origin of coordinates is the centroid of the triangle, and the latter lies on the xy-plane. Boldface letters denote vectors. The same letters in italics denote the magnitudes of these vectors while a caret over a letter denotes a unit vector. The vector $\mathbf{r}_l$ is the position vector to the l-the vertex of the triangle, as shown in figure 1.1.

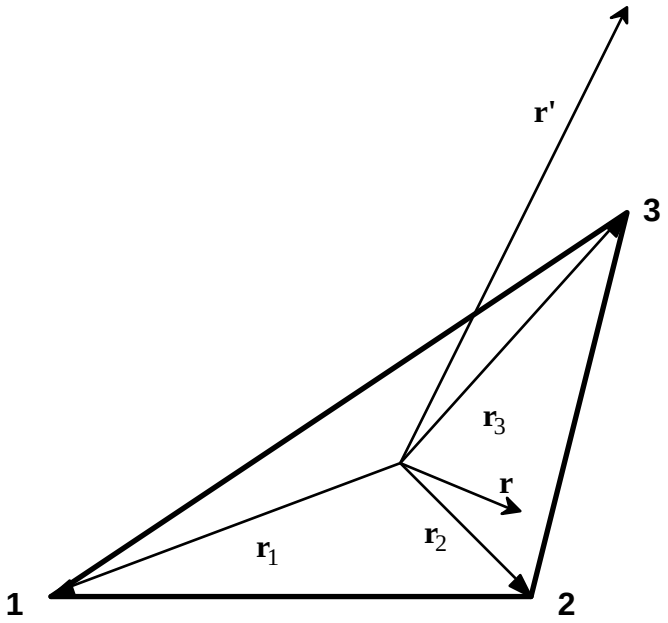

Figure 1.1: The integration triangle

We note that

$$\mathbf{I}^{(l)}(\mathbf{r}') = \int_T \frac{(\mathbf{r}-\mathbf{r}_l)\mathrm{e}^{-ikR}}{R}\,dS = \int_T \frac{(\mathbf{r}-\mathbf{r}')\mathrm{e}^{-ikR}}{R}\,dS - (\mathbf{r}_l-\mathbf{r}')\int_T \frac{\mathrm{e}^{-ikR}}{R}\,dS$$

$$= -\frac{1}{ik}\int_T \nabla\left(\mathrm{e}^{-ikR}\right)dS - (\mathbf{r}_l-\mathbf{r}')\int_T \frac{\mathrm{e}^{-ikR}}{R}\,dS = -\frac{1}{ik}\int_T \nabla_S\left(\mathrm{e}^{-ikR}\right)dS - \frac{1}{ik}\int_T \hat{z}\frac{\partial}{\partial z}\left(\mathrm{e}^{-ikR}\right)dS$$

$$-(\mathbf{r}_l-\boldsymbol{\rho}')\int_T \frac{\mathrm{e}^{-ikR}}{R}\,dS + \hat{z}z'\int_T \frac{\mathrm{e}^{-ikR}}{R}\,dS = -\frac{1}{ik}\int_T \nabla_S\left(\mathrm{e}^{-ikR}\right)dS - (\mathbf{r}_l-\boldsymbol{\rho}')\int_T \frac{\mathrm{e}^{-ikR}}{R}\,dS \tag{1.4}$$

where $\hat{\nu}$ is the exterior unit normal to the side of a triangle, lying on the plane of the triangle. The last integral in this expression (the Scalar integral) also appears by itself in the MoM and, thus, it is one of the integrals that needs to be evaluated. The integral before it can be converted to a line integral around the triangle's boundary using a standard identity ([2], p. 503)

$$\mathbf{I}^{(l)}(\mathbf{r}') = \int_T \frac{(\mathbf{r}-\mathbf{r}_l)\mathrm{e}^{-ikR}}{R}\,dS = -\frac{1}{ik}\int_{\partial T} \hat{\nu}\left(\mathrm{e}^{-ikR}\right)ds - (\mathbf{r}_l-\boldsymbol{\rho}')\int_T \frac{\mathrm{e}^{-ikR}}{R}\,dS \tag{1.5}$$

We can proceed one step further and measure all distances in wavelengths. We note that

$$\int_{\partial T'} ds' \to \lambda\int_{\partial T} ds\,, \quad \int_{T'} dS' \to \lambda^2\int_T dS \tag{1.6}$$

when we move from measuring length in meters to length in wavelengths. With this in mind, and dividing all distances by wavelength, we get from (1.5)

$$\mathbf{I}^{(l)}(\mathbf{r}') = -\frac{\lambda^2}{i2\pi}\int_{\partial T} \hat{\nu}\left(\mathrm{e}^{-i2\pi R}\right)ds - \lambda^2(\mathbf{r}_l-\boldsymbol{\rho}')\int_T \frac{\mathrm{e}^{-i2\pi R}}{R}\,dS \tag{1.7}$$

where all distances, including triangle dimensions, are measured in wavelengths. We note that both integrals are independent of the index *l*, and that, although the first one is a vector integral, it is in essence a vector sum of three Scalar integrals, each defined over a side of the triangle.

The objective of this report is to calculate the integrals in (1.7) to a pre-assigned number of significant digits. Neither of these integrals can be evaluated analytically. The integrands, however, can be replaced by functions that we know how to integrate and that can approximate the actual integrands arbitrarily closely. The obvious way to proceed is to expand the exponential function in a Maclaurin series about $R=0$ and truncate after the required number of terms. This works well when *R* is small, so that the number of terms for agreement to the required number of significant digits is also small. This translates to the observation point being near the integration triangle. The observation point, however, can be any point in space, except for points on the three sides of the triangle. Thus, as the observation point recedes from the triangle, more and

more terms are required in the Maclaurin sum and there comes a point when this method becomes counter-productive due to the large amount of time required to compute this sum. We attempt to get around this difficulty by multiplying and dividing (1.7) by a common factor; we thus write

$$\mathbf{I}^{(l)}(\mathbf{r}') = -\lambda^2 \frac{\mathrm{e}^{-i2\pi r'}}{i2\pi} \int_{\partial T} \hat{\nu} \left[\mathrm{e}^{-i2\pi(R-r')} \right] ds - \lambda^2 (\mathbf{r}_l - \boldsymbol{\rho}') \mathrm{e}^{-i2\pi r'} \int_T \frac{\mathrm{e}^{-i2\pi(R-r')}}{R} dS \,. \tag{1.8}$$

We can show that the argument of the exponential in this case is bounded. The centroid of a triangle divides each median in a 2:1 ratio. The longer of the two parts is the distance from the centroid to the vertex of the median. Thus, the largest distance from the centroid to a point on the triangle is equal to two thirds the longest of the three medians. But a median is shorter than the longer of the two adjacent sides; thus, the longest distance from the centroid to the triangle's perimeter is less than two thirds the length of the triangle's longest side. We combine this with the fact that the side of a triangle (in this case that formed by the observation, integration and centroid points) is always greater than the difference of the other two sides to obtain the bound

$$\left| R - r' \right| \le r < \frac{2}{3} l_{\max} \tag{1.9}$$

where $l_{\max}$ is the length of the longest side of the triangle. Though this is not a strict bound, it is a bound that holds for all observation points; thus, no matter how far away the observation point is from the integration triangle, the number of terms in the expansion will be the same as for a point near the triangle. Moreover, for an actual grid, we can search among all triangles for the longest side and use that value in (1.9). In this way, we do not have to test all triangles separately, conserving a lot of compute time.

We proceed now to expand (1.8) in a Maclaurin series and keep the first *N* terms

$$\mathbf{I}_N^{(l)}(\mathbf{r}') = \lambda^2 \mathrm{e}^{-i2\pi r'} \sum_{n=0}^{N-1} \frac{(-i2\pi)^{n-1}}{n!} \int_{\partial T} \hat{\nu} (R - r')^n \, ds - \lambda^2 (\mathbf{r}_l - \boldsymbol{\rho}') \mathrm{e}^{-i2\pi r'} \sum_{n=0}^{N-1} \frac{(-i2\pi)^n}{n!} \int_T \frac{(R - r')^n}{R} dS \,. \tag{1.10}$$

In determining the number of terms *N*, we use Taylor's Theorem with a Remainder ([3], p. 113). If we require a number *M* of correct significant digits, then we proceed as follows to determine the number of terms. The series for the sine is

$$\frac{\sin\left[2\pi (R - r') \right]}{2\pi (R - r')} = \sum_{n=0}^{N-1} \frac{(-1)^n \left[2\pi (R - r') \right]^{2n}}{(2n+1)!} + R_s \left(N, 2\pi (R - r') \right) \tag{1.11}$$

where R_s is the remainder of the series and is bounded by the first omitted term

$$\left|R_s\left(N,2\pi\left(R-r'\right)\right)\right| \le \frac{\left[2\pi\left|R-r'\right|_{\max}\right]^{2N}}{(2N+1)!} < \frac{\left(\frac{4\pi}{3}l_{\max}\right)^{2N}}{(2N+1)!}. \tag{1.12}$$

We can then write for the relative error

$$\begin{aligned}
&\frac{\left|\frac{\sin\left[2\pi\left(R-r'\right)\right]}{2\pi\left(R-r'\right)} - \sum_{n=0}^{N-1}\frac{(-1)^n\left[2\pi\left(R-r'\right)\right]^{2n}}{(2n+1)!}\right|}{\left|\frac{\sin\left[2\pi\left(R-r'\right)\right]}{2\pi\left(R-r'\right)}\right|} \\
&= \frac{\left|R_s\left(N,2\pi\left(R-r'\right)\right)\right|}{\left|\frac{\sin\left[2\pi\left(R-r'\right)\right]}{2\pi\left(R-r'\right)}\right|} < \frac{\left(\frac{4\pi}{3}l_{\max}\right)^{2N}}{(2N+1)!\left|\frac{\sin\left[2\pi\left|R-r'\right|_{\max}\right]}{2\pi\left|R-r'\right|_{\max}}\right|} \le \frac{\left(\frac{4\pi}{3}l_{\max}\right)^{2N}}{(2N+1)!\left|\frac{\sin\left(\frac{4\pi}{3}l_{\max}\right)}{\frac{4\pi}{3}l_{\max}}\right|}.
\end{aligned} \tag{1.13}$$

The number of terms is determined by requiring that the relative error is smaller than 5 divided by the number 10 raised to the number of significant digits *M* plus one, or

$$\frac{\left(\frac{4\pi}{3}l_{\max}\right)^{2N}}{(2N+1)!} < 5\cdot 10^{-M-1}\left|\frac{\sin\left(\frac{4\pi}{3}l_{\max}\right)}{\frac{4\pi}{3}l_{\max}}\right|. \tag{1.14}$$

Once the triangle's dimensions are known, we can solve this expression for *N*.

In this discussion we have assumed that the argument of the sine function is small; in practice, the longest side of a triangle does not exceed one tenth of a wavelength and, hence, the largest argument is approximately equal to $0.4\pi/3$ radians or 24 deg. This means that the trigonometric functions in the original integrals hardly exhibit an oscillatory behavior.

The argument for the cosine function is slightly more complicated and is driven by the fact that the integral of the leading term of the first sum in (1.10) is equal to zero. This can be seen most clearly in (1.4) where the leading term in the expansion is a constant (1) and, hence, its

surface gradient is zero. Thus, the first contributor to the integral is the second term in the cosine expansion. We then proceed to re-write the relevant integral in the form

$$\mathbf{I} = \int_{\partial T} \hat{\nu} \left\{ \cos\left[k\left(R - r' \right) \right] - 1 \right\} ds \,. \tag{1.15}$$

We expand now the new integrand into a Maclaurin series

$$\cos\left[2\pi\left(R - r' \right) \right] - 1 = \sum_{n=1}^{\infty} \frac{(-1)^n \left[2\pi\left(R - r' \right) \right]^{2n}}{(2n)!} = -\left[2\pi\left(R - r' \right) \right]^2 \sum_{n=0}^{\infty} \frac{(-1)^n \left[2\pi\left(R - r' \right) \right]^{2n}}{(2n+2)!} \tag{1.16}$$

We consider now the termination of the last power series after N terms

$$\frac{1 - \cos\left[2\pi\left(R - r' \right) \right]}{\left[2\pi\left(R - r' \right) \right]^2} = \sum_{n=0}^{N-1} \frac{(-1)^n \left[2\pi\left(R - r' \right) \right]^{2n}}{(2n+2)!} + R_c\left(N, 2\pi\left(R - r' \right) \right). \tag{1.17}$$

We plot the left-hand side of this equation in figure 1.2. We see that, in the range of interest, it is strictly decreasing as its argument increases.

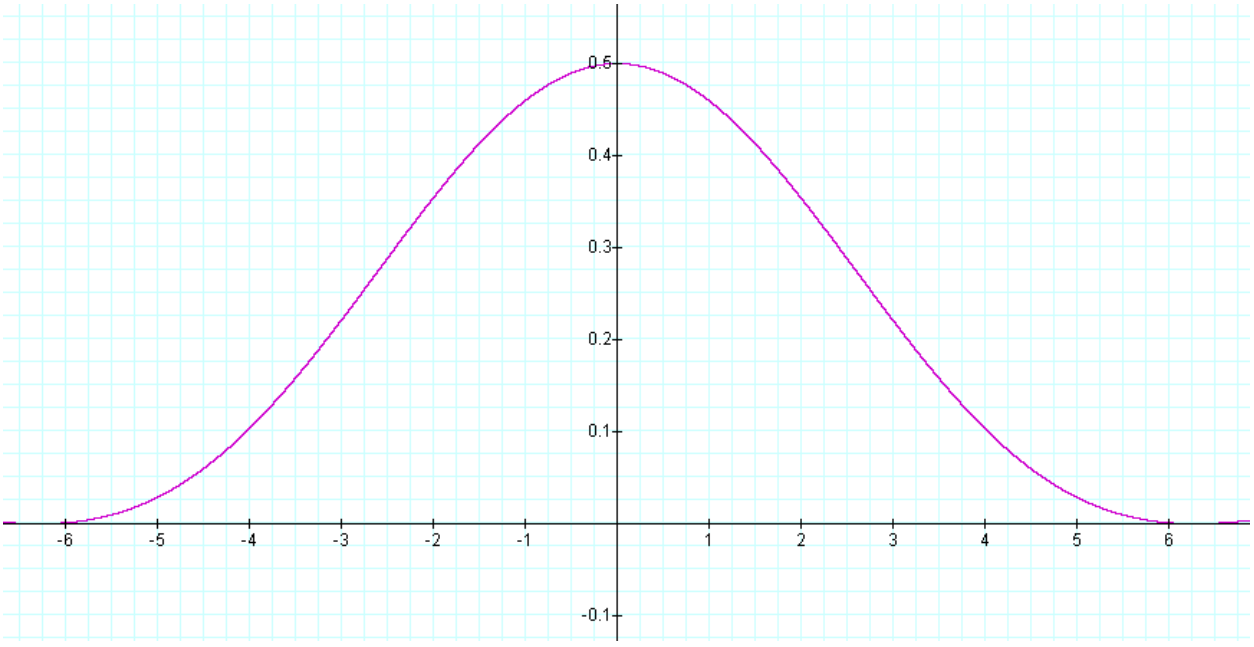

Figure 1.2: Plot of the left-hand side of (1.17)

The remainder in (1.17) is bounded by

$$\left|R_c\left(N,2\pi\left(R-r'\right)\right)\right| \le \frac{\left(k\left|R-r'\right|_{\max}\right)^{2N}}{\left(2N+2\right)!} < \frac{\left(\frac{4\pi}{3}l_{\max}\right)^{2N}}{\left(2N+2\right)!}. \tag{1.18}$$

Taking to account the monotonicity of the function, we can write for the relative error

$$\frac{\left|R_c\left(N,2\pi\left(R-r'\right)\right)\right|}{\left|\frac{1-\cos\left[2\pi\left(R-r'\right)\right]}{\left[2\pi\left(R-r'\right)\right]^2}\right|} \le \frac{\left(\frac{4\pi}{3}l_{\max}\right)^{2N}}{\left(2N+2\right)!\left|\frac{1-\cos\left(\frac{4\pi}{3}l_{\max}\right)}{\left(\frac{4\pi}{3}l_{\max}\right)^2}\right|} \tag{1.19}$$

and we set the criterion for determining N to be

$$\frac{\left(\frac{4\pi}{3}l_{\max}\right)^{2N}}{\left(2N+2\right)!} < 5\cdot 10^{-(M+1)}\left|\frac{1-\cos\left(\frac{4\pi}{3}l_{\max}\right)}{\left(\frac{4\pi}{3}l_{\max}\right)^2}\right|. \tag{1.20}$$

Using criteria (1.14) and (1.20) for the sine and cosine, and assuming that the largest side of a triangle is less or equal to one tenth of a wavelength, we arrive at table 1.1. This table gives the number of terms required to guarantee a certain number of significant digits (SD). We see that, for single precision (7 SD), we need a total of 8 terms while, for double (15 SD), we need a total of 14. We see that only on one occasion (6 SD) does the number of terms between sine and cosine differ. Finally, the criteria we use are universal, i.e., they are independent of the location of the observation point and the shape of the triangle. Thus, once we decide on the number of significant digits, we can calculate the number of terms once and for all provided we know the largest side among all triangles in a grid.

Table 1.1: Number of terms required to guarantee a given number of significant digits (SD). Largest side of triangle less than or equal to a tenth of a wavelength.

Number of SD	Sine	Cosine
4	3	3
5	3	3
6	4	3
7	4	4
8	4	4
9	5	5
10	5	5
11	5	5
12	6	6
13	6	6
14	6	6
15	7	7

As mentioned above, using the same identity that allowed us to convert the first integral to a line integral, we can show that the zeroth-order term in the line integral of (1.10) does not contribute. Down-shifting the index by one we get

$$\mathbf{I}_N^{(l)}(\mathbf{r}') = \lambda^2 \mathrm{e}^{-i2\pi r'} \sum_{n=0}^{N-2} \frac{(-i2\pi)^n}{(n+1)!} \int_{\partial T} \hat{\nu} (R - r')^{n+1} \, ds - \lambda^2 (\mathbf{r}_l - \boldsymbol{\rho}') \mathrm{e}^{-i2\pi r'} \sum_{n=0}^{N-1} \frac{(-i2\pi)^n}{n!} \int_T \frac{(R - r')^n}{R} \, dS$$

$$= \lambda^2 \mathrm{e}^{-i2\pi r'} \sum_{n=0}^{N-2} \frac{(-i2\pi)^n}{(n+1)!} \mathbf{I}_{(n)}(\mathbf{r}') - \lambda^2 (\mathbf{r}_l - \boldsymbol{\rho}') \mathrm{e}^{-i2\pi r'} \sum_{n=0}^{N-1} \frac{(-i2\pi)^n}{(n+1)!} I_{(n)}(\mathbf{r}'), \quad l = 1,2,3 \tag{1.21}$$

where

$$\mathbf{I}_{(n)}(\mathbf{r}') = \int_{\partial T} \hat{\nu} (R - r')^{n+1} \, ds, \quad I_{(n)}(\mathbf{r}') = (n+1) \int_T \frac{(R - r')^n}{R} \, dS. \tag{1.22}$$

It is these two integrals that we must compute analytically. The first is a line integral while the second is a surface integral. In Appendix A we employ the Gordon-Bilow transformation to convert the surface integral to a line integral [4], [5]. From (A.1) and (A.42), we have that

$$I_{(n)}(\mathbf{r}') = \sum_{j=1}^{3} \hat{\nu}_j \cdot (\mathbf{r}_{j+1} - \boldsymbol{\rho}') \int_{s_j} \frac{\left(\sqrt{\rho^2 + h^2} - r'\right)^{n+1} - \left(|h| - r'\right)^{n+1}}{\rho^2} \, ds \tag{1.23}$$

where s_j is the *j*-th side of the triangle and $\hat{\nu}_j$ is the exterior unit normal to it, lying on the triangle's plane, while ρ is the distance between the integration point and the projection of the observation point on the triangle's plane. In this notation

$$\mathbf{I}_{(n)}(\mathbf{r}') = \sum_{j=1}^{3} \hat{\nu}_j \int_{s_j} \left(\sqrt{\rho^2 + h^2} - r' \right)^{n+1} ds \,. \tag{1.24}$$

We evaluate these integrals in the next section.

2. EVALUATION OF LINE INTEGRALS

We begin by writing (1.23) in the form

$$I_{(n)}(\mathbf{r}') = \sum_{j=1}^{3} \hat{\nu}_j \cdot \left(\mathbf{r}_{j+1} - \boldsymbol{\rho}' \right) K_{n,j}(\mathbf{r}') \tag{2.1}$$

where

$$K_{n,j}(\mathbf{r}') = \int_{s_j} \frac{\left(\sqrt{\rho^2 + h^2} - r' \right)^{n+1} - \left(|h| - r' \right)^{n+1}}{\rho^2} ds \,, \quad n = 0,1,2,\ldots . \tag{2.2}$$

From this

$$K_{0,j} = \int_{s_j} \frac{\sqrt{\rho^2 + h^2} - |h|}{\rho^2} ds \tag{2.3}$$

$$K_{1,j} = s_j - 2r' K_{0,j} \tag{2.4}$$

$$K_{n+1,j} = V_{n-1,j} - 2r' K_{n,j} - \rho'^2 K_{n-1,j} \,, \quad n = 1,2,\ldots \tag{2.5}$$

where

$$V_{n,j}(\mathbf{r}') = \int_{s_j} \left(\sqrt{\rho^2 + h^2} - r' \right)^{n+1} ds \,, \quad n = 0,1,2,\ldots . \tag{2.6}$$

Comparing the last integral to that in (1.24), we find that we can write

$$\mathbf{I}_{(n)}(\mathbf{r}') = \sum_{j=1}^{3} \hat{\nu}_j V_{n,j}(\mathbf{r}') \,. \tag{2.7}$$

Before proceeding with the evaluation of the integrals in (2.6), we summarize some essential definitions

$$\mathbf{r} = \mathbf{r}_{j+1} + s\hat{t}_j\,, \quad j = 1,2,3 \tag{2.8}$$

with the indices running cyclically. We also write

$$\mathbf{r}' = x'\hat{x} + y'\hat{y} + h\hat{z} = \boldsymbol{\rho}' + h\hat{z}\,, \quad \mathbf{r}_l = x_l\hat{x} + y_l\hat{y}\,. \tag{2.9}$$

and

$$\mathbf{a}_{j+1} = \mathbf{r}_{j+1} - \boldsymbol{\rho}'\,, \quad \tau = s + \hat{t}_j \cdot \mathbf{a}_{j+1}\,, \quad A_j = \left|\hat{t}_j \times \left(\hat{t}_j \times \mathbf{a}_{j+1}\right)\right|, \quad \rho = \left|\mathbf{r} - \boldsymbol{\rho}'\right| = \left|\mathbf{a}_{j+1} + s\hat{t}_j\right|. \tag{2.10}$$

From these we can write

$$\rho^2 = s^2 + 2\hat{t}_j \cdot \mathbf{a}_{j+1}s + \left|\mathbf{a}_{j+1}\right|^2 = \left(s + \hat{t}_j \cdot \mathbf{a}_{j+1}\right)^2 + \left|\mathbf{a}_{j+1}\right|^2 - \left(\hat{t}_j \cdot \mathbf{a}_{j+1}\right)^2 = \left(s + \hat{t}_j \cdot \mathbf{a}_{j+1}\right)^2 + A_j^{\,2} = \tau^2 + A_j^{\,2} \tag{2.11}$$

We also define

$$\mathbf{b}_j = \mathbf{r}_j - \mathbf{r}'; \quad B_j = \sqrt{A_j^{\,2} + h^2}\,, \quad j = 1,2,3 \tag{2.12}$$

The geometric significance of these quantities is shown in figures. 2.1 and 2.2.

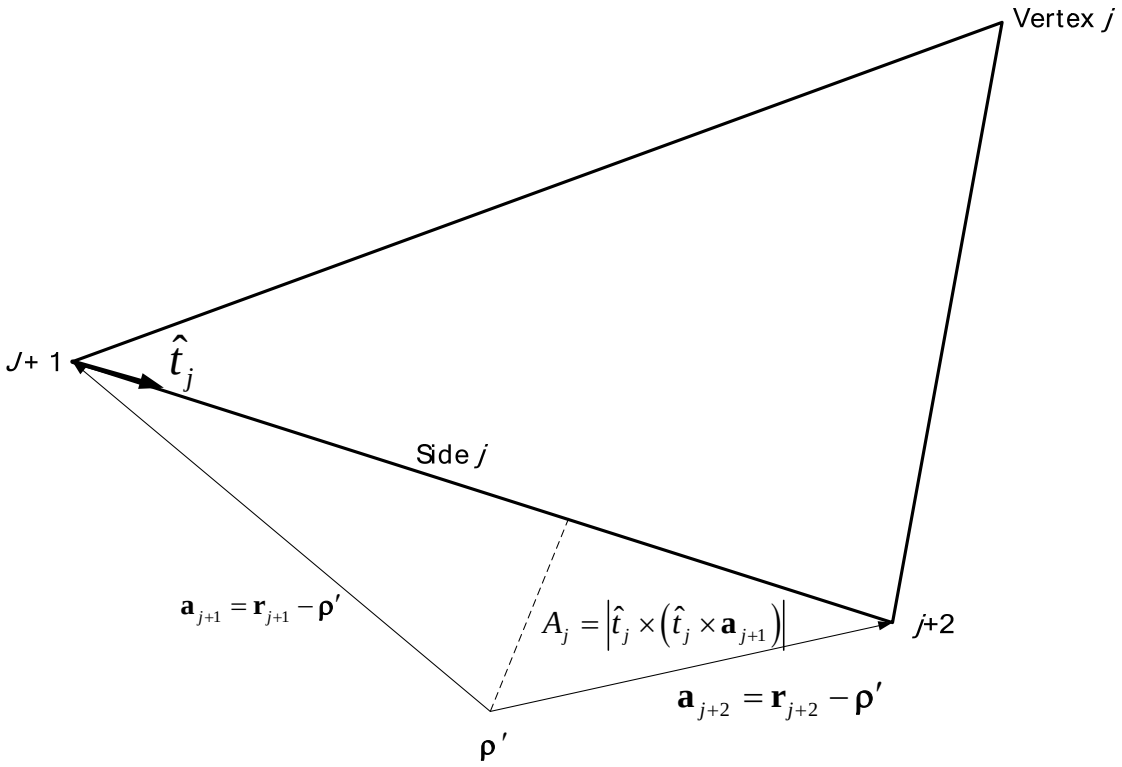

Figure 2.1: Geometrical meaning of the quantities in Equation (2.10)

2.1 EVALUATION OF $V_{n,j}$

For $\hat{t}_j \cdot \mathbf{b}_{j+2} > \hat{t}_j \cdot \mathbf{b}_{j+1} > 0$, we make the transformation

$$\tau = B_j \tan\theta\,, \quad d\tau = B_j \sec^2\theta d\theta \tag{2.13}$$

and write for (2.6)

$$V_{n,j} = \int_{\hat{t}_j\cdot\mathbf{b}_{j+1}}^{\hat{t}_j\cdot\mathbf{b}_{j+2}} \left(\sqrt{\tau^2 + B_j{}^2} - r'\right)^{n+1} d\tau = B_j \int_{\arctan\left(\frac{\hat{t}_j\cdot\mathbf{b}_{j+1}}{B_j}\right)}^{\arctan\left(\frac{\hat{t}_j\cdot\mathbf{b}_{j+2}}{B_j}\right)} \left(B_j \sec\theta - r'\right)^{n+1} \sec^2\theta d\theta$$

$$= \sum_{m=0}^{n+1} \left(\frac{(n+1)!}{m!(n+1-m)!}\right) B_j{}^{m+1} (-r')^{n+1-m} \int_{\arctan\left(\frac{\hat{t}_j\cdot\mathbf{b}_{j+1}}{B_j}\right)}^{\arctan\left(\frac{\hat{t}_j\cdot\mathbf{b}_{j+2}}{B_j}\right)} \sec^{m+2}\theta d\theta\,. \tag{2.14}$$

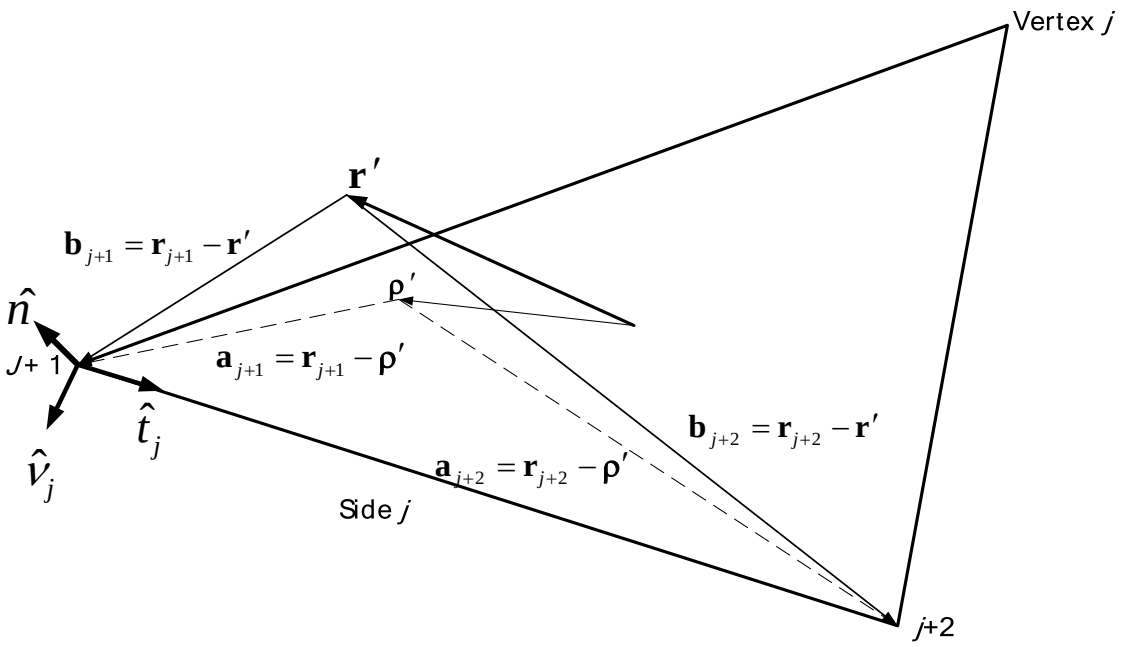

Figure 2.2: Local rectangular coordinates and various vectors

Let

$$v_{m,j} = B_j^{\,m+1} \int_{\arctan\left(\frac{\hat{t}_j\cdot\mathbf{b}_{j+1}}{B_j}\right)}^{\arctan\left(\frac{\hat{t}_j\cdot\mathbf{b}_{j+2}}{B_j}\right)} \sec^{m+2}\theta d\theta\,, \quad m = 0,1,2,... \tag{2.15}$$

Then

$$v_{0,j} = B_j \int_{\arctan\left(\frac{\hat{t}_j\cdot\mathbf{b}_{j+1}}{B_j}\right)}^{\arctan\left(\frac{\hat{t}_j\cdot\mathbf{b}_{j+2}}{B_j}\right)} \sec^2\theta d\theta = B_j \tan\theta \Bigg|_{\arctan\left(\frac{\hat{t}_j\cdot\mathbf{b}_{j+1}}{B_j}\right)}^{\arctan\left(\frac{\hat{t}_j\cdot\mathbf{b}_{j+2}}{B_j}\right)} = \hat{t}_j\cdot\mathbf{b}_{j+2} - \hat{t}_j\cdot\mathbf{b}_{j+1} = s_j \tag{2.16}$$

while

$$v_{1,j} = B_j^{\,2} \int_{\arctan\left(\frac{\hat{t}_j\cdot\mathbf{b}_{j+1}}{\sqrt{h^2+A_j^{\,2}}}\right)}^{\arctan\left(\frac{\hat{t}_j\cdot\mathbf{b}_{j+2}}{\sqrt{h^2+A_j^{\,2}}}\right)} \sec^3\theta d\theta = B_j^{\,2}\sec\theta\tan\theta \Bigg|_{\arctan\left(\frac{\hat{t}_j\cdot\mathbf{b}_{j+1}}{\sqrt{h^2+A_j^{\,2}}}\right)}^{\arctan\left(\frac{\hat{t}_j\cdot\mathbf{b}_{j+2}}{\sqrt{h^2+A_j^{\,2}}}\right)}$$

$$- B_j^{\,2} \int_{\arctan\left(\frac{\hat{t}_j \cdot \mathbf{b}_{j+1}}{B_j}\right)}^{\arctan\left(\frac{\hat{t}_j \cdot \mathbf{b}_{j+2}}{B_j}\right)} \sec\theta \tan^2\theta d\theta$$

$$= B_j^{\,2}\left[1+\frac{\left(\hat{t}_j \cdot \mathbf{b}_{j+2}\right)^2}{B_j^{\,2}}\right]^{1/2}\left(\frac{\hat{t}_j \cdot \mathbf{b}_{j+2}}{B_j}\right) - \left[1+\frac{\left(\hat{t}_j \cdot \mathbf{b}_{j+1}\right)^2}{B_j^{\,2}}\right]^{1/2}\left(\frac{\hat{t}_j \cdot \mathbf{b}_{j+1}}{B_j}\right) - v_{1,j} + B_j^{\,2} \int_{\arctan\left(\frac{\hat{t}_j \cdot \mathbf{b}_{j+1}}{B_j}\right)}^{\arctan\left(\frac{\hat{t}_j \cdot \mathbf{b}_{j+2}}{B_j}\right)} \sec\theta d\theta$$

$$= \left|\mathbf{b}_{j+2}\right|\left(\hat{t}_j \cdot \mathbf{b}_{j+2}\right) - \left|\mathbf{b}_{j+1}\right|\left(\hat{t}_j \cdot \mathbf{b}_{j+1}\right) - v_{1,j} + B_j^{\,2} \int_{\arctan\left(\frac{\hat{t}_j \cdot \mathbf{b}_{j+1}}{B_j}\right)}^{\arctan\left(\frac{\hat{t}_j \cdot \mathbf{b}_{j+2}}{B_j}\right)} \sec\theta d\theta \qquad (2.17)$$

so that

$$v_{1,j} = \frac{1}{2}\left\{\left|\mathbf{b}_{j+2}\right|\left(\hat{t}_j \cdot \mathbf{b}_{j+2}\right) - \left|\mathbf{b}_{j+1}\right|\left(\hat{t}_j \cdot \mathbf{b}_{j+1}\right)\right.$$
$$\left. + B_j^{\,2}\left[\ln\left|\sqrt{1+\left(\frac{\hat{t}_j \cdot \mathbf{b}_{j+2}}{B_j}\right)^2}+\left(\frac{\hat{t}_j \cdot \mathbf{b}_{j+2}}{B_j}\right)\right| - \ln\left|\sqrt{1+\left(\frac{\hat{t}_j \cdot \mathbf{b}_{j+1}}{B_j}\right)^2}+\left(\frac{\hat{t}_j \cdot \mathbf{b}_{j+1}}{B_j}\right)\right|\right]\right\}$$

$$= \frac{1}{2}\left\{\left|\mathbf{b}_{j+2}\right|\left(\hat{t}_j \cdot \mathbf{b}_{j+2}\right) - \left|\mathbf{b}_{j+1}\right|\left(\hat{t}_j \cdot \mathbf{b}_{j+1}\right) + B_j^{\,2}\left[\ln\left|\frac{\left|\mathbf{b}_{j+2}\right| + \hat{t}_j \cdot \mathbf{b}_{j+2}}{B_j}\right| - \ln\left|\frac{\left|\mathbf{b}_{j+1}\right| + \hat{t}_j \cdot \mathbf{b}_{j+1}}{B_j}\right|\right]\right\}$$

$$= \frac{1}{2}\left\{\left|\mathbf{b}_{j+2}\right|\left(\hat{t}_j \cdot \mathbf{b}_{j+2}\right) - \left|\mathbf{b}_{j+1}\right|\left(\hat{t}_j \cdot \mathbf{b}_{j+1}\right) + B_j^{\,2}\ln\left|\frac{\left|\mathbf{b}_{j+2}\right| + \hat{t}_j \cdot \mathbf{b}_{j+2}}{\left|\mathbf{b}_{j+1}\right| + \hat{t}_j \cdot \mathbf{b}_{j+1}}\right|\right\}. \qquad (2.18)$$

In general,

$$v_{m,j} = B_j^{\,m+1} \int_{\arctan\left(\frac{\hat{t}_j\cdot\mathbf{b}_{j+1}}{B_j}\right)}^{\arctan\left(\frac{\hat{t}_j\cdot\mathbf{b}_{j+2}}{B_j}\right)} \sec^{m+2}\theta d\theta = B_j^{\,m+1}\sec^m\theta\tan\theta \Bigg|_{\arctan\left(\frac{\hat{t}_j\cdot\mathbf{b}_{j+1}}{B_j}\right)}^{\arctan\left(\frac{\hat{t}_j\cdot\mathbf{b}_{j+2}}{B_j}\right)}$$

$$-mB_j^{\,m+1} \int_{\arctan\left(\frac{\hat{t}_j\cdot\mathbf{b}_{j+1}}{B_j}\right)}^{\arctan\left(\frac{\hat{t}_j\cdot\mathbf{b}_{j+2}}{B_j}\right)} \sec^m\theta\tan^2\theta d\theta = B_j^{\,m+1}\sec^m\theta\tan\theta \Bigg|_{\arctan\left(\frac{\hat{t}_j\cdot\mathbf{b}_{j+1}}{B_j}\right)}^{\arctan\left(\frac{\hat{t}_j\cdot\mathbf{b}_{j+2}}{B_j}\right)} - m\left(v_{m,j} - B_j^{\,2}v_{m-2,j}\right) \tag{2.19}$$

or

$$v_{m,j} = \frac{B_j^{\,m+1}}{m+1}\left\{\left[1+\left(\frac{\hat{t}_j\cdot\mathbf{b}_{j+2}}{B_j}\right)^2\right]^{m/2}\left(\frac{\hat{t}_j\cdot\mathbf{b}_{j+2}}{B_j}\right) - \left[1+\left(\frac{\hat{t}_j\cdot\mathbf{b}_{j+1}}{B_j}\right)^2\right]^{m/2}\left(\frac{\hat{t}_j\cdot\mathbf{b}_{j+1}}{B_j}\right)\right\} + \frac{mB_j^{\,2}}{m+1}v_{m-2,j}$$

$$= \frac{1}{m+1}\left\{\left|\mathbf{b}_{j+2}\right|^m\left(\hat{t}_j\cdot\mathbf{b}_{j+2}\right) - \left|\mathbf{b}_{j+1}\right|^m\left(\hat{t}_j\cdot\mathbf{b}_{j+1}\right)\right\} + \frac{m}{m+1}B_j^{\,2}v_{m-2,j}\,, \quad m = 2,3,\ldots. \tag{2.20}$$

This completes the evaluation of (2.15). From (2.14) and (2.15)

$$V_{n,j} = \sum_{m=0}^{n+1}\left[\frac{(n+1)!}{m!(n+1-m)!}\right](-r')^{n+1-m}\,v_{m,j}\,, \quad n = 0,1,2,\ldots. \tag{2.21}$$

We examine now the case where $\hat{t}_j\cdot\mathbf{b}_{j+1} < \hat{t}_j\cdot\mathbf{b}_{j+2} < 0$. From (2.6)

$$V_{n,j} = \int_{\hat{t}_j\cdot\mathbf{b}_{j+1}}^{\hat{t}_j\cdot\mathbf{b}_{j+2}}\left(\sqrt{\tau^2+B_j^{\,2}} - r'\right)^{n+1}d\tau = \int_{\left|\hat{t}_j\cdot\mathbf{b}_{j+2}\right|}^{\left|\hat{t}_j\cdot\mathbf{b}_{j+1}\right|}\left(\sqrt{\tau^2+B_j^{\,2}} - r'\right)^{n+1}d\tau$$

$$= \sum_{m=0}^{n+1}\left(\frac{(n+1)!}{m!(n+1-m)!}\right)B_j^{\,m+1}(-r')^{n+1-m}\int_{\arctan\left(\frac{\left|\hat{t}_j\cdot\mathbf{b}_{j+2}\right|}{B_j}\right)}^{\arctan\left(\frac{\left|\hat{t}_j\cdot\mathbf{b}_{j+1}\right|}{B_j}\right)}\sec^{m+2}\theta d\theta\,. \tag{2.22}$$

Proceeding as above,

$$v_{m,j} = B_j^{\,m+1} \int_{\arctan\left(\frac{|\hat{t}_j\cdot\mathbf{b}_{j+2}|}{B_j}\right)}^{\arctan\left(\frac{|\hat{t}_j\cdot\mathbf{b}_{j+1}|}{B_j}\right)} \sec^{m+2}\theta d\theta\,, \quad m = 0,1,2,... \tag{2.23}$$

$$v_{0,j} = B_j \int_{\arctan\left(\frac{|\hat{t}_j\cdot\mathbf{b}_{j+2}|}{B_j}\right)}^{\arctan\left(\frac{|\hat{t}_j\cdot\mathbf{b}_{j+1}|}{B_j}\right)} \sec^2\theta d\theta = B_j \tan\theta \Bigg|_{\arctan\left(\frac{|\hat{t}_j\cdot\mathbf{b}_{j+2}|}{B_j}\right)}^{\arctan\left(\frac{|\hat{t}_j\cdot\mathbf{b}_{j+1}|}{B_j}\right)} = |\hat{t}_j\cdot\mathbf{b}_{j+1}| - |\hat{t}_j\cdot\mathbf{b}_{j+2}| = s_j \tag{2.24}$$

$$v_{1,j} = \frac{1}{2}\left\{|\mathbf{b}_{j+1}||\hat{t}_j\cdot\mathbf{b}_{j+1}| - |\mathbf{b}_{j+2}||\hat{t}_j\cdot\mathbf{b}_{j+2}| + B_j^{\,2}\ln\left|\frac{|\mathbf{b}_{j+1}| + |\hat{t}_j\cdot\mathbf{b}_{j+1}|}{|\mathbf{b}_{j+2}| + |\hat{t}_j\cdot\mathbf{b}_{j+2}|}\right|\right\} \tag{2.25}$$

$$v_{m,j} = \frac{1}{m+1}\left\{|\mathbf{b}_{j+1}|^m|\hat{t}_j\cdot\mathbf{b}_{j+1}| - |\mathbf{b}_{j+2}|^m|\hat{t}_j\cdot\mathbf{b}_{j+2}|\right\} + \frac{m}{m+1}B_j^{\,2}v_{m-2,j}\,, \quad m = 2,3,... \tag{2.26}$$

For the case,

$$\hat{t}_j\cdot\mathbf{b}_{j+1} \le 0\,, \quad \hat{t}_j\cdot\mathbf{b}_{j+2} \ge 0 \tag{2.27}$$

we write from (2.6)

$$\begin{aligned} V_{n,j} &= \int_{\hat{t}_j\cdot\mathbf{b}_{j+1}}^{\hat{t}_j\cdot\mathbf{b}_{j+2}} \left(\sqrt{\tau^2 + B_j^{\,2}} - r'\right)^{n+1} d\tau = \int_{\hat{t}_j\cdot\mathbf{b}_{j+1}}^{0} \left(\sqrt{\tau^2 + B_j^{\,2}} - r'\right)^{n+1} d\tau + \int_0^{\hat{t}_j\cdot\mathbf{b}_{j+2}} \left(\sqrt{\tau^2 + B_j^{\,2}} - r'\right)^{n+1} d\tau \\ &= \int_0^{|\hat{t}_j\cdot\mathbf{b}_{j+1}|} \left(\sqrt{\tau^2 + B_j^{\,2}} - r'\right)^{n+1} d\tau + \int_0^{\hat{t}_j\cdot\mathbf{b}_{j+2}} \left(\sqrt{\tau^2 + B_j^{\,2}} - r'\right)^{n+1} d\tau \\ &= \sum_{m=0}^{n+1}\left(\frac{(n+1)!}{m!(n+1-m)!}\right) B_j^{\,m+1}(-r')^{n+1-m} \left\{\int_0^{\arctan\left(\frac{|\hat{t}_j\cdot\mathbf{b}_{j+1}|}{B_j}\right)} \sec^{m+2}\theta d\theta + \int_0^{\arctan\left(\frac{\hat{t}_j\cdot\mathbf{b}_{j+2}}{B_j}\right)} \sec^{m+2}\theta d\theta\right\}. \end{aligned} \tag{2.28}$$

In this case, (2.15) becomes

$$v_{m,j} = B_j^{\,m+1}\left\{\int_0^{\arctan\left(\frac{\left|\hat{t}_j\cdot\mathbf{b}_{j+1}\right|}{B_j}\right)} \sec^{m+2}\theta d\theta + \int_0^{\arctan\left(\frac{\hat{t}_j\cdot\mathbf{b}_{j+2}}{B_j}\right)} \sec^{m+2}\theta d\theta\right\}, \quad m = 0,1,2,... \tag{2.29}$$

so that

$$v_{0,j} = B_j\left\{\int_0^{\arctan\left(\frac{\left|\hat{t}_j\cdot\mathbf{b}_{j+1}\right|}{B_j}\right)} \sec^{2}\theta d\theta + \int_0^{\arctan\left(\frac{\hat{t}_j\cdot\mathbf{b}_{j+2}}{B_j}\right)} \sec^{2}\theta d\theta\right\} = \left|\hat{t}_j\cdot\mathbf{b}_{j+1}\right| + \hat{t}_j\cdot\mathbf{b}_{j+2} = s_j \tag{2.30}$$

$$v_{1,j} = \frac{1}{2}\left\{\left|\mathbf{b}_{j+1}\right|\left|\hat{t}_j\cdot\mathbf{b}_{j+1}\right| + \left|\mathbf{b}_{j+2}\right|\left(\hat{t}_j\cdot\mathbf{b}_{j+2}\right) + B_j^{\,2}\ln\left|\frac{\left(\left|\mathbf{b}_{j+1}\right| + \left|\hat{t}_j\cdot\mathbf{b}_{j+1}\right|\right)\left(\left|\mathbf{b}_{j+2}\right| + \hat{t}_j\cdot\mathbf{b}_{j+2}\right)}{B_j^{\,2}}\right|\right\} \tag{2. 31}$$

$$v_{m,j} = \frac{1}{m+1}\left\{\left|\mathbf{b}_{j+1}\right|^m\left|\hat{t}_j\cdot\mathbf{b}_{j+1}\right| + \left|\mathbf{b}_{j+2}\right|^m\left(\hat{t}_j\cdot\mathbf{b}_{j+2}\right)\right\} + \frac{m}{m+1}B_j^{\,2}v_{m-2,j}\,, \quad m = 2,3,... \tag{2.32}$$

This concludes the evaluation of (2.6). The iteration formulas (2.20), (2.26) and (2.32) do not converge everywhere. In Appendix B, we show that, for the iteration to be stable, we need $0 \le B_j < 1$.

We also mention that there are other ways of evaluating these integrals but they do not appear to have an advantage over the present one.

2.2. EVALUATION OF $K_{0,j}$

We turn to the evaluation of (2.3) and write

$$K_{0,j} = \int_{s_j}\frac{\left(\rho^2+h^2\right)^{\frac{1}{2}} - \left|h\right|}{\rho^2}ds = \int_{s_j}\frac{ds}{\left(\rho^2+h^2\right)^{\frac{1}{2}} + \left|h\right|} = \int_0^{s_j}\frac{ds}{R+\left|h\right|}\,. \tag{2.33}$$

We make the transformation

$$R^2 = \left(s + \hat{t}_j \cdot \mathbf{a}_{j+1}\right)^2 + B_j{}^2 \Rightarrow s + \hat{t}_j \cdot \mathbf{a}_{j+1} = \pm\sqrt{R^2 - B_j{}^2}\,, \quad ds = \frac{\pm R dR}{\sqrt{R^2 - B_j{}^2}} \tag{2.34}$$

and consider observation points in the region $\hat{t}_j \cdot \mathbf{b}_{j+2} > \hat{t}_j \cdot \mathbf{b}_{j+1} > 0$. In this case, the appropriate sign in (2.34) is the positive one. From the last two statements

$$K_{0,j} = \int_{|\mathbf{b}_{j+1}|}^{|\mathbf{b}_{j+2}|} \frac{R dR}{\left(R + |h|\right)\sqrt{R^2 - B_j{}^2}} = \int_{|\mathbf{b}_{j+1}|}^{|\mathbf{b}_{j+2}|} \frac{dR}{\sqrt{R^2 - B_j{}^2}} - |h| \int_{|\mathbf{b}_{j+1}|}^{|\mathbf{b}_{j+2}|} \frac{dR}{\left(R + |h|\right)\sqrt{R^2 - B_j{}^2}} = I_1 - I_2 \tag{2.35}$$

We let

$$R = B_j \cosh(u)\,, \quad dR = B_j \sinh(u)\, du \tag{2.36}$$

and write

$$I_1 = \int_{|\mathbf{b}_{j+1}|}^{|\mathbf{b}_{j+2}|} \frac{dR}{\sqrt{R^2 - B_j{}^2}} = \int_{\cosh^{-1}\left(\frac{|\mathbf{b}_{j+1}|}{B_j}\right)}^{\cosh^{-1}\left(\frac{|\mathbf{b}_{j+2}|}{B_j}\right)} du = \cosh^{-1}\left(\frac{|\mathbf{b}_{j+2}|}{B_j}\right) - \cosh^{-1}\left(\frac{|\mathbf{b}_{j+1}|}{B_j}\right)$$

$$= \ln\left(\frac{|\mathbf{b}_{j+2}| + \sqrt{|\mathbf{b}_{j+2}|^2 - B_j{}^2}}{B_j}\right) - \ln\left(\frac{|\mathbf{b}_{j+1}| + \sqrt{|\mathbf{b}_{j+1}|^2 - B_j{}^2}}{B_j}\right)$$

$$= \ln\left(\frac{|\mathbf{b}_{j+2}| + \sqrt{|\mathbf{b}_{j+2}|^2 - B_j{}^2}}{|\mathbf{b}_{j+1}| + \sqrt{|\mathbf{b}_{j+1}|^2 - B_j{}^2}}\right) = \ln\left(\frac{|\mathbf{b}_{j+2}| + |\hat{t}_j \cdot \mathbf{b}_{j+2}|}{|\mathbf{b}_{j+1}| + |\hat{t}_j \cdot \mathbf{b}_{j+1}|}\right). \tag{2.37}$$

For the second integral in (2.35), we write

$$I_2 = |h| \int_{|\mathbf{b}_{j+1}|}^{|\mathbf{b}_{j+2}|} \frac{dR}{\left(R + |h|\right)\sqrt{R^2 - B_j{}^2}} = |h| \int_{|\mathbf{b}_{j+1}|}^{|\mathbf{b}_{j+2}|} \frac{\left(R - |h|\right) dR}{\left(R^2 - |h|^2\right)\sqrt{R^2 - B_j{}^2}}$$

$$= |h| \int_{|\mathbf{b}_{j+1}|}^{|\mathbf{b}_{j+2}|} \frac{R dR}{\left(R^2 - |h|^2\right)\sqrt{R^2 - B_j{}^2}} - |h|^2 \int_{|\mathbf{b}_{j+1}|}^{|\mathbf{b}_{j+2}|} \frac{dR}{\left(R^2 - |h|^2\right)\sqrt{R^2 - B_j{}^2}} = I_{21} - I_{22}\,. \tag{2.38}$$

In order to evaluate I_{21}, we let

$$u^2 = R^2 - B_j{}^2 \tag{2.39}$$

and write

$$I_{21} = |h| \int_{|\mathbf{b}_{j+1}|}^{|\mathbf{b}_{j+2}|} \frac{RdR}{\left(R^2 - |h|^2\right)\sqrt{R^2 - B_j{}^2}} = |h| \int_{|\hat{t}_j \cdot \mathbf{b}_{j+1}|}^{|\hat{t}_j \cdot \mathbf{b}_{j+2}|} \frac{du}{u^2 + A_j{}^2} \tag{2.40}$$

We now make the transformation

$$u = A_j \tan\psi \tag{2.41}$$

to get

$$I_{21} = |h| \int_{|\hat{t}_j \cdot \mathbf{b}_{j+1}|}^{|\hat{t}_j \cdot \mathbf{b}_{j+2}|} \frac{du}{u^2 + A_j{}^2} = \frac{|h|}{A_j} \int_{\tan^{-1}\left(\frac{|\hat{t}_j \cdot \mathbf{b}_{j+1}|}{A_j}\right)}^{\tan^{-1}\left(\frac{|\hat{t}_j \cdot \mathbf{b}_{j+2}|}{A_j}\right)} d\psi = \frac{|h|}{A_j}\left[\tan^{-1}\left(\frac{|\hat{t}_j \cdot \mathbf{b}_{j+2}|}{A_j}\right) - \tan^{-1}\left(\frac{|\hat{t}_j \cdot \mathbf{b}_{j+1}|}{A_j}\right)\right]. \tag{2.42}$$

For the integral I_{22} in (2.38), we let

$$v = \frac{R}{\sqrt{R^2 - B_j{}^2}}; \quad v^2\left(R^2 - B_j{}^2\right) = R^2 \quad \Rightarrow \quad R = B_j \frac{v}{\sqrt{v^2 - 1}} \tag{2.43}$$

so that

$$dR = B_j \frac{\sqrt{v^2 - 1} - \dfrac{v^2}{\sqrt{v^2 - 1}}}{v^2 - 1} dv = -\frac{B_j}{\left(v^2 - 1\right)^{3/2}} dv\,. \tag{2.44}$$

We can then write for I_{22} in (2.38)

$$I_{22} = |h|^2 \int_{|\mathbf{b}_{j+1}|}^{|\mathbf{b}_{j+2}|} \frac{dR}{\left(R^2 - |h|^2\right)\sqrt{R^2 - B_j^{\,2}}} = -|h|^2 \int_{\frac{|\mathbf{b}_{j+1}|}{|\hat{t}_j \cdot \mathbf{b}_{j+1}|}}^{\frac{|\mathbf{b}_{j+2}|}{|\hat{t}_j \cdot \mathbf{b}_{j+2}|}} \frac{dv}{\left(A_j v\right)^2 + |h|^2}. \tag{2.45}$$

We let next

$$w = \frac{A_j}{|h|} v \tag{2.46}$$

and write

$$I_{22} = -|h|^2 \int_{\frac{|\mathbf{b}_{j+1}|}{|\hat{t}_j \cdot \mathbf{b}_{j+1}|}}^{\frac{|\mathbf{b}_{j+2}|}{|\hat{t}_j \cdot \mathbf{b}_{j+2}|}} \frac{dv}{\left(A_j v\right)^2 + |h|^2} = -\frac{|h|}{A_j} \int_{\frac{A_j|\mathbf{b}_{j+1}|}{|h||\hat{t}_j \cdot \mathbf{b}_{j+1}|}}^{\frac{A_j|\mathbf{b}_{j+2}|}{|h||\hat{t}_j \cdot \mathbf{b}_{j+2}|}} \frac{dw}{w^2 + 1}$$

$$= \frac{|h|}{A_j}\left[\tan^{-1}\left(\frac{A_j\left|\mathbf{b}_{j+1}\right|}{|h|\left|\hat{t}_j \cdot \mathbf{b}_{j+1}\right|}\right) - \tan^{-1}\left(\frac{A_j\left|\mathbf{b}_{j+2}\right|}{|h|\left|\hat{t}_j \cdot \mathbf{b}_{j+2}\right|}\right)\right]. \tag{2.47}$$

From (2.38), (2.42) and (2.47), we have

$$I_2 = I_{21} - I_{22} = \frac{|h|}{A_j}\left[\tan^{-1}\left(\frac{\left|\hat{t}_j \cdot \mathbf{b}_{j+2}\right|}{A_j}\right) - \tan^{-1}\left(\frac{\left|\hat{t}_j \cdot \mathbf{b}_{j+1}\right|}{A_j}\right)\right]$$

$$+ \frac{|h|}{A_j}\left[\tan^{-1}\left(\frac{A_j\left|\mathbf{b}_{j+2}\right|}{|h|\left|\hat{t}_j \cdot \mathbf{b}_{j+2}\right|}\right) - \tan^{-1}\left(\frac{A_j\left|\mathbf{b}_{j+1}\right|}{|h|\left|\hat{t}_j \cdot \mathbf{b}_{j+1}\right|}\right)\right]. \tag{2.48}$$

From this, (2.35) and (2.37), we can write that

$$K_{0,j} = I_1 - I_2 = \ln\left(\frac{\left|\mathbf{b}_{j+2}\right| + \left|\hat{t}_j \cdot \mathbf{b}_{j+2}\right|}{\left|\mathbf{b}_{j+1}\right| + \left|\hat{t}_j \cdot \mathbf{b}_{j+1}\right|}\right) - \frac{|h|}{A_j}\left[\tan^{-1}\left(\frac{\left|\hat{t}_j \cdot \mathbf{b}_{j+2}\right|}{A_j}\right) - \tan^{-1}\left(\frac{\left|\hat{t}_j \cdot \mathbf{b}_{j+1}\right|}{A_j}\right)\right]$$

$$- \frac{|h|}{A_j}\left[\tan^{-1}\left(\frac{A_j\left|\mathbf{b}_{j+2}\right|}{|h|\left|\hat{t}_j \cdot \mathbf{b}_{j+2}\right|}\right) - \tan^{-1}\left(\frac{A_j\left|\mathbf{b}_{j+1}\right|}{|h|\left|\hat{t}_j \cdot \mathbf{b}_{j+1}\right|}\right)\right], \quad \hat{t}_j \cdot \mathbf{b}_{j+2} > \hat{t}_j \cdot \mathbf{b}_{j+1} > 0. \tag{2.49}$$

As we pointed out above, this formula is valid when the integration in (2.33) is over an interval of positive numbers. This is made explicit through the inequality in (2.49). Basically, and with respect to the *j*-th side of the triangle, we divide all of space into three sectors. They are formed by attaching an infinite plane at each end of the *j*-th side and normal to it. The inequality in (2.49) holds in one of the two sectors that do not contain the *j*-th side. In the other sector, the directions of the inequality are reversed. In this case, and by (2.34), we must introduce a negative sign in (2.35) or, simply, reverse the direction of integration; thus, from (2.49) we have

$$K_{0,j} = \ln\left(\frac{|\mathbf{b}_{j+1}| + |\hat{t}_j \cdot \mathbf{b}_{j+1}|}{|\mathbf{b}_{j+2}| + |\hat{t}_j \cdot \mathbf{b}_{j+2}|}\right) + \frac{|h|}{A_j}\left[\tan^{-1}\left(\frac{|\hat{t}_j \cdot \mathbf{b}_{j+2}|}{A_j}\right) - \tan^{-1}\left(\frac{|\hat{t}_j \cdot \mathbf{b}_{j+1}|}{A_j}\right)\right]$$
$$+ \frac{|h|}{A_j}\left[\tan^{-1}\left(\frac{A_j|\mathbf{b}_{j+2}|}{|h||\hat{t}_j \cdot \mathbf{b}_{j+2}|}\right) - \tan^{-1}\left(\frac{A_j|\mathbf{b}_{j+1}|}{|h||\hat{t}_j \cdot \mathbf{b}_{j+1}|}\right)\right], \quad \hat{t}_j \cdot \mathbf{b}_{j+1} < \hat{t}_j \cdot \mathbf{b}_{j+2} < 0\,. \tag{2.50}$$

The third case is when the observation point is in the space between the two planes. The corresponding inequalities are

$$\hat{t}_j \cdot \mathbf{b}_{j+1} \le 0\,, \quad \hat{t}_j \cdot \mathbf{b}_{j+2} \ge 0 \tag{2.51}$$

which necessitate splitting the interval of integration in two. The resulting expression is

$$K_{0,j} = \int_{B_j}^{|\mathbf{b}_{j+1}|} \frac{RdR}{(R+|h|)\sqrt{R^2 - B_j^{\,2}}} + \int_{B_j}^{|\mathbf{b}_{j+2}|} \frac{RdR}{(R+|h|)\sqrt{R^2 - B_j^{\,2}}}$$
$$= \ln\left(\frac{|\mathbf{b}_{j+1}| + |\hat{t}_j \cdot \mathbf{b}_{j+1}|}{B_j}\right) - \frac{|h|}{A_j}\tan^{-1}\left(\frac{|\hat{t}_j \cdot \mathbf{b}_{j+1}|}{A_j}\right) - \frac{|h|}{A_j}\left[\tan^{-1}\left(\frac{A_j|\mathbf{b}_{j+1}|}{|h||\hat{t}_j \cdot \mathbf{b}_{j+1}|}\right) - \frac{\pi}{2}\right]$$
$$+ \ln\left(\frac{|\mathbf{b}_{j+2}| + |\hat{t}_j \cdot \mathbf{b}_{j+2}|}{B_j}\right) - \frac{|h|}{A_j}\tan^{-1}\left(\frac{|\hat{t}_j \cdot \mathbf{b}_{j+2}|}{A_j}\right) - \frac{|h|}{A_j}\left[\tan^{-1}\left(\frac{A_j|\mathbf{b}_{j+2}|}{|h||\hat{t}_j \cdot \mathbf{b}_{j+2}|}\right) - \frac{\pi}{2}\right]$$
$$= \ln\left[\frac{\left(|\mathbf{b}_{j+1}| + |\hat{t}_j \cdot \mathbf{b}_{j+1}|\right)\left(|\mathbf{b}_{j+2}| + |\hat{t}_j \cdot \mathbf{b}_{j+2}|\right)}{B_j^{\,2}}\right] - \frac{|h|}{A_j}\left[\tan^{-1}\left(\frac{|\hat{t}_j \cdot \mathbf{b}_{j+1}|}{A_j}\right) + \tan^{-1}\left(\frac{|\hat{t}_j \cdot \mathbf{b}_{j+2}|}{A_j}\right)\right]$$
$$+ \frac{|h|}{A_j}\left[\cot^{-1}\left(\frac{A_j|\mathbf{b}_{j+1}|}{|h||\hat{t}_j \cdot \mathbf{b}_{j+1}|}\right) + \cot^{-1}\left(\frac{A_j|\mathbf{b}_{j+2}|}{|h||\hat{t}_j \cdot \mathbf{b}_{j+2}|}\right)\right]$$
$$= \ln\left[\frac{\left(|\mathbf{b}_{j+1}| + |\hat{t}_j \cdot \mathbf{b}_{j+1}|\right)\left(|\mathbf{b}_{j+2}| + |\hat{t}_j \cdot \mathbf{b}_{j+2}|\right)}{B_j^{\,2}}\right] - \frac{|h|}{A_j}\left[\tan^{-1}\left(\frac{|\hat{t}_j \cdot \mathbf{b}_{j+1}|}{A_j}\right) + \tan^{-1}\left(\frac{|\hat{t}_j \cdot \mathbf{b}_{j+2}|}{A_j}\right)\right]$$

$$+\frac{|h|}{A_j}\left[\tan^{-1}\left(\frac{|h|\left|\hat{t}_j\cdot\mathbf{b}_{j+1}\right|}{A_j\left|\mathbf{b}_{j+1}\right|}\right)+\tan^{-1}\left(\frac{|h|\left|\hat{t}_j\cdot\mathbf{b}_{j+2}\right|}{A_j\left|\mathbf{b}_{j+2}\right|}\right)\right],\quad \hat{t}_j\cdot\mathbf{b}_{j+1}\le 0\,,\quad \hat{t}_j\cdot\mathbf{b}_{j+2}\ge 0\,. \tag{2.52}$$

We revisit (2.49) and combine the first and third arctangents according to the formula

$$\tan^{-1}(x)+\tan^{-1}(y)=\begin{cases}\tan^{-1}\left(\dfrac{x+y}{1-xy}\right), & xy<1\\ \pi+\tan^{-1}\left(\dfrac{x+y}{1-xy}\right), & x>0\,,\quad xy>1\end{cases} \tag{2.53}$$

Since

$$\frac{\left|\hat{t}_j\cdot\mathbf{b}_{j+2}\right|}{A_j}\cdot\frac{A_j\left|\mathbf{b}_{j+2}\right|}{|h|\left|\hat{t}_j\cdot\mathbf{b}_{j+2}\right|}=\frac{\left|\mathbf{b}_{j+2}\right|}{|h|}>1 \tag{2.54}$$

we use the lower formula in (2.53) and write

$$\tan^{-1}\left(\frac{\left|\hat{t}_j\cdot\mathbf{b}_{j+2}\right|}{A_j}\right)+\tan^{-1}\left(\frac{A_j\left|\mathbf{b}_{j+2}\right|}{|h|\left|\hat{t}_j\cdot\mathbf{b}_{j+2}\right|}\right)=\pi+\tan^{-1}\left(\frac{\dfrac{\left|\hat{t}_j\cdot\mathbf{b}_{j+2}\right|}{A_j}+\dfrac{A_j\left|\mathbf{b}_{j+2}\right|}{|h|\left|\hat{t}_j\cdot\mathbf{b}_{j+2}\right|}}{1-\dfrac{\left|\mathbf{b}_{j+2}\right|}{|h|}}\right)$$

$$=\pi+\tan^{-1}\left(\frac{|h|\dfrac{\left|\hat{t}_j\cdot\mathbf{b}_{j+2}\right|}{A_j}+\dfrac{A_j\left|\mathbf{b}_{j+2}\right|}{\left|\hat{t}_j\cdot\mathbf{b}_{j+2}\right|}}{|h|-\left|\mathbf{b}_{j+2}\right|}\right)=\pi-\tan^{-1}\left[\frac{|h|\dfrac{\left|\hat{t}_j\cdot\mathbf{b}_{j+2}\right|}{A_j}+\dfrac{A_j\left|\mathbf{b}_{j+2}\right|}{\left|\hat{t}_j\cdot\mathbf{b}_{j+2}\right|}}{\left|\mathbf{b}_{j+2}\right|^2-|h|^2}\left(|h|+\left|\mathbf{b}_{j+2}\right|\right)\right]$$

$$=\pi-\tan^{-1}\left[\frac{|h|\left|\hat{t}_j\cdot\mathbf{b}_{j+2}\right|^2+A_j{}^2\left|\mathbf{b}_{j+2}\right|}{A_j\left|\hat{t}_j\cdot\mathbf{b}_{j+2}\right|\left|\mathbf{a}_{j+2}\right|^2}\left(|h|+\left|\mathbf{b}_{j+2}\right|\right)\right]$$

$$=\pi-\tan^{-1}\left[\frac{|h|\left(\left|\mathbf{a}_{j+2}\right|^2-A_j{}^2\right)+A_j{}^2\left|\mathbf{b}_{j+2}\right|}{A_j\left|\hat{t}_j\cdot\mathbf{b}_{j+2}\right|\left|\mathbf{a}_{j+2}\right|^2}\left(|h|+\left|\mathbf{b}_{j+2}\right|\right)\right]$$

$$=\pi-\tan^{-1}\left[\frac{|h|\left(|h|+\left|\mathbf{b}_{j+2}\right|\right)}{A_j\left|\hat{t}_j\cdot\mathbf{b}_{j+2}\right|}+\frac{A_j}{\left|\hat{t}_j\cdot\mathbf{b}_{j+2}\right|}\right]=\pi-\tan^{-1}\left[\frac{|h|\left(|h|+\left|\mathbf{b}_{j+2}\right|\right)+A_j{}^2}{A_j\left|\hat{t}_j\cdot\mathbf{b}_{j+2}\right|}\right]. \tag{2.55}$$

Similarly,

$$\tan^{-1}\left(\frac{\left|\hat{t}_j\cdot\mathbf{b}_{j+1}\right|}{A_j}\right)+\tan^{-1}\left(\frac{A_j\left|\mathbf{b}_{j+1}\right|}{|h|\left|\hat{t}_j\cdot\mathbf{b}_{j+1}\right|}\right)=\pi-\tan^{-1}\left[\frac{|h|\left(|h|+\left|\mathbf{b}_{j+1}\right|\right)+A_j{}^2}{A_j\left|\hat{t}_j\cdot\mathbf{b}_{j+1}\right|}\right]. \tag{2.56}$$

Substitution of the last two expressions in (2.49) yields

$$K_{0,j}=\ln\left(\frac{\left|\mathbf{b}_{j+2}\right|+\left|\hat{t}_j\cdot\mathbf{b}_{j+2}\right|}{\left|\mathbf{b}_{j+1}\right|+\left|\hat{t}_j\cdot\mathbf{b}_{j+1}\right|}\right)+\frac{|h|}{A_j}\left\{\tan^{-1}\left[\frac{|h|\left(|h|+\left|\mathbf{b}_{j+2}\right|\right)+A_j{}^2}{A_j\left|\hat{t}_j\cdot\mathbf{b}_{j+2}\right|}\right]\right.$$
$$\left.-\tan^{-1}\left[\frac{|h|\left(|h|+\left|\mathbf{b}_{j+1}\right|\right)+A_j{}^2}{A_j\left|\hat{t}_j\cdot\mathbf{b}_{j+1}\right|}\right]\right\},\quad \hat{t}_j\cdot\mathbf{b}_{j+2}>\hat{t}_j\cdot\mathbf{b}_{j+1}>0\,. \tag{2.57}$$

As $A_j\to 0$, we use the well known expansion

$$\tan^{-1}(x)=\frac{\pi}{2}-\sum_{k=0}^{\infty}\frac{(-1)^k}{(2k+1)x^{2k+1}},\quad |x|\ge 1 \tag{2.58}$$

to obtain an estimate for A_j so that only the first term in the series will be required for a specified number of significant digits. We thus set

$$\frac{A_j\left|\hat{t}_j\cdot\mathbf{b}_{j+2}\right|}{|h|\left(|h|+\left|\mathbf{b}_{j+2}\right|\right)+A_j{}^2}<\sqrt{3\cdot 10^{-M}} \tag{2.59}$$

and by means of

$$\frac{A_j\left|\hat{t}_j\cdot\mathbf{b}_{j+2}\right|}{|h|\left(|h|+\left|\mathbf{b}_{j+2}\right|\right)+A_j{}^2}<\frac{A_j\left|\hat{t}_j\cdot\mathbf{b}_{j+2}\right|}{|h|\left(|h|+\left|\mathbf{b}_{j+2}\right|\right)} \tag{2.60}$$

we obtain the estimate

$$A_j < \sqrt{3\cdot 10^{-M}}\,\frac{|h|\left(|h|+\left|\mathbf{b}_{j+2}\right|\right)}{\left|\hat{t}_j\cdot\mathbf{b}_{j+2}\right|}. \tag{2.61}$$

For these values of A_j, we replace (2.57) by

$$K_{0,j} = \ln\left(\frac{\left|\mathbf{b}_{j+2}\right|+\left|\hat{t}_j\cdot\mathbf{b}_{j+2}\right|}{\left|\mathbf{b}_{j+1}\right|+\left|\hat{t}_j\cdot\mathbf{b}_{j+1}\right|}\right)-\frac{|h|}{A_j}\left\{\frac{\pi}{2}-\frac{A_j\left|\hat{t}_j\cdot\mathbf{b}_{j+1}\right|}{|h|\left(|h|+\left|\mathbf{b}_{j+1}\right|\right)+A_j{}^2}-\frac{\pi}{2}+\frac{A_j\left|\hat{t}_j\cdot\mathbf{b}_{j+2}\right|}{|h|\left(|h|+\left|\mathbf{b}_{j+2}\right|\right)+A_j{}^2}\right\}$$

$$=\ln\left(\frac{\left|\mathbf{b}_{j+2}\right|+\left|\hat{t}_j\cdot\mathbf{b}_{j+2}\right|}{\left|\mathbf{b}_{j+1}\right|+\left|\hat{t}_j\cdot\mathbf{b}_{j+1}\right|}\right)-|h|\left\{\frac{\left|\hat{t}_j\cdot\mathbf{b}_{j+2}\right|}{|h|\left(|h|+\left|\mathbf{b}_{j+2}\right|\right)+A_j{}^2}-\frac{\left|\hat{t}_j\cdot\mathbf{b}_{j+1}\right|}{|h|\left(|h|+\left|\mathbf{b}_{j+1}\right|\right)+A_j{}^2}\right\}$$

$$\hat{t}_j\cdot\mathbf{b}_{j+2} > \hat{t}_j\cdot\mathbf{b}_{j+1} > 0. \tag{2.62}$$

Moreover, if $h=0$, then

$$K_{0,j} = \ln\left(\frac{\left|\mathbf{b}_{j+2}\right|+\left|\hat{t}_j\cdot\mathbf{b}_{j+2}\right|}{\left|\mathbf{b}_{j+1}\right|+\left|\hat{t}_j\cdot\mathbf{b}_{j+1}\right|}\right),\quad h=0,\quad \hat{t}_j\cdot\mathbf{b}_{j+2} > \hat{t}_j\cdot\mathbf{b}_{j+1} > 0. \tag{2.63}$$

Similarly, in place of (C.18) we write

$$K_{0,j} = -\ln\left(\frac{\left|\mathbf{b}_{j+2}\right|+\left|\hat{t}_j\cdot\mathbf{b}_{j+2}\right|}{\left|\mathbf{b}_{j+1}\right|+\left|\hat{t}_j\cdot\mathbf{b}_{j+1}\right|}\right)-\frac{|h|}{A_j}\left\{\tan^{-1}\left[\frac{|h|\left(|h|+\left|\mathbf{b}_{j+2}\right|\right)+A_j{}^2}{A_j\left|\hat{t}_j\cdot\mathbf{b}_{j+2}\right|}\right]\right.$$

$$\left.-\tan^{-1}\left[\frac{|h|\left(|h|+\left|\mathbf{b}_{j+1}\right|\right)+A_j{}^2}{A_j\left|\hat{t}_j\cdot\mathbf{b}_{j+1}\right|}\right]\right\},\quad \hat{t}_j\cdot\mathbf{b}_{j+1} < \hat{t}_j\cdot\mathbf{b}_{j+2} < 0 \tag{2.64}$$

and, if

$$A_j < \sqrt{3\cdot 10^{-M}}\,\frac{|h|\left(|h|+\left|\mathbf{b}_{j+1}\right|\right)}{\left|\hat{t}_j\cdot\mathbf{b}_{j+1}\right|} \tag{2.65}$$

then

$$K_{0,j} = -\ln\left(\frac{\left|\mathbf{b}_{j+2}\right| + \left|\hat{t}_j \cdot \mathbf{b}_{j+2}\right|}{\left|\mathbf{b}_{j+1}\right| + \left|\hat{t}_j \cdot \mathbf{b}_{j+1}\right|}\right) + |h|\left\{\frac{\left|\hat{t}_j \cdot \mathbf{b}_{j+2}\right|}{|h|\left(|h| + \left|\mathbf{b}_{j+2}\right|\right) + A_j^{\,2}} - \frac{\left|\hat{t}_j \cdot \mathbf{b}_{j+1}\right|}{|h|\left(|h| + \left|\mathbf{b}_{j+1}\right|\right) + A_j^{\,2}}\right\} \tag{2.66}$$

while, if $h = 0$,

$$K_{0,j} = -\ln\left(\frac{\left|\mathbf{b}_{j+2}\right| + \left|\hat{t}_j \cdot \mathbf{b}_{j+2}\right|}{\left|\mathbf{b}_{j+1}\right| + \left|\hat{t}_j \cdot \mathbf{b}_{j+1}\right|}\right), \quad h = 0\,, \quad \hat{t}_j \cdot \mathbf{b}_{j+1} < \hat{t}_j \cdot \mathbf{b}_{j+2} < 0\,. \tag{2.67}$$

In (2.52), we recall that if $h = 0$, then $A_j > 0$. Also, if $A_j = 0$, then $|h| > 0$. Otherwise, the observation point would lie on the *j*-th side of the triangle. In this expression, we combine arctangents according to the formula

$$\tan^{-1}(x) - \tan^{-1}(y) = \tan^{-1}\left(\frac{x-y}{1+xy}\right), \quad xy > -1\,. \tag{2.68}$$

In place of (2.52) we write

$$\begin{aligned}
K_{0,j} &= \ln\left[\frac{\left(\left|\mathbf{b}_{j+1}\right| + \left|\hat{t}_j \cdot \mathbf{b}_{j+1}\right|\right)\left(\left|\mathbf{b}_{j+2}\right| + \left|\hat{t}_j \cdot \mathbf{b}_{j+2}\right|\right)}{B_j^{\,2}}\right] - \frac{|h|}{A_j}\left[\tan^{-1}\left(\frac{\left|\hat{t}_j \cdot \mathbf{b}_{j+1}\right|}{A_j}\right) + \tan^{-1}\left(\frac{\left|\hat{t}_j \cdot \mathbf{b}_{j+2}\right|}{A_j}\right)\right] \\
&+ \frac{|h|}{A_j}\left[\tan^{-1}\left(\frac{|h|\left|\hat{t}_j \cdot \mathbf{b}_{j+1}\right|}{A_j\left|\mathbf{b}_{j+1}\right|}\right) + \tan^{-1}\left(\frac{|h|\left|\hat{t}_j \cdot \mathbf{b}_{j+2}\right|}{A_j\left|\mathbf{b}_{j+2}\right|}\right)\right] \\
&= \ln\left[\frac{\left(\left|\mathbf{b}_{j+1}\right| + \left|\hat{t}_j \cdot \mathbf{b}_{j+1}\right|\right)\left(\left|\mathbf{b}_{j+2}\right| + \left|\hat{t}_j \cdot \mathbf{b}_{j+2}\right|\right)}{B_j^{\,2}}\right] - \frac{|h|}{A_j}\left[\tan^{-1}\left(\frac{\left|\hat{t}_j \cdot \mathbf{b}_{j+1}\right|}{A_j}\right) - \tan^{-1}\left(\frac{|h|\left|\hat{t}_j \cdot \mathbf{b}_{j+1}\right|}{A_j\left|\mathbf{b}_{j+1}\right|}\right)\right] \\
&- \frac{|h|}{A_j}\left[\tan^{-1}\left(\frac{\left|\hat{t}_j \cdot \mathbf{b}_{j+2}\right|}{A_j}\right) - \tan^{-1}\left(\frac{|h|\left|\hat{t}_j \cdot \mathbf{b}_{j+2}\right|}{A_j\left|\mathbf{b}_{j+2}\right|}\right)\right] \\
&= \ln\left[\frac{\left(\left|\mathbf{b}_{j+1}\right| + \left|\hat{t}_j \cdot \mathbf{b}_{j+1}\right|\right)\left(\left|\mathbf{b}_{j+2}\right| + \left|\hat{t}_j \cdot \mathbf{b}_{j+2}\right|\right)}{B_j^{\,2}}\right] - \frac{|h|}{A_j}\tan^{-1}\left[\frac{\dfrac{\left|\hat{t}_j \cdot \mathbf{b}_{j+1}\right|}{A_j} - \dfrac{|h|\left|\hat{t}_j \cdot \mathbf{b}_{j+1}\right|}{A_j\left|\mathbf{b}_{j+1}\right|}}{1 + \dfrac{\left|\hat{t}_j \cdot \mathbf{b}_{j+1}\right|}{A_j}\dfrac{|h|\left|\hat{t}_j \cdot \mathbf{b}_{j+1}\right|}{A_j\left|\mathbf{b}_{j+1}\right|}}\right]
\end{aligned}$$

$$
-\frac{|h|}{A_j}\tan^{-1}\left[\frac{\dfrac{\left|\hat{t}_j\cdot\mathbf{b}_{j+2}\right|}{A_j}-\dfrac{|h|\left|\hat{t}_j\cdot\mathbf{b}_{j+2}\right|}{A_j\left|\mathbf{b}_{j+2}\right|}}{1+\dfrac{\left|\hat{t}_j\cdot\mathbf{b}_{j+2}\right|}{A_j}\dfrac{|h|\left|\hat{t}_j\cdot\mathbf{b}_{j+2}\right|}{A_j\left|\mathbf{b}_{j+2}\right|}}\right]
$$

$$
=\ln\left[\frac{\left(\left|\mathbf{b}_{j+1}\right|+\left|\hat{t}_j\cdot\mathbf{b}_{j+1}\right|\right)\left(\left|\mathbf{b}_{j+2}\right|+\left|\hat{t}_j\cdot\mathbf{b}_{j+2}\right|\right)}{B_j^{\,2}}\right]-\frac{|h|}{A_j}\tan^{-1}\left[\frac{\left|\hat{t}_j\cdot\mathbf{b}_{j+1}\right|\left(\left|\mathbf{b}_{j+1}\right|-|h|\right)}{A_j^{\,2}\left|\mathbf{b}_{j+1}\right|+|h|\left|\hat{t}_j\cdot\mathbf{b}_{j+1}\right|^2}A_j\right]
$$

$$
-\frac{|h|}{A_j}\tan^{-1}\left[\frac{\left|\hat{t}_j\cdot\mathbf{b}_{j+2}\right|\left(\left|\mathbf{b}_{j+2}\right|-|h|\right)}{A_j^{\,2}\left|\mathbf{b}_{j+2}\right|+|h|\left|\hat{t}_j\cdot\mathbf{b}_{j+2}\right|^2}A_j\right]
$$

$$
=\ln\left[\frac{\left(\left|\mathbf{b}_{j+1}\right|+\left|\hat{t}_j\cdot\mathbf{b}_{j+1}\right|\right)\left(\left|\mathbf{b}_{j+2}\right|+\left|\hat{t}_j\cdot\mathbf{b}_{j+2}\right|\right)}{B_j^{\,2}}\right]-\frac{|h|}{A_j}\tan^{-1}\left[\frac{\left|\hat{t}_j\cdot\mathbf{b}_{j+1}\right|\left(\left|\mathbf{b}_{j+1}\right|-|h|\right)}{A_j^{\,2}\left|\mathbf{b}_{j+1}\right|+|h|\left(\left|\mathbf{b}_{j+1}\right|^2-A_j^{\,2}-h^2\right)}A_j\right]
$$

$$
-\frac{|h|}{A_j}\tan^{-1}\left[\frac{\left|\hat{t}_j\cdot\mathbf{b}_{j+2}\right|\left(\left|\mathbf{b}_{j+2}\right|-|h|\right)}{A_j^{\,2}\left|\mathbf{b}_{j+2}\right|+|h|\left(\left|\mathbf{b}_{j+2}\right|^2-A_j^{\,2}-h^2\right)}A_j\right]
$$

$$
=\ln\left[\frac{\left(\left|\mathbf{b}_{j+1}\right|+\left|\hat{t}_j\cdot\mathbf{b}_{j+1}\right|\right)\left(\left|\mathbf{b}_{j+2}\right|+\left|\hat{t}_j\cdot\mathbf{b}_{j+2}\right|\right)}{B_j^{\,2}}\right]-\frac{|h|}{A_j}\tan^{-1}\left[\frac{\left|\hat{t}_j\cdot\mathbf{b}_{j+1}\right|A_j}{A_j^{\,2}+|h|\left(\left|\mathbf{b}_{j+1}\right|+|h|\right)}\right]
$$

$$
-\frac{|h|}{A_j}\tan^{-1}\left[\frac{\left|\hat{t}_j\cdot\mathbf{b}_{j+2}\right|A_j}{A_j^{\,2}+|h|\left(\left|\mathbf{b}_{j+2}\right|+|h|\right)}\right],\quad \hat{t}_j\cdot\mathbf{b}_{j+1}\le 0\,,\quad \hat{t}_j\cdot\mathbf{b}_{j+2}\ge 0\,. \tag{2.69}
$$

We consider now the case $A_j\to 0$. From

$$
\tan^{-1}(x)=\sum_{k=0}^{\infty}\frac{(-1)^k\,x^{2k+1}}{2k+1},\quad |x|\le 1 \tag{2.70}
$$

we have that

$$
\tan^{-1}\left(10^{-8}\right)=10^{-8}\left[1-\frac{10^{-16}}{3}+\frac{10^{-24}}{5}-\ldots\right]. \tag{2.71}
$$

Thus, for arguments less than or equal to 10^{-8}, the second and subsequent terms do not contribute in a machine that uses double precision. We can then replace the arctangent by its argument. If

$$\frac{\left|\hat{t}_j \cdot \mathbf{b}_{j+1}\right| A_j}{A_j{}^2 + |h|\left(\left|\mathbf{b}_{j+1}\right| + |h|\right)} < 10^{-8} \tag{2.72}$$

we replace (2.69) by

$$K_{0,j} = \ln\left[\frac{\left(\left|\mathbf{b}_{j+1}\right| + \left|\hat{t}_j \cdot \mathbf{b}_{j+1}\right|\right)\left(\left|\mathbf{b}_{j+2}\right| + \left|\hat{t}_j \cdot \mathbf{b}_{j+2}\right|\right)}{B_j{}^2}\right] - \frac{\left|\hat{t}_j \cdot \mathbf{b}_{j+1}\right||h|}{A_j{}^2 + |h|\left(\left|\mathbf{b}_{j+1}\right| + |h|\right)}$$
$$-\frac{|h|}{A_j}\tan^{-1}\left[\frac{\left|\hat{t}_j \cdot \mathbf{b}_{j+2}\right| A_j}{A_j{}^2 + |h|\left(\left|\mathbf{b}_{j+2}\right| + |h|\right)}\right], \quad \hat{t}_j \cdot \mathbf{b}_{j+1} \le 0, \quad \hat{t}_j \cdot \mathbf{b}_{j+2} \ge 0 \tag{2.73}$$

while, if

$$\frac{\left|\hat{t}_j \cdot \mathbf{b}_{j+2}\right| A_j}{A_j{}^2 + |h|\left(\left|\mathbf{b}_{j+2}\right| + |h|\right)} < 10^{-8} \tag{2.74}$$

then we replace (2.69) by

$$K_{0,j} = \ln\left[\frac{\left(\left|\mathbf{b}_{j+1}\right| + \left|\hat{t}_j \cdot \mathbf{b}_{j+1}\right|\right)\left(\left|\mathbf{b}_{j+2}\right| + \left|\hat{t}_j \cdot \mathbf{b}_{j+2}\right|\right)}{B_j{}^2}\right] - \frac{|h|}{A_j}\tan^{-1}\left[\frac{\left|\hat{t}_j \cdot \mathbf{b}_{j+1}\right| A_j}{A_j{}^2 + |h|\left(\left|\mathbf{b}_{j+1}\right| + |h|\right)}\right]$$
$$-\frac{\left|\hat{t}_j \cdot \mathbf{b}_{j+2}\right||h|}{A_j{}^2 + |h|\left(\left|\mathbf{b}_{j+2}\right| + |h|\right)}, \quad \hat{t}_j \cdot \mathbf{b}_{j+1} \le 0, \quad \hat{t}_j \cdot \mathbf{b}_{j+2} \ge 0. \tag{2.75}$$

If both (2.72) and (2.74) obtain, then we replace (2.69) by

$$K_{0,j} = \ln\left[\frac{\left(\left|\mathbf{b}_{j+1}\right| + \left|\hat{t}_j \cdot \mathbf{b}_{j+1}\right|\right)\left(\left|\mathbf{b}_{j+2}\right| + \left|\hat{t}_j \cdot \mathbf{b}_{j+2}\right|\right)}{B_j{}^2}\right] - \frac{\left|\hat{t}_j \cdot \mathbf{b}_{j+1}\right||h|}{A_j{}^2 + |h|\left(\left|\mathbf{b}_{j+1}\right| + |h|\right)}$$
$$-\frac{\left|\hat{t}_j \cdot \mathbf{b}_{j+2}\right||h|}{A_j{}^2 + |h|\left(\left|\mathbf{b}_{j+2}\right| + |h|\right)}, \quad \hat{t}_j \cdot \mathbf{b}_{j+1} \le 0, \quad \hat{t}_j \cdot \mathbf{b}_{j+2} \ge 0. \tag{2.76}$$

If $h = 0$, then $A_j \neq 0$ and

$$K_{0,j} = \ln\left[\frac{\left(\left|\mathbf{b}_{j+1}\right| + \left|\hat{t}_j \cdot \mathbf{b}_{j+1}\right|\right)\left(\left|\mathbf{b}_{j+2}\right| + \left|\hat{t}_j \cdot \mathbf{b}_{j+2}\right|\right)}{B_j^{\,2}}\right], \quad h = 0\,, \quad \hat{t}_j \cdot \mathbf{b}_{j+1} \le 0\,, \quad \hat{t}_j \cdot \mathbf{b}_{j+2} \ge 0\,. \tag{2.77}$$

We note that (2.74) can be used in place of (2.61), and (2.72) in place of (2.59). In connection with this, we show that these inequalities hold for both corners of an edge. We first recall that

$$a > b\,, \quad c > 0 \quad \Rightarrow \quad \frac{a}{b} > \frac{a+c}{b+c}\,. \tag{2.78}$$

This follows from

$$a > b \quad \Rightarrow \quad ac > bc \quad \Rightarrow \quad ac + ab > bc + ab \quad \Rightarrow \quad a\left(b+c\right) > b\left(a+c\right). \tag{2.79}$$

For the case in (2.57), consider

$$\left(\frac{\left|\hat{t}_j \cdot \mathbf{b}_{j+2}\right|}{\left|\hat{t}_j \cdot \mathbf{b}_{j+1}\right|}\right)^2 = \frac{\left|\mathbf{b}_{j+2}\right|^2 - \left(\left|h\right|^2 + A_j^{\,2}\right)}{\left|\mathbf{b}_{j+1}\right|^2 - \left(\left|h\right|^2 + A_j^{\,2}\right)} > \frac{\left|\mathbf{b}_{j+2}\right|^2}{\left|\mathbf{b}_{j+1}\right|^2} \tag{2.80}$$

from which

$$\frac{\left|\hat{t}_j \cdot \mathbf{b}_{j+2}\right|}{\left|\hat{t}_j \cdot \mathbf{b}_{j+1}\right|} > \frac{\left|\mathbf{b}_{j+2}\right|}{\left|\mathbf{b}_{j+1}\right|} > \frac{\left|h\right| + \left|\mathbf{b}_{j+2}\right|}{\left|h\right| + \left|\mathbf{b}_{j+1}\right|} \quad \Rightarrow \quad \frac{\left|\hat{t}_j \cdot \mathbf{b}_{j+2}\right|}{\left|\hat{t}_j \cdot \mathbf{b}_{j+1}\right|} > \frac{\left|h\right| + \left|\mathbf{b}_{j+2}\right|}{\left|h\right| + \left|\mathbf{b}_{j+1}\right|} \tag{2.81}$$

or

$$\frac{\left|\hat{t}_j \cdot \mathbf{b}_{j+1}\right|}{\left|h\right| + \left|\mathbf{b}_{j+1}\right|} < \frac{\left|\hat{t}_j \cdot \mathbf{b}_{j+2}\right|}{\left|h\right| + \left|\mathbf{b}_{j+2}\right|}\,. \tag{2.82}$$

If we examine (2.60), we see that, in light of (2.82), (2.61) holds for both vertices *j*+1 and *j*+2. The same can be said about (2.69).

In Appendix C we present an alternate way of computing $K_{0,j}$. The rest of the $K_{n,j}$ can be computed from the iteration formulas (2.4) and (2.5). In Appendix C, we show that the iteration formula does not converge for all positions of the observation point. We discuss this issue in the next section.

3. COMMON REGION OF VALIDITY OF INTEGRAL EVALUATION

In Appendix B, we show that the iteration formula (2.5) converges provided (B.14), namely

$$\begin{aligned} &|h| \le \frac{1-\rho'^2}{2} \quad \text{, if } 0 \le \rho' < 1 \text{ and } |h| > 0 \\ &0 \le \rho' < 1 \qquad \text{, if } |h| = 0 \end{aligned} . \tag{3.1}$$

holds; similarly, (2.20), (2.26) and (2. 32) converge provided (B.19) is satisfied:

$$0 \le B_j < 1 . \tag{3.2}$$

We also noted that these two statements do not imply one another. In this section, we prove that both are satisfied within a sphere centered at the centroid of the triangle and radius equal to 0.5. The proof is as follows.

We note that

$$r' = \sqrt{\rho'^2 + h^2} < 0.5 \quad \Rightarrow \quad \rho' < 0.5 , \quad |h| < 0.5 \tag{3.3}$$

from which we get that

$$|h| < \sqrt{0.25 - \rho'^2} = \frac{1}{2}\sqrt{1 - 4\rho'^2} \le \frac{1}{2}\sqrt{1 - 4\rho'^2 + \left(2\rho'^2\right)^2} = \frac{1}{2}\left(1 - 2\rho'^2\right) \le \frac{1}{2}\left(1 - \rho'^2\right) \tag{3.4}$$

so that (3.1) is satisfied.

We also note that

$$\left|\mathbf{b}_{j+1}\right| = \sqrt{B_j^{\,2} + \left(\hat{t}_j \cdot \mathbf{b}_{j+1}\right)^2} \quad \Rightarrow \quad B_j \le \left|\mathbf{b}_{j+1}\right| , \quad j = 1,2,3 . \tag{3.5}$$

Also, by construction, B_j is non-negative. But

$$\left|\mathbf{b}_{j+1}\right| = \left|\mathbf{r}' - \mathbf{r}_{j+1}\right| < 1 \tag{3.6}$$

since the observation point $\mathbf{r}'$ and any of the three vertices $\mathbf{r}_{j+1}$ of the triangle are inside the sphere. From (3.5) and (3.6) we conclude that (3.2) is satisfied.

Thus, our method is guaranteed to work when the observation point is less than half a wavelength away from the triangle's centroid. A question we may ask in connection with this

conclusion is: how does it compare in speed with the original Maclaurin expansion where we expand exp(*ikR*)? In table 3.1, we present the same information as in table 1.1 except that this time we use the unaltered Maclaurin series. The observation point on the sphere, half a wavelength away from the centroid of the triangle. If we let it lie on the triangle's plane, then, in the worst of situations, the point on the triangle farthest from it is the vertex with the property that (a) it corresponds to the smallest angle of the triangle and, (b), the straight-line segment connecting it to the observation point passes through the centroid of the triangle. With this in mind, a bound on *R* is

$$R \le 0.5 + \frac{2}{3} l_{\max} = \frac{1}{2} + \frac{2}{30} = \frac{17}{30} \tag{3.7}$$

or

$$2\pi R \le \pi \frac{17}{15}. \tag{3.8}$$

We use this as an argument in (1.14) and (1.20) to fill table 3.1 We see that, for the observation point on the half-wavelength sphere, we require at least twice as many terms as in table 1.1. Certainly, as the radius of the sphere becomes smaller, so is the number of terms. From (3.7) we see that *R* is minimized for the sphere of zero radius; thus, the unaltered method requires as few terms as the altered one only when the observation point is the triangle's centroid.

Table 3.1: Number of terms required to guarantee a given number of significant digits (SD) for the unaltered integral. Largest side of triangle less than or equal to a tenth of a wavelength and observation point is half a wavelength away from centroid.

Number of SD	Sine	Cosine
4	8	8
5	9	8
6	10	9
7	10	9
8	11	10
9	11	11
10	12	11
11	13	12
12	13	12
13	14	13
14	14	13
15	15	14

4. VALIDATION

We compare here results of our method with those of Khayat and Wilton [6]. They compute the second (Scalar) integral in (1.7), i.e., the integral of the free-space Green's function

$$I(\mathbf{r}') = \int_T \frac{e^{-ikR}}{R} dS \, . \tag{4.1}$$

The integration triangle is shown in figure 4.1. It is an isosceles right triangle whose equal legs have length 1 m. The wavelength is equal to 10 m. The result of Rossi and Cullen is from [7] and appears in table I of [6], where it is used as a reference (benchmark). The first Khayat and Wilton row refers to the 36-point result in table I of [6], while the last row comes from table II in [6], with a reported accuracy of 14 significant digits (SD).

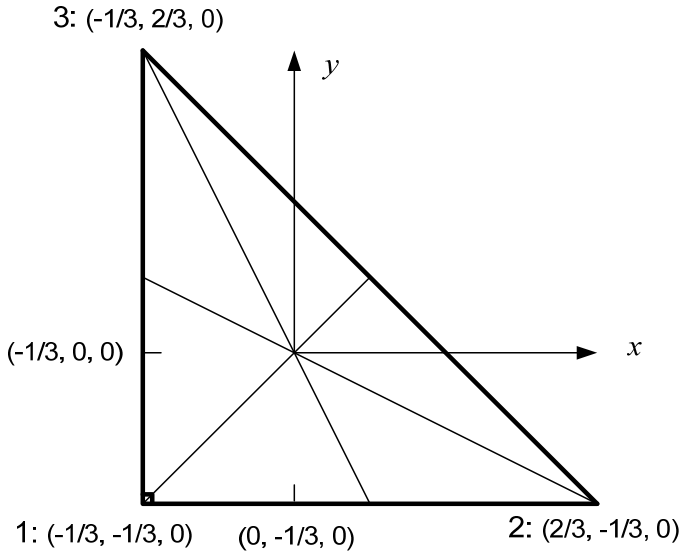

Figure 4.1: The Khayat-Wilton triangle

The results of the comparison are shown in table 4.1. The four observation points lie on the right angle's bisector. Their coordinates are given with respect to an origin located at the vertex of the right angle, as in [6]. According to (1.14) and (1.20), the number of terms required for seven SD is 8 (total), while, for 15 SD, it is 14n (total).

In table 4.2, we show the difference between our result for 15 SD and that of Khayat and Wilton for 14 SD. We have rounded our results to 14 SD. There is almost perfect agreement.

In table 4.3, we display the remaining points computed in [6] to 14 SD. In this case, we move away from the observation point of Case 1 along the normal to the triangle and compute the integral at three observation points. The integrand now is not singular as in the first four cases

but the proximity of the observation point to the integration triangle makes it behave as if it were. In table 4.4, we plot the difference between our results and those of Khayat and Wilton. We get excellent agreement in general except for the real part of Case 5 where we note a significant difference. We placed a fine grid around this point and found that the Khayat and Wilton result falls off the curve. In an exchange of correspondence, the authors of [2] verified the correctness of our result using both the original approach and a modified one [8].

Table 4.1: Comparison of present approach to results in references 6 and 7. Observation point is inside the triangle and its coordinates are given with respect to an origin centered at the right-angle vertex.

Observation point location (x, y, z) in m	Case 1 (0.1, 0.1, 0.0)	Case 2 (0.2, 0.2, 0.0)	Case 3 (0.3, 0.3, 0.0)	Case 4 (0.4, 0.4, 0.0)
Our result (7 SD)	1.89857266168680 -i 0.309643085617962	2.246285006785350 -i 0.311143518184329	2.381002978088960 -i 0.311826316300869	2.283869854898920 -i 0.311688243312515
Our result (15 SD)	1.89857266176846 -i 0.309643085636859	2.246285006965140 -i 0.311143518212247	2.381002978727480 -i 0.311826316345215	2.283869855108430 -i 0.311688243332126
Khayat and Wilton	1.898579 –i 0.3096492	2.246288 –i 0.3111477	2.381009 –i 0.3118314	2.283890 –i 0.3116960
Rossi and Cullen Mathematica (6 SD)	1.89857 –i 0.309643	2.24628 –i 0.311144	2.38099 –i 0.311826	2.28386 –i 0.311688
Khayat and Wilton (14 SD)	1.89857266176845 –i 0.30964308563686	2.24628500696514 –i 0.31114351821225	2.38100297872747 –i 0.31182631634521	2.28386985510842 –i 0.31168824333213

Table 4.2: Difference between our results (15 SD rounded to 14) and those of Khayat and Wilton (14 SD): real and imaginary parts.

The points below are for K&W's coordinate system (centered at the right angle). Our system is centered at the centroid.	Re{K&W 14 SD} - Re{our method, DP, 14 Taylor Terms}	Im{K&W 14 SD} - Im{our method, DP, 14 Taylor Terms}
Case 1: (.1, .1, 0)	0.0000000000001	0.00000000000000
Case 2: (.2, .2, 0)	0.0000000000001	0.00000000000000
Case 3: (.3, .3, 0)	0.0000000000000	0.00000000000001
Case 4: (.4, .4, 0)	0.0000000000000	0.00000000000000

Table 4.3: Observation point near integration triangle.
Observation point coordinates (0.1, 0.1, *z*).

Case	5, $z = 0.0001$	6, $z = 0.01$	7, $z = 0.1$
Re{$I_{(14)}$}	1.897944525246840	1.837558164829700	1.429705163246540
Re{K&W}	1.89795445129807	1.83755816482970	1.42970516324653
Im{$I_{(14)}$}	-0.309643085431937	-0.309641036420311	-0.309438204123196
Im{K&W}	-0.30964308543194	-0.30964103642031	-0.30943820412320

Table 4.4: Differences for Cases 5 – 7 between our results and those of Khayat and Wilton.

Case	Re{K&W, 14 SD} - Re{our method, 15 SD, 14 Taylor Terms}	Im{K&W, 14 SD} - Re{our method, 15 SD, 14 Taylor Terms}
Case 5: (.1, .1, 0.0001)	0.00000992605123	0.00000000000000
Case 6: (.1, .1, 0.01)	0.00000000000000	0.00000000000000
Case 7: (.1, .1, 0.1)	-0.00000000000001	0.00000000000000

This concludes our validation tests. We will discuss validation further in the second part of this report.

5. CONCLUSIONS

We have introduced a new method for computing the inner integral of the impedance elements in the Rao-Wilton-Glisson [1] formulation of the method of moments in electromagnetics (Sections 1 and 2). The distinguishing feature of this method is that it can compute the integral to a prescribed precision. We know of no other method that can do this. The method is valid for all observation points that lie within a sphere with center the triangle's centroid and radius of one half of a wavelength (Section 3). This restriction is because the two iteration formulas we use do not converge everywhere in space but have a common domain of convergence in the interior of this sphere. There are also points outside this sphere where we have convergence; they are of no consequence, however, since we can find faster ways of obtaining the same accuracy outside this sphere. This is the subject of the second part of this report.

APPENDIX A
CONVERSION OF $I_{(n)}$ TO A LINE INTEGRAL

Consider the integral

$$\mathbf{J}_{(n)}^{(l)}(\mathbf{r}') = -(\mathbf{r}_l - \boldsymbol{\rho}')\, I_{(n)}(\mathbf{r}')$$

$$= (n+1)\int_T \left[(x'-x_l)\,\hat{x} + (y'-y_l)\,\hat{y}\right] \frac{\left[\sqrt{(x-x')^2 + (y-y')^2 + h^2} - r'\right]^n}{\sqrt{(x-x')^2 + (y-y')^2 + h^2}}\, dxdy \tag{A.1}$$

and use the transformation

$$\xi = x - x', \quad \eta = y - y' \tag{A.2}$$

to write

$$\mathbf{J}_{(n)}^{(l)} = (n+1)\int_T (c_l\hat{x} + b_l\hat{y}) \frac{\left(\sqrt{\xi^2+\eta^2+h^2} - r'\right)^n}{\sqrt{\xi^2+\eta^2+h^2}}\, d\xi d\eta \tag{A.3}$$

where

$$c_l = x' - x_l, \quad b_l = y' - y_l. \tag{A.4}$$

We define

$$\mathbf{v}_{(n)}^{(l)}(\xi,\eta) = (n+1)(c_l\hat{x} + b_l\hat{y}) \frac{\left(\sqrt{\xi^2+\eta^2+h^2} - r'\right)^n}{\sqrt{\xi^2+\eta^2+h^2}} \tag{A.5}$$

and rewrite it as a complex-valued function

$$v_{(n)}^{(l)}(\xi,\eta) = (n+1)(c_l + ib_l) \frac{\left(\sqrt{\xi^2+\eta^2+h^2} - r'\right)^n}{\sqrt{\xi^2+\eta^2+h^2}}. \tag{A.6}$$

We make next the transformation

$$\zeta = \xi + i\eta\,, \quad \zeta^* = \xi - i\eta \quad \Rightarrow \quad \xi = \frac{\zeta + \zeta^*}{2}\,, \quad \eta = \frac{\zeta - \zeta^*}{2i} \tag{A.7}$$

to get

$$V_{(n)}^{(l)}(\zeta,\zeta^*) = (n+1)(c_l + ib_l)\frac{\left(\sqrt{\zeta\zeta^* + h^2} - r'\right)^n}{\sqrt{\zeta\zeta^* + h^2}}. \tag{A.8}$$

We need the following integral

$$I_{(n)}^{(l)}(\zeta,\zeta^*) = \frac{1}{2}\int^{\zeta^*} V_{(n)}^{(l)}(\zeta,\tau)\,d\tau = (n+1)\frac{c_l + ib_l}{2}\int^{\zeta^*} \frac{\left(\sqrt{\zeta\tau + h^2} - r'\right)^n}{\sqrt{\zeta\tau + h^2}}\,d\tau$$

$$= \frac{(c_l + ib_l)\left(\sqrt{\zeta\zeta^* + h^2} - r'\right)^{n+1}}{\zeta}. \tag{A.9}$$

We proceed to define functions *f* and *g* as

$$f_{(n)}^{(l)}(\xi,\eta) = \mathrm{Re}\left\{I_{(n)}^{(l)}(\zeta,\zeta^*)\right\} = \mathrm{Re}\left\{\frac{(\xi - i\eta)(c_l + ib_l)\left(\sqrt{\xi^2 + \eta^2 + h^2} - r'\right)^{n+1}}{(n+1)\left(\xi^2 + \eta^2\right)}\right\}$$

$$= \frac{c_l\xi + b_l\eta}{\xi^2 + \eta^2}\left(\sqrt{\xi^2 + \eta^2 + h^2} - r'\right)^{n+1} = \frac{c_l\xi + b_l\eta}{\rho^2}\left(\sqrt{\rho^2 + h^2} - r'\right)^{n+1} \tag{A.10}$$

$$g_{(n)}^{(l)}(\xi,\eta) = \mathrm{Im}\left\{I_{(n)}^{(l)}(\zeta,\zeta^*)\right\} = \mathrm{Im}\left\{\frac{(\xi - i\eta)(c_l + ib_l)\left(\sqrt{\xi^2 + \eta^2 + h^2} - r'\right)^{n+1}}{(n+1)\left(\xi^2 + \eta^2\right)}\right\}$$

$$= \frac{b_l\xi - c_l\eta}{\xi^2 + \eta^2}\left(\sqrt{\xi^2 + \eta^2 + h^2} - r'\right)^{n+1} = \frac{b_l\xi - c_l\eta}{\rho^2}\left(\sqrt{\rho^2 + h^2} - r'\right)^{n+1} \tag{A.11}$$

where

$$\rho = \sqrt{\xi^2 + \eta^2}\,. \tag{A.12}$$

For (A.5) we can now write

$$\mathbf{v}_{(n)}^{(l)}(\xi,\eta)=\nabla f_{(n)}^{(l)}(\xi,\eta)+\hat{z}\times\nabla g_{(n)}^{(l)}(\xi,\eta)\,. \tag{A.13}$$

We re-adjust (A.11) and (A.12) so as to remove the singularity at $\rho=0$. To this end, we compute the asymptotic form of these expressions as $\rho\to 0$. We let

$$\xi=\rho\cos\varphi\,,\quad \eta=\rho\sin\varphi \tag{A.14}$$

and substitute in (A.10) and (A.11) to get

$$f_{(n)}^{(l)}(\xi,\eta)=\frac{c_l\cos\varphi+b_l\sin\varphi}{\rho}\left(\sqrt{\rho^2+h^2}-r'\right)^{n+1} \tag{A.15}$$

$$g_{(n)}^{(l)}(\xi,\eta)=\frac{b_l\cos\varphi-c_l\sin\varphi}{\rho}\left(\sqrt{\rho^2+h^2}-r'\right)^{n+1}. \tag{A.16}$$

Through a direct calculation, we find that

$$f_{(n)}^{(l)}(\xi,\eta)=\frac{c_l\cos\varphi+b_l\sin\varphi}{\rho}\left(|h|-r'\right)^{n+1}+O(1)\,,\ \rho\to 0 \tag{A.17}$$

$$g_{(n)}^{(l)}(\xi,\eta)=\frac{b_l\cos\varphi-c_l\sin\varphi}{\rho}\left(|h|-r'\right)^{n+1}+O(1)\,,\ \rho\to 0\,. \tag{A.18}$$

We define

$$f_{0(n)}^{(l)}(\xi,\eta)=\frac{c_l\cos\varphi+b_l\sin\varphi}{\rho}\left(|h|-r'\right)^{n+1},\quad g_{0(n)}^{(l)}(\xi,\eta)=\frac{b_l\cos\varphi-c_l\sin\varphi}{\rho}\left(|h|-r'\right)^{n+1}. \tag{A.19}$$

These two expressions satisfy the Cauchy-Riemann conditions. Thus, we can subtract them from the corresponding ones in (A.10) and (A.11) and, also, use (A.1) to generate functions that do not have a singularity at $\rho=0$

$$\tilde{f}_{(n)}^{(l)}(\xi,\eta)=\frac{c_l\xi+b_l\eta}{\rho^2}\left[\left(\sqrt{\rho^2+h^2}-r'\right)^{n+1}-\left(|h|-r'\right)^{n+1}\right] \tag{A.20}$$

$$\tilde{g}_{(n)}^{(l)}(\xi,\eta)=\frac{b_l\xi-c_l\eta}{\rho^2}\left[\left(\sqrt{\rho^2+h^2}-r'\right)^{n+1}-\left(|h|-r'\right)^{n+1}\right]. \tag{A.21}$$

From [4], we have that, in general, if **v** is of the form (A.13), then

$$\int_D \mathbf{v}(x,y)dxdy = \int_{\partial D} f(x,y)\hat{\nu}ds + \int_{\partial D} g(x,y)\hat{t}ds\,. \tag{A.22}$$

where $\hat{\nu}$ is the normal to a triangle's side while $\hat{t}$ is the tangent to it and is positively oriented with respect to the normal to the triangle. Both lie on the triangle's plane. From (A.3), (B20), and (A.21), we can then write

$$\begin{aligned}\mathbf{J}_{(n)}^{(l)} &= \int_{\partial T} \frac{c_l\xi + b_l\eta}{\rho^2}\left[\left(\sqrt{\rho^2+h^2}-r'\right)^{n+1} - \left(|h|-r'\right)^{n+1}\right]\hat{\nu}ds \\ &+ \int_{\partial T} \frac{b_l\xi - c_l\eta}{\rho^2}\left[\left(\sqrt{\rho^2+h^2}-r'\right)^{n+1} - \left(|h|-r'\right)^{n+1}\right]\hat{t}ds\,.\end{aligned} \tag{A.22}$$

We introduce rectangular coordinates

$$\left(\hat{\nu}_j, \hat{t}_j, \hat{n}\right), \quad \hat{n} = \hat{z}\,, \quad \hat{\nu}_j = \hat{t}_j \times \hat{n}\,, \quad j = 1,2,3 \tag{A.23}$$

on each side of the triangle, with origin the endpoint that we encounter first in going around the triangle in the positive sense with respect to the normal $\hat{n}$. Specifically, for side 1, it is the point $\mathbf{r}_2$; for side 2 the point $\mathbf{r}_3$; and for side 3 the point $\mathbf{r}_1$. Note that these coordinates bear the index of the side they belong to. With this notation, (A.22) becomes

$$\begin{aligned}\mathbf{J}_{(n)}^{(l)} &= \sum_{j=1}^{3}\hat{\nu}_j \int_{s_j}\left\{\frac{c_l\xi + b_l\eta}{\rho^2}\left[\left(\sqrt{\rho^2+h^2}-r'\right)^{n+1} - \left(|h|-r'\right)^{n+1}\right]\right\}ds \\ &+ \sum_{j=1}^{3}\hat{t}_j \int_{s_j}\frac{b_l\xi - c_l\eta}{\rho^2}\left[\left(\sqrt{\rho^2+h^2}-r'\right)^{n+1} - \left(|h|-r'\right)^{n+1}\right]ds\,.\end{aligned} \tag{A.24}$$

For the position vector to the *j*-th side, we write

$$\mathbf{r} = \mathbf{r}_{j+1} + s\hat{t}_j\,, \quad j = 1,2,3 \tag{A.25}$$

with the indices running cyclically. We also write

$$\mathbf{r}' = x'\hat{x} + y'\hat{y} + h\hat{z} = \boldsymbol{\rho}' + h\hat{z}\,, \quad \mathbf{r}_l = x_l\hat{x} + y_l\hat{y}\,. \tag{A.26}$$

From these and (A.24), we have that

$$\xi c_l + \eta b_l = \left(\mathbf{r} - \boldsymbol{\rho}'\right)\cdot\left(\boldsymbol{\rho}' - \mathbf{r}_l\right) \tag{A.27}$$

and

$$\xi b_l - \eta c_l = (x-x')(y'-y_l) - (y-y')(x'-x_l) = \hat{z}\cdot\left[(\mathbf{r}-\boldsymbol{\rho}')\times(\boldsymbol{\rho}'-\mathbf{r}_l)\right] = \left[(\boldsymbol{\rho}'-\mathbf{r}_l)\times\hat{z}\right]\cdot(\mathbf{r}-\boldsymbol{\rho}') \tag{A.28}$$

We substitute these in (A.24)

$$\mathbf{J}_{(n)}^{(l)} = \sum_{j=1}^{3}\hat{\nu}_j \int_{s_j}\left\{\frac{(\mathbf{r}-\boldsymbol{\rho}')\cdot(\boldsymbol{\rho}'-\mathbf{r}_l)}{\rho^2}\left[\left(\sqrt{\rho^2+h^2}-r'\right)^{n+1} - \left(|h|-r'\right)^{n+1}\right]\right\} ds$$
$$+\sum_{j=1}^{3}\hat{t}_j \int_{s_j}\frac{\left[(\boldsymbol{\rho}'-\mathbf{r}_l)\times\hat{z}\right]\cdot(\mathbf{r}-\boldsymbol{\rho}')}{\rho^2}\left[\left(\sqrt{\rho^2+h^2}-r'\right)^{n+1} - \left(|h|-r'\right)^{n+1}\right] ds\,. \tag{A.29}$$

We can further write this as

$$\mathbf{J}_{(n)}^{(l)} = \sum_{j=1}^{3}\int_{s_j}\frac{\hat{\nu}_j\left[(\mathbf{r}-\boldsymbol{\rho}')\cdot(\boldsymbol{\rho}'-\mathbf{r}_l)\right] + \hat{t}_j\left\{\left[(\boldsymbol{\rho}'-\mathbf{r}_l)\times\hat{z}\right]\cdot(\mathbf{r}-\boldsymbol{\rho}')\right\}}{\rho^2}\left[\left(\sqrt{\rho^2+h^2}-r'\right)^{n+1} - \left(|h|-r'\right)^{n+1}\right] ds \tag{A.30}$$

We define

$$\mathbf{a}_{j+1} = a_{j+1}\hat{a}_{j+1} = \mathbf{r}_{j+1} - \boldsymbol{\rho}', \quad \rho = |\mathbf{r}-\boldsymbol{\rho}'| = \left|\mathbf{a}_{j+1} + s\hat{t}_j\right| \tag{A.31}$$

and write

$$\hat{\nu}_j\left[(\mathbf{r}-\boldsymbol{\rho}')\cdot(\boldsymbol{\rho}'-\mathbf{r}_l)\right] + \hat{t}_j\left\{\left[(\boldsymbol{\rho}'-\mathbf{r}_l)\times\hat{z}\right]\cdot(\mathbf{r}-\boldsymbol{\rho}')\right\}$$
$$= -\hat{\nu}_j\left[(\mathbf{r}-\boldsymbol{\rho}')\cdot\mathbf{a}_l\right] - \hat{t}_j\left\{\left[\mathbf{a}_l\times\hat{z}\right]\cdot(\mathbf{r}-\boldsymbol{\rho}')\right\} = -a_l\left\{\hat{\nu}_j\left[(\mathbf{r}-\boldsymbol{\rho}')\cdot\hat{a}_l\right] + \hat{t}_j\left\{\left[\hat{a}_l\times\hat{z}\right]\cdot(\mathbf{r}-\boldsymbol{\rho}')\right\}\right\} \tag{A.32}$$

We resolve the vectors in (A.32) along the directions $(\hat{a}_l, \hat{z}\times\hat{a}_l, \hat{z})$

$$\hat{\nu}_j\left[(\mathbf{r}-\boldsymbol{\rho}')\cdot\hat{a}_l\right] + \hat{t}_j\left[(\hat{a}_l\times\hat{z})\cdot(\mathbf{r}-\boldsymbol{\rho}')\right]$$
$$= \left\{\hat{a}_l\left(\hat{a}_l\cdot\hat{\nu}_j\right) + \left(\hat{z}\times\hat{a}_l\right)\left[\left(\hat{z}\times\hat{a}_l\right)\cdot\hat{\nu}_j\right]\right\}\left[(\mathbf{r}-\boldsymbol{\rho}')\cdot\hat{a}_l\right]$$
$$+\left\{\hat{a}_l\left(\hat{a}_l\cdot\hat{t}_j\right) + \left(\hat{z}\times\hat{a}_l\right)\left[\left(\hat{z}\times\hat{a}_l\right)\cdot\hat{t}_j\right]\right\}\left[(\hat{a}_l\times\hat{z})\cdot(\mathbf{r}-\boldsymbol{\rho}')\right]$$
$$= \hat{a}_l\left\{\left(\hat{a}_l\cdot\hat{\nu}_j\right)\left[(\mathbf{r}-\boldsymbol{\rho}')\cdot\hat{a}_l\right] + \left(\hat{a}_l\cdot\hat{t}_j\right)\left[(\hat{a}_l\times\hat{z})\cdot(\mathbf{r}-\boldsymbol{\rho}')\right]\right\}$$

$$
\begin{aligned}
&+(\hat{z}\times\hat{a}_l)\left\{\left[(\hat{z}\times\hat{a}_l)\cdot\hat{\nu}_j\right]\left[(\mathbf{r}-\boldsymbol{\rho}')\cdot\hat{a}_l\right]+\left[(\hat{z}\times\hat{a}_l)\cdot\hat{t}_j\right]\left[(\hat{a}_l\times\hat{z})\cdot(\mathbf{r}-\boldsymbol{\rho}')\right]\right\}\\
&=\hat{a}_l\left\{(\hat{a}_l\cdot\hat{\nu}_j)\left[(\mathbf{r}-\boldsymbol{\rho}')\cdot\hat{a}_l\right]+\left[\hat{a}_l\cdot(\hat{z}\times\hat{\nu}_j)\right]\left[(\hat{a}_l\times\hat{z})\cdot(\mathbf{r}-\boldsymbol{\rho}')\right]\right\}\\
&\quad+(\hat{z}\times\hat{a}_l)\left\{\left[(\hat{z}\times\hat{a}_l)\cdot(\hat{t}_j\times\hat{z})\right]\left[(\mathbf{r}-\boldsymbol{\rho}')\cdot\hat{a}_l\right]+\left[(\hat{z}\times\hat{a}_l)\cdot\hat{t}_j\right]\left[(\hat{a}_l\times\hat{z})\cdot(\mathbf{r}-\boldsymbol{\rho}')\right]\right\}\\
&=\hat{a}_l\left\{(\hat{a}_l\cdot\hat{\nu}_j)\hat{a}_l+\left[\hat{\nu}_j\cdot(\hat{z}\times\hat{a}_l)\right](\hat{z}\times\hat{a}_l)\right\}\cdot(\mathbf{r}-\boldsymbol{\rho}')\\
&\quad-(\hat{z}\times\hat{a}_l)\left\{(\hat{t}_j\cdot\hat{a}_l)\hat{a}_l+\left[(\hat{z}\times\hat{a}_l)\cdot\hat{t}_j\right](\hat{z}\times\hat{a}_l)\right\}\cdot(\mathbf{r}-\boldsymbol{\rho}')\\
&=\hat{a}_l\left[\hat{\nu}_j\cdot(\mathbf{r}-\boldsymbol{\rho}')\right]-(\hat{z}\times\hat{a}_l)\left[\hat{t}_j\cdot(\mathbf{r}-\boldsymbol{\rho}')\right].
\end{aligned}
\tag{A.33}
$$

Substitution in (A.32) gives

$$
\hat{\nu}_j\left[(\mathbf{r}-\boldsymbol{\rho}')\cdot(\boldsymbol{\rho}'-\mathbf{r}_l)\right]+\hat{t}_j\left\{\left[(\boldsymbol{\rho}'-\mathbf{r}_l)\times\hat{z}\right]\cdot(\mathbf{r}-\boldsymbol{\rho}')\right\}=-\mathbf{a}_l\left[\hat{\nu}_j\cdot(\mathbf{r}-\boldsymbol{\rho}')\right]+(\hat{z}\times\mathbf{a}_l)\left[\hat{t}_j\cdot(\mathbf{r}-\boldsymbol{\rho}')\right]
\tag{A.34}
$$

and this in (A.30)

$$
\begin{aligned}
\mathbf{J}_{(n)}^{(l)}&=-\mathbf{a}_l\sum_{j=1}^{3}\int_{s_j}\frac{\hat{\nu}_j\cdot(\mathbf{r}-\boldsymbol{\rho}')}{\rho^2}\left[\left(\sqrt{\rho^2+h^2}-r'\right)^{n+1}-\left(|h|-r'\right)^{n+1}\right]ds\\
&+(\hat{z}\times\mathbf{a}_l)\sum_{j=1}^{3}\int_{s_j}\frac{\hat{t}_j\cdot(\mathbf{r}-\boldsymbol{\rho}')}{\rho^2}\left[\left(\sqrt{\rho^2+h^2}-r'\right)^{n+1}-\left(|h|-r'\right)^{n+1}\right]ds\,.
\end{aligned}
\tag{A.35}
$$

Since the original expression in (A.6) does not have a component along $\hat{z}\times\mathbf{a}_l$, this term must be zero in (A.35). We can show this by using Stokes' theorem

$$
\sum_{j=1}^{3}\int_{s_j}\frac{\hat{t}_j\cdot(\mathbf{r}-\boldsymbol{\rho}')}{\rho^2}\left[\left(\sqrt{\rho^2+h^2}-r'\right)^{n+1}-\left(|h|-r'\right)^{n+1}\right]ds=\int_T\hat{z}\cdot\nabla\times\left[(\mathbf{r}-\boldsymbol{\rho}')F(\rho)\right]ds
\tag{A.36}
$$

with

$$
F(\rho)=\frac{\left(\sqrt{\rho^2+h^2}-r'\right)^{n+1}-\left(|h|-r'\right)^{n+1}}{\rho^2}\,.
\tag{A.37}
$$

But

$$
\nabla\times\left[(\mathbf{r}-\boldsymbol{\rho}')F(\rho)\right]=\nabla F(\rho)\times(\mathbf{r}-\boldsymbol{\rho}')=\frac{dF(\rho)}{d\rho}\nabla\rho\times(\mathbf{r}-\boldsymbol{\rho}')
\tag{A.38}
$$

and

$$\nabla\rho = \nabla\left|\mathbf{r}-\boldsymbol{\rho}'\right| = \frac{\mathbf{r}-\boldsymbol{\rho}'}{\rho}. \tag{A.39}$$

Thus, (A.38) is zero and, hence, the integral over the triangle in (A.36) is zero. We can then replace (A.35) by

$$\mathbf{J}_{(n)}^{(l)} = -\mathbf{a}_l \sum_{j=1}^{3} \int_{s_j} \frac{\hat{\nu}_j \cdot \left(\mathbf{r}-\boldsymbol{\rho}'\right)}{\rho^2} \left[\left(\sqrt{\rho^2+h^2} - r'\right)^{n+1} - \left(|h| - r'\right)^{n+1} \right] ds\,. \tag{A.40}$$

But

$$\hat{\nu}_j \cdot \left(\mathbf{r}-\boldsymbol{\rho}'\right) = \hat{\nu}_j \cdot \left(\mathbf{r}_{j+1}-\boldsymbol{\rho}'\right), \quad j = 1,2,3 \tag{A.41}$$

and (A.40) takes the simpler form

$$\mathbf{J}_{(n)}^{(l)} = -\mathbf{a}_l \sum_{j=1}^{3} \hat{\nu}_j \cdot \left(\mathbf{r}_{j+1}-\boldsymbol{\rho}'\right) \int_{s_j} \frac{\left(\sqrt{\rho^2+h^2} - r'\right)^{n+1} - \left(|h| - r'\right)^{n+1}}{\rho^2} ds\,. \tag{A.42}$$

APPENDIX B
REGIONS OF CONVERGENCE OF ITERATION FORMULAS

We begin with the iteration formula (2.5) which we write in the form

$$Y_{n+1,j} = AY_{n,j} + X_{n,j}\ , \quad n = 0,1,2,... \tag{B.1}$$

where

$$Y_{n,j} = \begin{bmatrix} K_{n,j} \\ K_{n+1,j} \end{bmatrix}, \quad X_{n,j} = \begin{bmatrix} 0 \\ V_{n,j} \end{bmatrix}, \quad A = \begin{bmatrix} 0 & 1 \\ -\rho'^2 & -2r' \end{bmatrix}. \tag{B.2}$$

According to ([9], p. 371), the solution of this difference equation is

$$Y_{n,j} = A^n Y_{0,j} + \sum_{m=1}^{n-1} A^{n-m} X_{m-1,j}\ , \quad n = 1,2,... \tag{B.3}$$

The stability of this solution is determined by the homogeneous part of (2.5) which we rewrite as

$$K_{n+2,j} + 2r'K_{n+1,j} + \rho'^2 K_{n,j} = 0\ , \quad n = 0,1,2,... \tag{B.4}$$

Seeking solutions of the form

$$K_{n,j} = \mu^n \tag{B.5}$$

we end up with the characteristic equation

$$\mu^2 + 2r'\mu + \rho'^2 = 0 \tag{B.6}$$

whose roots are

$$\mu_{\pm} = -r' \pm \sqrt{r'^2 - \rho'^2} = -r' \pm |h|\ . \tag{B.7}$$

We thus have the two solutions

$$K_{n,j+} = \mu_+^{\ n}\ , \quad K_{n,j-} = \mu_-^{\ n}\ . \tag{B.8}$$

According to ([10], Theorem 7.2.9.6), a necessary and sufficient condition for the two solutions to satisfy the stability condition

$$\lim_{n\to\infty}\frac{K_{n,j\pm}}{n}=0 \tag{B.9}$$

is that $|\mu_{\pm}|\le 1$ and, if equality holds, then the root must be simple. This implies that

$$r'-|h|\le 1,\quad r'+|h|\le 1 \tag{B.10}$$

or that

$$r'+|h|\le 1. \tag{B.11}$$

For the two roots to be equal, we must have $h=0$, in which case

$$\mu_{\pm}=-r',\quad h=0 \tag{B.12}$$

and for a stable solution we must have

$$r'<1. \tag{B.13}$$

From this and (B.11), we have the two conditions

$$\begin{array}{ll} |h|\le\dfrac{1-\rho'^2}{2} & ,\ \text{if } 0\le\rho'<1 \text{ and } |h|>0 \\ 0\le\rho'<1 & ,\ \text{if } |h|=0 \end{array}. \tag{B.14}$$

We graph this in figure B.1.

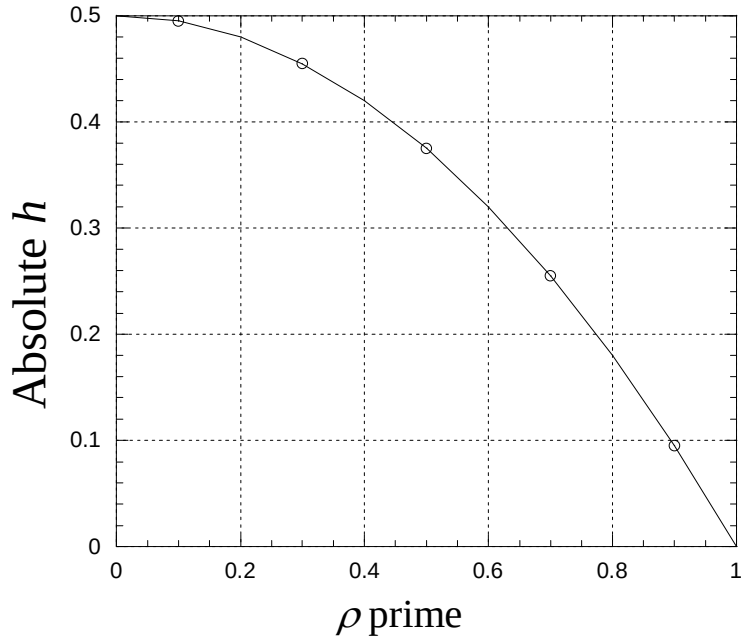

Figure B.1: Relation between $|h|$ and ρ' for stability. The stable region is the one below the curve and bounded by the two axes. The point (1, 0) is excluded.

We turn next to the stability of the iteration formulas (2.20), (2.26) and (2.32). Our discussion is motivated by comments in ([11], p. 142). The homogeneous part of all three equations under consideration is

$$v_{m+2,j} = \frac{m+2}{m+3} B_j^{\,2} v_{m,j}\,, \quad m = 0,1,2,\ldots\,. \tag{B.15}$$

This is not an easy equation to solve since the coefficients depend on the independent variable. We can, however, proceed as follows in our test for stability. We let

$$\gamma = \frac{m+2}{m+3}, \quad 0 < \gamma < 1 \tag{B.16}$$

and treat γ as a constant. We proceed as above to obtain a characteristic equation

$$\mu^2 = \gamma B_j^{\,2} \tag{B.17}$$

with the obvious solutions

$$\mu_{\pm} = \pm\sqrt{\gamma} B_j\,. \tag{B.18}$$

Since $\gamma < 1$, for the solutions $\left(\sqrt{\gamma} B_j\right)^m$ and $\left(-\sqrt{\gamma} B_j\right)^m$ to be stable, we need B_j to be less or equal to one

$$0 \le B_j < 1. \tag{B.19}$$

We recall that we obtain B_j by dropping the normal from the observation point to the line that contains the *j*-th side of the triangle. This distance is B_j.

We wish to point out that (B.19) does not imply (B.14) and conversely. This is unfortunate because both inequalities have to be satisfied simultaneously. As examples, think of an observation point on the plane of the triangle that lies on the extension of one of the sides of the triangle. Then, for that side, $B_j = 0$ while r' can be greater than one. If we now consider an observation point right above the centroid of the triangle and at a distance greater than 0.5, then (B.14) is not satisfied while (B.19) possibly could.

APPENDIX C
AN ALTERNATE WAY OF COMPUTING $K_{0,j}$

We assume the inequalities in (2.49) and let

$$\tau = B_j \tan\alpha \,. \tag{C.1}$$

We then get

$$K_{0,j} = \int_{\tan^{-1}\left(\frac{\hat{t}_j\cdot\mathbf{b}_{j+1}}{B_j}\right)}^{\tan^{-1}\left(\frac{\hat{t}_j\cdot\mathbf{b}_{j+2}}{B_j}\right)} \frac{B_j \sec^2\alpha\, d\alpha}{B_j\sec\alpha + |h|} = B_j \int_{\tan^{-1}\left(\frac{\hat{t}_j\cdot\mathbf{b}_{j+1}}{B_j}\right)}^{\tan^{-1}\left(\frac{\hat{t}_j\cdot\mathbf{b}_{j+2}}{B_j}\right)} \frac{d\alpha}{\cos\alpha\left(B_j + |h|\cos\alpha\right)}\,. \tag{C.2}$$

We now let

$$u = \tan\left(\frac{\alpha}{2}\right), \quad du = \frac{1}{2}\sec^2\left(\frac{\alpha}{2}\right)d\alpha = \frac{1+u^2}{2}d\alpha\,, \quad \cos\alpha = \frac{1-u^2}{1+u^2} \tag{C.3}$$

and substitute in (C.2)

$$K_{0,j} = 2B_j \int_{\tan\left[\frac{1}{2}\tan^{-1}\left(\frac{\hat{t}_j\cdot\mathbf{b}_{j+1}}{B_j}\right)\right]}^{\tan\left[\frac{1}{2}\tan^{-1}\left(\frac{\hat{t}_j\cdot\mathbf{b}_{j+2}}{B_j}\right)\right]} \frac{du}{\left(\frac{1-u^2}{1+u^2}\right)\left(B_j + |h|\frac{1-u^2}{1+u^2}\right)\left(1+u^2\right)}$$

$$= 2B_j \int_{\tan\left[\frac{1}{2}\tan^{-1}\left(\frac{\hat{t}_j\cdot\mathbf{b}_{j+1}}{B_j}\right)\right]}^{\tan\left[\frac{1}{2}\tan^{-1}\left(\frac{\hat{t}_j\cdot\mathbf{b}_{j+2}}{B_j}\right)\right]} \frac{\left(1+u^2\right)du}{\left(1-u^2\right)\left[\left(B_j - |h|\right)u^2 + B_j + |h|\right]}$$

$$= \int_{\tan\left[\frac{1}{2}\tan^{-1}\left(\frac{\hat{t}_j\cdot\mathbf{b}_{j+1}}{B_j}\right)\right]}^{\tan\left[\frac{1}{2}\tan^{-1}\left(\frac{\hat{t}_j\cdot\mathbf{b}_{j+2}}{B_j}\right)\right]} \left[\frac{1}{1-u} + \frac{1}{1+u}\right]du - 2\frac{|h|}{B_j - |h|}\int_{\tan\left[\frac{1}{2}\tan^{-1}\left(\frac{\hat{t}_j\cdot\mathbf{b}_{j+1}}{B_j}\right)\right]}^{\tan\left[\frac{1}{2}\tan^{-1}\left(\frac{\hat{t}_j\cdot\mathbf{b}_{j+2}}{B_j}\right)\right]} \frac{du}{u^2 + \frac{B_j + |h|}{B_j - |h|}}$$

$$= -\ln|1-u|\Bigg|_{\tan\left[\frac{1}{2}\tan^{-1}\left(\frac{\hat{t}_j\cdot\mathbf{b}_{j+1}}{B_j}\right)\right]}^{\tan\left[\frac{1}{2}\tan^{-1}\left(\frac{\hat{t}_j\cdot\mathbf{b}_{j+2}}{B_j}\right)\right]} + \ln|1+u|\Bigg|_{\tan\left[\frac{1}{2}\tan^{-1}\left(\frac{\hat{t}_j\cdot\mathbf{b}_{j+1}}{B_j}\right)\right]}^{\tan\left[\frac{1}{2}\tan^{-1}\left(\frac{\hat{t}_j\cdot\mathbf{b}_{j+2}}{B_j}\right)\right]}$$

$$
\begin{aligned}
&-2\frac{|h|}{B_j-|h|}\sqrt{\frac{B_j-|h|}{B_j+|h|}}\left[\tan^{-1}\left(\sqrt{\frac{B_j-|h|}{B_j+|h|}}\tan\left[\frac{1}{2}\tan^{-1}\left(\frac{\hat{t}_j\cdot\mathbf{b}_{j+2}}{B_j}\right)\right]\right)-\tan^{-1}\left(\sqrt{\frac{B_j-|h|}{B_j+|h|}}\tan\left[\frac{1}{2}\tan^{-1}\left(\frac{\hat{t}_j\cdot\mathbf{b}_{j+1}}{B_j}\right)\right]\right)\right]\\
&=\ln\left|\frac{1+\tan\left[\frac{1}{2}\tan^{-1}\left(\frac{\hat{t}_j\cdot\mathbf{b}_{j+2}}{B_j}\right)\right]}{1-\tan\left[\frac{1}{2}\tan^{-1}\left(\frac{\hat{t}_j\cdot\mathbf{b}_{j+2}}{B_j}\right)\right]}\right|-\ln\left|\frac{1+\tan\left[\frac{1}{2}\tan^{-1}\left(\frac{\hat{t}_j\cdot\mathbf{b}_{j+1}}{B_j}\right)\right]}{1-\tan\left[\frac{1}{2}\tan^{-1}\left(\frac{\hat{t}_j\cdot\mathbf{b}_{j+1}}{B_j}\right)\right]}\right|\\
&-2\frac{|h|}{A_j}\left[\tan^{-1}\left(\frac{A_j}{B_j+|h|}\tan\left[\frac{1}{2}\tan^{-1}\left(\frac{\hat{t}_j\cdot\mathbf{b}_{j+2}}{B_j}\right)\right]\right)-\tan^{-1}\left(\frac{A_j}{B_j+|h|}\tan\left[\frac{1}{2}\tan^{-1}\left(\frac{\hat{t}_j\cdot\mathbf{b}_{j+1}}{B_j}\right)\right]\right)\right]\\
&=\ln\left\{\left|\frac{1+\tan\left[\frac{1}{2}\tan^{-1}\left(\frac{\hat{t}_j\cdot\mathbf{b}_{j+2}}{B_j}\right)\right]}{1-\tan\left[\frac{1}{2}\tan^{-1}\left(\frac{\hat{t}_j\cdot\mathbf{b}_{j+2}}{B_j}\right)\right]}\right|\left|\frac{1-\tan\left[\frac{1}{2}\tan^{-1}\left(\frac{\hat{t}_j\cdot\mathbf{b}_{j+1}}{B_j}\right)\right]}{1+\tan\left[\frac{1}{2}\tan^{-1}\left(\frac{\hat{t}_j\cdot\mathbf{b}_{j+1}}{B_j}\right)\right]}\right|\right\}\\
&-2\frac{|h|}{A_j}\tan^{-1}\left\{\frac{\frac{A_j}{B_j+|h|}\left\{\tan\left[\frac{1}{2}\tan^{-1}\left(\frac{\hat{t}_j\cdot\mathbf{b}_{j+2}}{B_j}\right)\right]-\tan\left[\frac{1}{2}\tan^{-1}\left(\frac{\hat{t}_j\cdot\mathbf{b}_{j+1}}{B_j}\right)\right]\right\}}{1+\left(\frac{A_j}{B_j+|h|}\right)^2\tan\left[\frac{1}{2}\tan^{-1}\left(\frac{\hat{t}_j\cdot\mathbf{b}_{j+2}}{B_j}\right)\right]\tan\left[\frac{1}{2}\tan^{-1}\left(\frac{\hat{t}_j\cdot\mathbf{b}_{j+1}}{B_j}\right)\right]}\right\}.
\end{aligned}
\tag{C.4}
$$

The last line in (C.4) can be written in a variety of ways by applying trigonometric and inverse trigonometric identities to the numerator. Finally, we remind that this formula is valid when the conditions in (2.49) are satisfied. We would also have to consider the other two cases.

REFERENCES

1. M. Rao, D. R. Wilton, and A. W. Glisson, "Electromagnetic Scattering by surfaces of arbitrary shape", *IEEE Trans. Antennas Propagat.*, vol. AP-30, no. 3, pp. 409-418, 1982.

2. Van Bladel, *Electromagnetic Fields*. New York: McGraw-Hill, 1964

3. M. Apostol, *Mathematical Analysis*, 2nd ed. Reading, MA: Addison Wesley, 1974.

4. A. Gordon and H. J. Bilow, "Reduction of Surface Integrals to Contour Integrals", *IEEE Trans. Antennas Propagat.*, vol. 50, no. 3, pp. 308-311, 2002.

5. S. Asvestas and H. J. Bilow, "Line-integral approach to computing impedance matrix elements", *IEEE Trans. Antennas Propagat.*, vol. 55, no. 10, pp. 2767-2772, 2007.

6. A. Khayat and D. R. Wilton, "Numerical evaluation of singular and near-singular potential integrals", *IEEE Trans. Antennas Propagat.*, vol. 53, no. 10, pp. 3180-3190, 2005.

7. Rossi and P. J. Cullen, "On the fully numerical evaluation of the linear-shape function times the 3-D Green's function on a plane triangle", *IEEE Trans Microwave Theory Tech*, Vol. 47, No. 4, pp. 398-402, 1999.

8. A. Khayat, D. R. Wilton and P. W. Fink, "An improved transformation and optimized sampling Scheme for numerical evaluation of singular and near-singular potentials", to appear in the *IEEE Antennas and Wireless Propagat. Letters*.

9. Dahlquist and Å. Björck, *Numerical Methods*. Englewood Cliffs, NJ: Prentice-Hall, 1974.

10. Stoer and R. Bulirsch, *Introduction to Numerical Analysis*. New York: Springer-Verlag, 1980.

11. H. Press et al., *Numerical Recipes*. Cambridge: Cambridge University Press, 1986.

PART 2. NUMERICAL EVALUATION OF INTEGRALS

1. STATEMENT OF PROBLEM AND APPROACH

In the first part of this report, we developed a method for computing the integral

$$\mathbf{I}^{(l)}(\mathbf{r}') = \int_T \frac{\mathbf{f}^{(l)}(\mathbf{r})\mathrm{e}^{-ikR}}{R} dS\,, \quad \mathbf{f}^{(l)}(\mathbf{r}) = \mathbf{r} - \mathbf{r}_l\,, \quad l = 1,2,3\,. \tag{1.1}$$

Here

$$R = \sqrt{r'^2 - 2\mathbf{r}'\cdot\mathbf{r} + r^2} = \sqrt{\left(x - x'\right)^2 + \left(y - y'\right)^2 + h^2} \tag{1.2}$$

with

$$\mathbf{r} = x\hat{x} + y\hat{y}\,, \quad \mathbf{r}' = x'\hat{x} + y'\hat{y} + h\hat{z} \tag{1.3}$$

and the region of integration *T* being the triangle in figure 1.1. The origin of coordinates is the centroid of the triangle, and the latter lies on the *xy*-plane. Boldface letters denote vectors. The same letters in italics denote the magnitudes of these vectors while a caret over a letter denotes a unit vector. The vector $\mathbf{r}_l$ is the position vector to the *l*-th vertex of the triangle, as shown in figure 1.

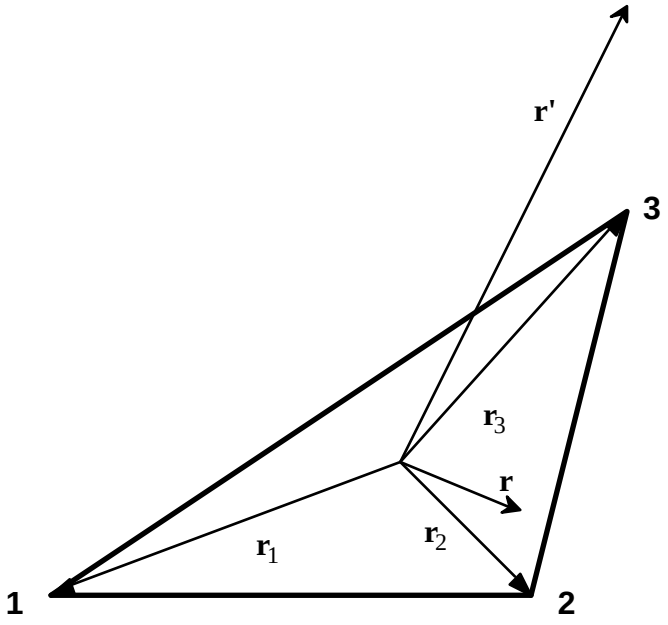

Figure 1.1: The Integration Triangle

In Part 1, we found it convenient to measure distances in wavelengths and, hence, we rewrite the original integral in the form

$$\mathbf{I}^{(l)}(\mathbf{r}') = \lambda^2 \int_T \frac{\mathbf{f}^{(l)}(\mathbf{r}) \mathrm{e}^{-i2\pi R}}{R} dS\,, \quad \mathbf{f}^{(l)}(\mathbf{r}) = \mathbf{r} - \mathbf{r}_l\,, \quad l = 1,2,3 \tag{1.4}$$

with all distances in wavelengths (λ). We also found it convenient to introduce the phase factor $\exp(-i2\pi r')$ and write

$$\mathbf{I}^{(l)}(\mathbf{r}') = \lambda^2 \mathrm{e}^{-i2\pi r'} \int_T \frac{\mathbf{f}^{(l)}(\mathbf{r}) \mathrm{e}^{-i2\pi (R - r')}}{R} dS\,, \quad \mathbf{f}^{(l)}(\mathbf{r}) = \mathbf{r} - \mathbf{r}_l\,, \quad l = 1,2,3\,. \tag{1.5}$$

We reached the conclusion that we can compute the integral in (1.5) to a prescribed precision by approximating the exponential with its Maclaurin series expansion. We can do this for observation points in the interior of a sphere with center the triangle's centroid and radius of half a wavelength. We also found that the number of terms depends only on the number of significant digits required and the longest side of the triangle but not on the position of the observation point within the sphere or the shape of the triangle.

Since the observation point may lie anywhere in space (but on the three sides of the triangle), we must develop a method that provides answers to (1.5) for observation points outside the half-wavelength sphere and for prescribed accuracy. We describe below a procedure we developed for doing show. Where we do not use the method of Part 1, we use cubatures[2] to evaluate (1.5) to a prescribed number of significant digits. The general strategy is as follows.

1. Collect available cubatures for triangles.
2. Develop a set of testing triangles.
3. For a prescribed accuracy, develop a program that provides timing information for the cubatures and our method in Part 1 to run over the set of triangles.
4. For observation points inside the half-wavelength sphere but not on the triangle, run our method and those cubatures that are faster than our method. Determine where those cubatures provide the required accuracy by comparing their answer to that of our method. Based on this, define a new sphere, concentric with the old one but of radius less or equal to that of the old one.
5. For observation points outside the new sphere, order all cubatures according to increasing size (number of points employed in cubature). Define a convergence criterion for the sequence of cubatures.
6. For a judiciously selected set of observation points and all triangles, run the sequence of cubatures. Using the results, define a set of spheres concentric with the sphere in 4,

[2] By *cubature* we mean a numerical method for evaluating a surface integral; we reserve the word *quadrature* for a numerical method for evaluating a line integral.

above. In the space between two successive spheres, choose the smallest cubature that has converged. This is the cubature to be used in this region for the prescribed accuracy.

In the following sections, we present the details of this plan.

2. AVAILABLE CUBATURES AND THEIR TIMING

The cubatures for triangles that we use come from three sources [1], [2], [3]. They range in size from 3 points to 175 points. We have employed all the cubatures in table 5.1 of [1] as well as a 46-point one that Dr. Taylor sent us. The latter integrates a 15-deg polynomial exactly. We have also used a 175-point cubature that Prof. H. Xiao kindly supplied to us. It integrates a 30-deg polynomial. The only cubature coming from [3] is the 7-point one, with a misprint corrected. We used it because it is a popular one in the electromagnetics community. Our guess is that it can at best integrate a 4-deg polynomial exactly. We exhibit all these cubatures in table 2.1 and plot the relationship between polynomial degree and cubature points in figure 2.1.

Table 2.1: Size of cubatures employed and maximum degree of polynomial they integrate exactly.

Number of cubature points	Maximum degree of polynomial that can be integrated exactly
3	2
6	4
7	4 (?)
10	5
15	7
21	9
28	11
36	13
45	14
46	15
55	16
66	18
78	20
91	21
105	23
120	25
175	30

The standard triangle over which these cubatures are defined is an equilateral triangle of side one. Originally, most of them were defined over a right triangle. We made the appropriate transformations to map this triangle into our standard equilateral triangle. We use this triangle to transform a cubature's points so that they apply to any other, arbitrarily shaped triangle.

We demonstrate our procedure using 7 significant digits (SD) as the required accuracy. *The number of significant digits is a variable in our programs.* For demonstration purposes, however, we have chosen 7 SD. This number corresponds to single precision (32 bits) in the IEEE-754 floating-point standard [4].

We also set the wavelength λ equal to one meter. This does not entail any loss of generality; it simply allows for easier calculating. *In our programs, the wavelength is a variable.*

We require that the longest side of the triangle is no longer than one tenth of a wavelength. In a general MoM code that uses our scheme, the entire grid would be scanned and the longest side would be found and used. Thus, *the length of the longest side in our programs is a variable*. For demonstrating our approach, however, we set the maximum side at less or equal to a tenth of a wavelength.

Finally, we mention that all our programming was done in C programming language.

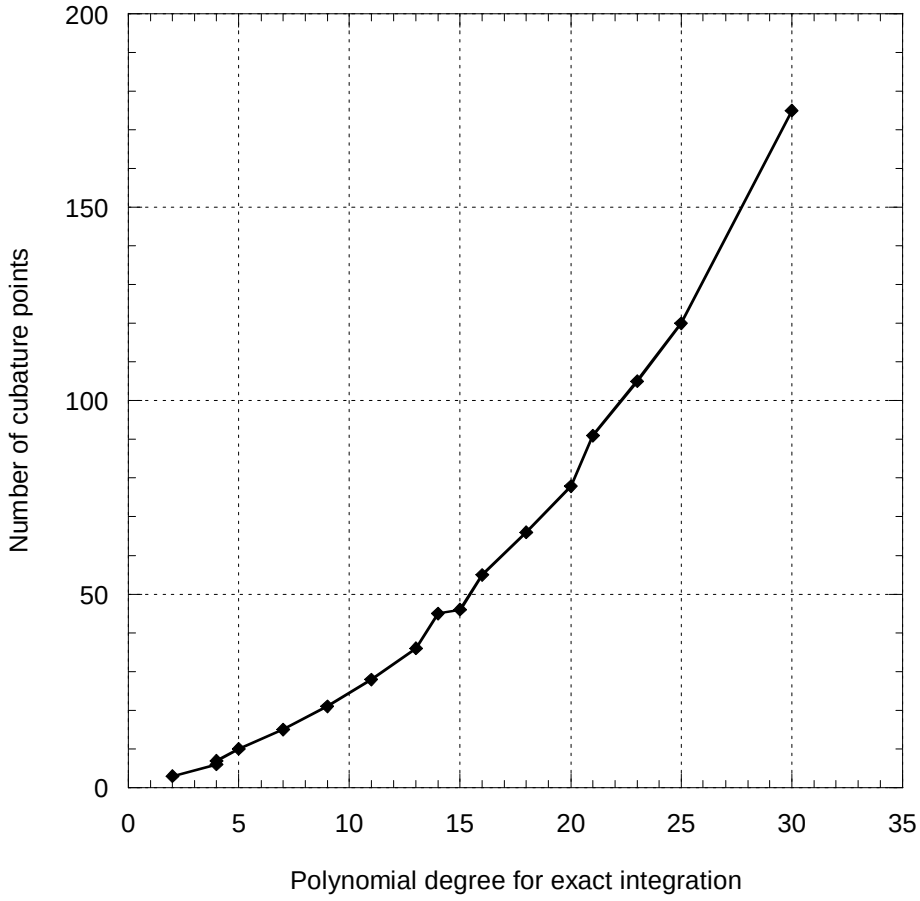

Figure 2.1: Cubature size (number of points) as a function of degree of polynomial that can be integrated exactly.

We proceed now with the timing of our method and that of the cubatures. We only need one test triangle since the cubatures take the same time over all triangles and since the number of terms in our method is fixed once the length of the maximum side is fixed. The timing algorithm took into account the time to transform from the standard (equilateral) triangle to the test triangle in figure 2.2. Although the two are identical in this case, this time must be accounted for in general. Subroutines were written in a way so as to make the timing comparison between our method and the cubatures as fair as possible. The results are shown in figure 2.3. Time is normalized to our method. All cubatures lie on a straight line since time to apply them is directly proportional to a cubature's number of points. We see that cubatures with 21 or fewer points are faster than our method, while cubatures with 28 or more points are slower. This does not mean that we discard cubatures that are slower. We shall use them below to establish convergence for the sequence of cubatures. Of immediate interest, however, are cubatures that are faster than our method.

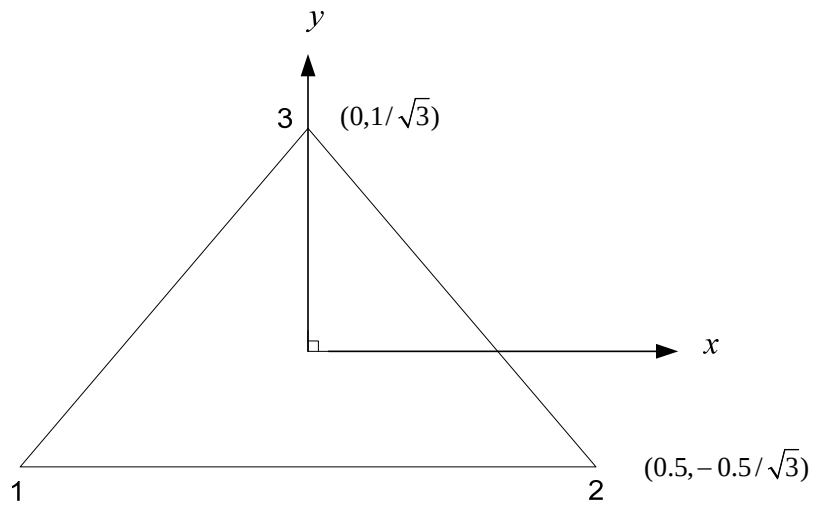

Figure 2.2: Equilateral test triangle for timing cubatures and our method.

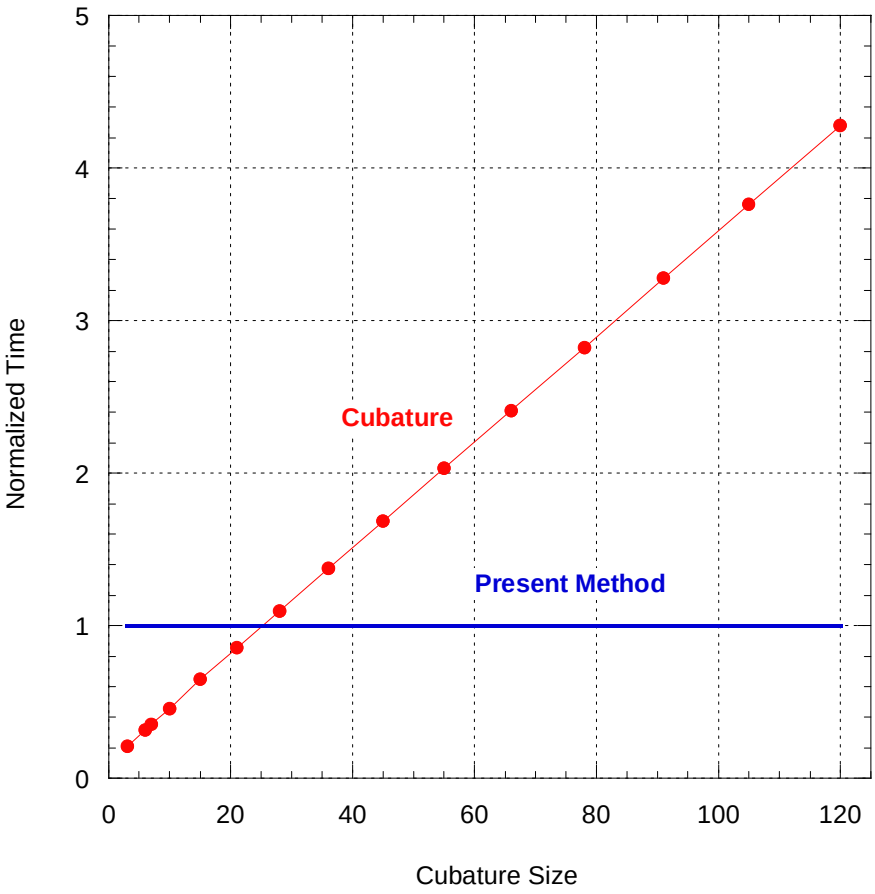

Figure 2.3: Cubature time normalized to that of our method (7 SD).

3. DIVISION OF OBSERVATION SPACE INTO SPHERICAL REGIONS

In the previous section we determined that cubatures with 21 or fewer points are faster than our method. In this section we resolve the question of whether we can use them within the sphere of application of our method and obtain the required 7-SD accuracy. We also determine which cubature to use in the rest of the observation space. To this end we introduce a set of 25 test triangles. These triangles are shown in Appendix A. They have been chosen deterministically rather than through a random process that, say, generates triangle vertices randomly subject to the condition that the longest side of a triangle cannot be larger than $\lambda/10$. We feel that our set of triangles is representative of those we encounter in practice, containing both well behaved and nearly pathological ones.

We also generated a set of approximately 10,000 observation points spread on a hemisphere above each of these triangles and with center the centroid of the triangle. This number is the same for all 25 triangles once the radius of the hemisphere has been fixed. It will, however, vary from hemisphere to hemisphere. Observation points on a hemisphere below a triangle are not

necessary since we have symmetry with respect to the triangle's plane. The points are evenly spread with respect to the observation angles. We also used a set of randomly chosen points with, essentially, the same outcome. In the tables below we present the results for the set of evenly spaced points.

Using the set of triangles and the set of observation points, we computed the three integrals in (1.5). These are vectors that lie in the triangle's plane and their components are complex numbers; thus, we have 3 vectors of 2 components each, with the components a pair of real numbers each, a total of 12 real numbers. We also computed the scalar integral that results when we eliminate the vector function from the integrand of (1.5). This is a complex number and, hence, it contributes two more real numbers for a grand total of 14.

We next define what we mean by *average failure rate* (AFR) for a specific cubature. Suppose we have the correct 7-SD answer for every triangle and every observation point that lies on a given hemisphere. For one of the triangles (and for the specific cubature) we compute the 14 real numbers for all 10,000 or so observation points. We compare each such number to the correct 7-SD answer by forming the relative error and testing it to determine whether it satisfies the inequality.

$$\left|\frac{(\text{computed number})-(\text{correct to 7-SD number})}{\text{correct to 7-SD number}}\right| < 5\cdot 10^{-8}. \tag{3.1}$$

We count a failure if this inequality is not satisfied. The total number of failures over all observation points (those that are at the same distance from the centroid of a triangle), and for a specific triangle and cubature is the *failure rate* (FR). We express this in percent. As an example, if we have 1,500 failures out of 10,000 observation points tested, then the FR is (1,500/10,000)x100 = 15%.

For a fixed cubature and hemisphere, we find the FR for each of the 25 test triangles. We then average the 25 numbers to obtain an AFR for the specific hemisphere and cubature. Besides the AFR, we also keep track of the minimum FR (MinFR) and maximum FR (MaxFR). These two numbers come out of two triangles, the one that has the minimum FR and the one that has the maximum FR. We present a sample of such an output in table 3.1. This table is for the 7-point cubature (C7) and for all the observation points on a hemisphere of radius $r' = 0.3\lambda$. We present AFR, MinFR and MaxFR for the scalar integral's real and imaginary part. We also present results for one of the vector integrals in (1.5). In this case, we have four entries since the vector integral has two components, each a complex number.

Table 3.1: Failure rates for the 7-point cubature and for the observation points on a hemisphere of radius $r' = 0.3\lambda$. (Isc real: real part of scalar integral; V1 x re: real part of the *x*-component of the vector integral in (1.5) with $l = 1$)

FR	Isc real	Isc Imag	V1 x re	V1 x im	V1 y re	V1 y im
AFR	33.04	0.00	89.85	23.90	93.15	3.65
MinFR	0.00	0.00	62.51	0.00	82.32	0.00
MaxFR	87.32	0.00	99.47	98.39	97.33	36.60

We next describe how we classify error. We are dealing with 14 entries and there are many ways to define error. We can work with each of the 14 entries separately. We can also work with all 14 entries at once and call a failure if a specified number of entries fail to produce 7 SD. Of the many possibilities, we choose what we consider a natural way. The scalar integral consists of two entries (real and imaginary); each vector integral consists of four entries, since it has two complex-valued components. We declare a failure for the scalar integral if any of its two real numbers fails the test (3.1); similarly, we declare a failure for any of the three vector integrals if any of its four real numbers fails the test (3.1). Under this scheme, we use the largest number of failures within each of the four groups of numbers to be the FR of that group. As an example, table 3.1 would reduce to table 3.2.

Table 3.2: Failure rates for the scalar and first vector integral in table 3.1 according to the rules described above.

FR	Isc	V1
AFR	33.04	93.15
MinFR	0.00	82.32
MaxFR	87.32	99.47

The last issue we need discuss before presenting numerical results is what we mean by convergence of the sequence of cubatures. We look at a single triangle and a single observation point and compute the set of 14 real numbers using all the cubatures, ordered from the smallest to the largest size. For each of the 14 entries we compare how this number changes as a function of cubature size. Specifically, we compare successive results and test them whether they agree to 7 SD. The test we use is

$$\left|\frac{C(n,m)-C(n+1,m)}{C(n+1,m)}\right| < 5\cdot 10^{-8}, \quad n = 1,2,...,17;, \quad m = 1,2,...,14 \tag{3.2}$$

where $C(n,m)$ stands for the result of the n^{th} cubature for the m^{th} real number. Here, we have placed the 17 cubatures of table 2.1 in an one-to-one correspondence with the natural numbers. For each *m*, we look for $\bar{n}$, the smallest *n* that satisfies(3.2). If (3.2) is satisfied for $\bar{n}+1$ and

$\bar{n}+2$ also, we declare the sequence to have converged and its value to be that of $\bar{n}+3$. In our program, *the number of successive comparisons is a variable*; thus, it can be smaller or larger than three.

We now present some tables with results we obtained using the triangles, observation points, cubatures and rules we described above. The raw data sets we used are too large to present here. As an example, in Appendix B we present raw data for the 10-point cubature for a limited number of r' values. It is from this kind of tables that we obtain the tables that follow.

In table 3.3, we present AFR results for the scalar integral and for the four cubatures that are faster than our method. The number of SD required is 7, as it is throughout this discussion. We see that cubature C7 and C10 are not reliable at any distance from the centroid; on the contrary, Cubature C15 can be applied for $r' \geq 0.2$ and C21 for $r' \geq 0.15$ wavelengths. We also see that the error starts increasing at large distances. We will return to this point. If we ignore the behavior at large distances, then C15 and C21 provide 7 SD with an AFR of less than 1% from the stated distances on. The contents of this table appear in graphical form in figure 3.1.

Table 3.3: Scalar integral AFR for four cubatures that are faster than our method. The number we present in each cell is the larger of the AFR for the real and imaginary parts of the integral.

r' (in wavelengths)	Isc AFR C7	Isc AFR C10	Isc AFR C15	Isc AFR C21
0.1	99.61	99.22	77.37	9.85
0.15	97.83	96.74	7.63	0.00
0.2	91.47	87.18	0.00	0.00
0.3	33.05	21.43	0.00	0.00
0.4	0.18	0.00	0.00	0.00
0.5	97.84	95.72	0.01	0.00
0.6	0.00	0.00	0.00	0.00
0.7	0.00	0.00	0.00	0.00
0.8	0.00	0.00	0.00	0.00
0.9	0.00	0.00	0.00	0.00
1	81.02	76.96	0.08	0.00
1.5	77.20	73.24	0.06	0.00
2	74.20	70.70	0.07	0.00
2.5	72.08	69.10	0.07	0.00
3	71.15	67.96	0.06	0.00
5	71.56	68.92	0.05	0.01
10	69.97	66.90	0.09	0.02
25	70.18	66.98	0.08	0.02
50	67.76	65.67	0.09	0.04
100	64.87	64.07	0.17	0.11

500	56.83	59.32	1.69	1.36
1000	56.92	60.67	3.77	2.99

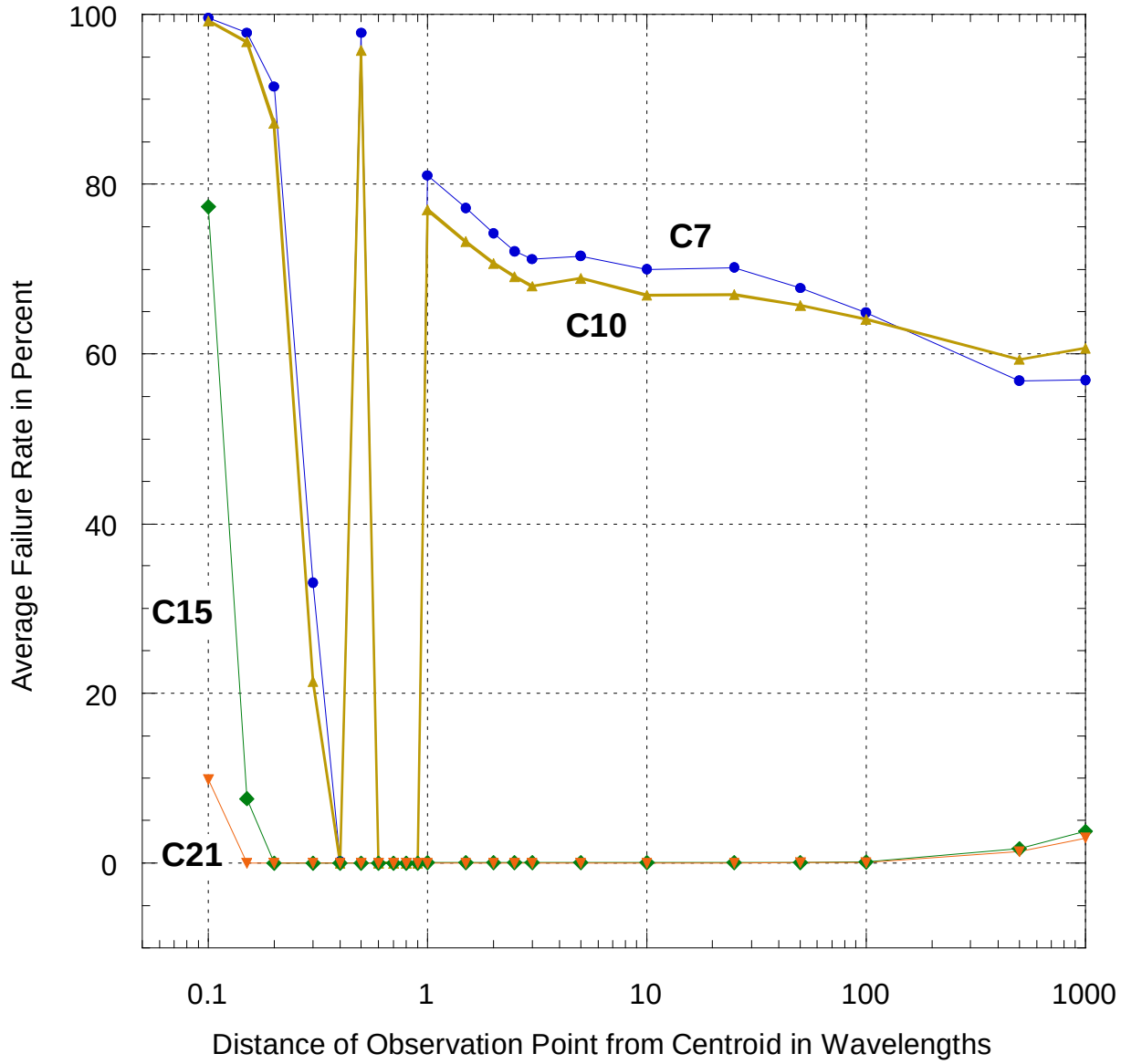

Figure 3.1: Data of table 3.3 in graphical form: AFR for scalar integral versus distance of observation point from centroid.

In Appendix C, we provide the same information for the three vector integrals. Based on these tables and the criterion that the AFR must be less than 1%, we can choose for each integral the sphere with radius r' outside of which we apply a cubature of a certain size. The most efficient (fastest) way of computing the four integrals, however, is a simultaneous computation of all four (see Appendix D); thus, it pays to use the same cubature and same radius r' for all four

integrals. To this end, we construct tables 3.4 and 3.5 where, using table 3.3 and the tables in Appendix C, we choose the maximum AFR for each of the cubatures C15 and C21 (we have eliminated the other two as not providing enough accuracy), respectively. We also present these results in graphical form in figure 3.2. From table 3.4, we see that we can use C15 outside a sphere of radius $r' = 0.4$ with an AFR of less than 1% while, from table 3.5, this radius becomes equal to 0.2. In figure 3.3, we display these findings and we call this conclusion a possible strategy for dividing the observation space.

Table 3.4: AFR for the four integrals using C15. The last column exhibits the maximum of the four columns preceding it.

r' (in wavelengths)	Isc AFR C15	V1 AFR C15	V2 AFR C15	V3 AFR C15	Maximum AFR
0.1	77.37	94.28	94.24	92.41	94.28
0.15	7.63	47.31	50.69	27.08	50.69
0.2	0.00	23.41	22.30	6.37	23.41
0.3	0.00	2.62	2.53	0.00	2.62
0.4	0.00	0.18	0.29	0.00	0.29
0.5	0.01	0.19	0.06	0.05	0.19
0.6	0.00	0.05	0.04	0.00	0.05
0.7	0.00	0.05	0.03	0.00	0.05
0.8	0.00	0.03	0.02	0.00	0.03
0.9	0.00	0.02	0.02	0.00	0.02
1	0.08	0.05	0.03	0.03	0.08
1.5	0.06	0.07	0.01	0.01	0.07
2	0.07	0.00	0.00	0.00	0.07
2.5	0.07	0.00	0.00	0.00	0.07
3	0.06	0.00	0.00	0.00	0.06
5	0.05	0.00	0.00	0.00	0.05
10	0.09	0.00	0.00	0.00	0.09
25	0.08	0.00	0.00	0.00	0.08
50	0.09	0.00	0.00	0.00	0.09
100	0.17	0.00	0.00	0.00	0.17
500	1.69	0.00	0.00	0.00	1.69
1000	3.77	0.00	0.00	0.00	3.77

Table 3.5: AFR for the four integrals using C21. The last column exhibits the maximum of the four columns preceding it.

r' (in wavelengths)	Isc AFR C21	V1 AFR C21	V2 AFR C21	V3 AFR C21	Maximum AFR
0.1	9.85	55.88	48.52	30.45	55.88
0.15	0.00	4.26	5.32	0.01	5.32
0.2	0.00	0.34	0.57	0.00	0.57
0.3	0.00	0.02	0.02	0.00	0.02
0.4	0.00	0.00	0.00	0.00	0.00
0.5	0.00	0.00	0.00	0.00	0.00
0.6	0.00	0.00	0.00	0.00	0.00
0.7	0.00	0.00	0.00	0.00	0.00
0.8	0.00	0.00	0.00	0.00	0.00
0.9	0.00	0.00	0.00	0.00	0.00
1	0.00	0.00	0.00	0.00	0.00
1.5	0.00	0.00	0.00	0.00	0.00
2	0.00	0.00	0.00	0.00	0.00
2.5	0.00	0.00	0.00	0.00	0.00
3	0.00	0.00	0.00	0.00	0.00
5	0.01	0.00	0.00	0.00	0.01
10	0.02	0.00	0.00	0.00	0.02
25	0.02	0.00	0.00	0.00	0.02
50	0.04	0.00	0.00	0.00	0.04
100	0.11	0.00	0.00	0.00	0.11
500	1.36	0.00	0.00	0.00	1.36
1000	2.99	0.00	0.00	0.00	2.99

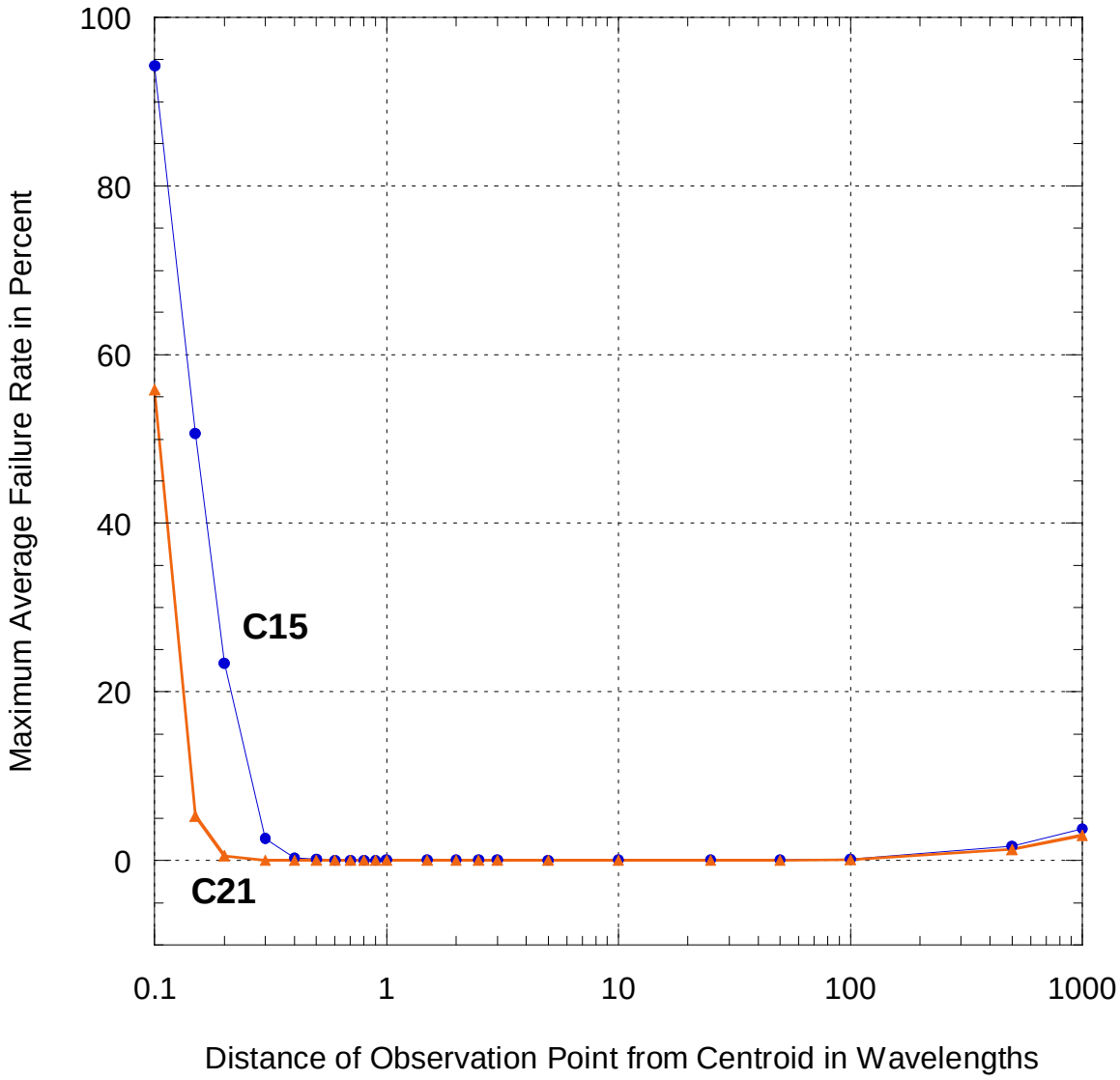

Figure 3.2: Graphical form of right-hand columns of tables 3.4 and 3.5: Maximum AFR as a function of distance of observation point from centroid.

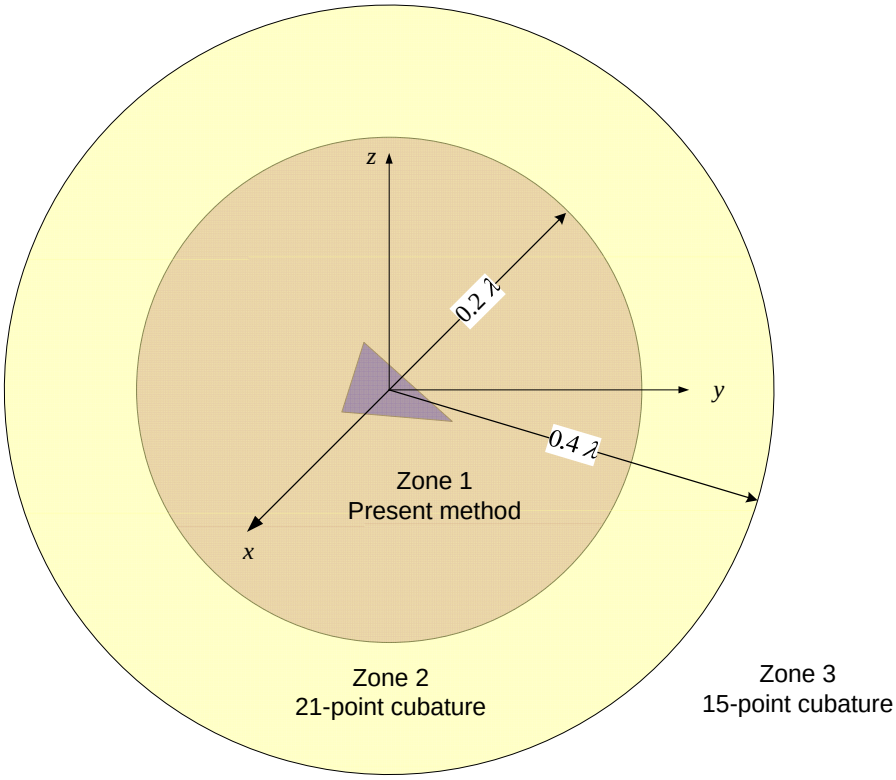

Figure 3.3: A possible zoning strategy for 7 SD based on a less than 1% AFR.

Another possible strategy for dividing the observation space is to use the MaxFR. In Appendix E, we present the relevant tables and use them to construct tables 3.6 and 3.7, and we also display their contents graphically in figure 3.4. Using these tables, we present in figure 3.5 another possible strategy based on a MaxFR of less than 1%.

Table 3.6: MaxFR for the four integrals using C15. The last column exhibits the maximum of the four columns preceding it.

r' (in wavelengths)	Isc MaxFR C15	V1 MaxFR C15	V2 MaxFR C15	V3 MaxFR C15	Maximum MaxFR
0.1	96.40	99.79	99.62	97.53	99.79
0.15	26.46	97.46	97.46	79.99	97.46
0.2	0.00	76.93	81.28	29.22	81.28
0.3	0.00	15.12	15.92	0.00	15.92
0.4	0.00	2.73	7.19	0.00	7.19
0.5	0.03	2.78	1.45	0.14	2.78
0.6	0.00	0.59	0.67	0.00	0.67
0.7	0.00	1.15	0.25	0.00	1.15
0.8	0.00	0.28	0.34	0.00	0.34
0.9	0.00	0.16	0.45	0.00	0.45
1	0.22	1.18	0.11	0.06	1.18
1.5	0.18	1.82	0.03	0.02	1.82
2	0.17	0.03	0.03	0.02	0.17
2.5	0.17	0.01	0.01	0.01	0.17
3	0.15	0.02	0.02	0.02	0.15
5	0.26	0.04	0.07	0.02	0.26
10	0.31	0.04	0.09	0.02	0.31
25	0.14	0.02	0.04	0.01	0.14
50	0.19	0.01	0.08	0.01	0.19
100	0.34	0.03	0.09	0.04	0.34
500	2.80	0.01	0.04	0.01	2.80
1000	6.26	0.04	0.09	0.04	6.26

Table 3.7: MaxFR for the four integrals using C21. The last column exhibits the maximum of the four columns preceding it.

r' (in wavelengths)	Isc MaxFR C21	V1 MaxFR C21	V2 MaxFR C21	V3 MaxFR C21	Maximum MaxFR
0.1	54.96	97.44	94.77	65.99	97.44
0.15	0.00	18.31	31.32	0.26	31.32
0.2	0.00	2.06	5.03	0.00	5.03
0.3	0.00	0.11	0.30	0.00	0.30
0.4	0.00	0.05	0.01	0.00	0.05
0.5	0.01	0.01	0.02	0.00	0.02
0.6	0.00	0.01	0.00	0.00	0.01
0.7	0.00	0.00	0.00	0.00	0.00
0.8	0.00	0.00	0.00	0.00	0.00
0.9	0.00	0.00	0.00	0.00	0.00
1	0.01	0.00	0.00	0.01	0.01
1.5	0.01	0.01	0.00	0.00	0.01
2	0.01	0.00	0.00	0.00	0.01
2.5	0.02	0.00	0.00	0.00	0.02
3	0.02	0.00	0.00	0.00	0.02
5	0.02	0.00	0.00	0.00	0.02
10	0.06	0.00	0.00	0.00	0.06
25	0.06	0.00	0.00	0.00	0.06
50	0.13	0.00	0.00	0.01	0.13
100	0.25	0.01	0.01	0.00	0.25
500	2.34	0.01	0.02	0.01	2.34
1000	5.62	0.01	0.01	0.01	5.62

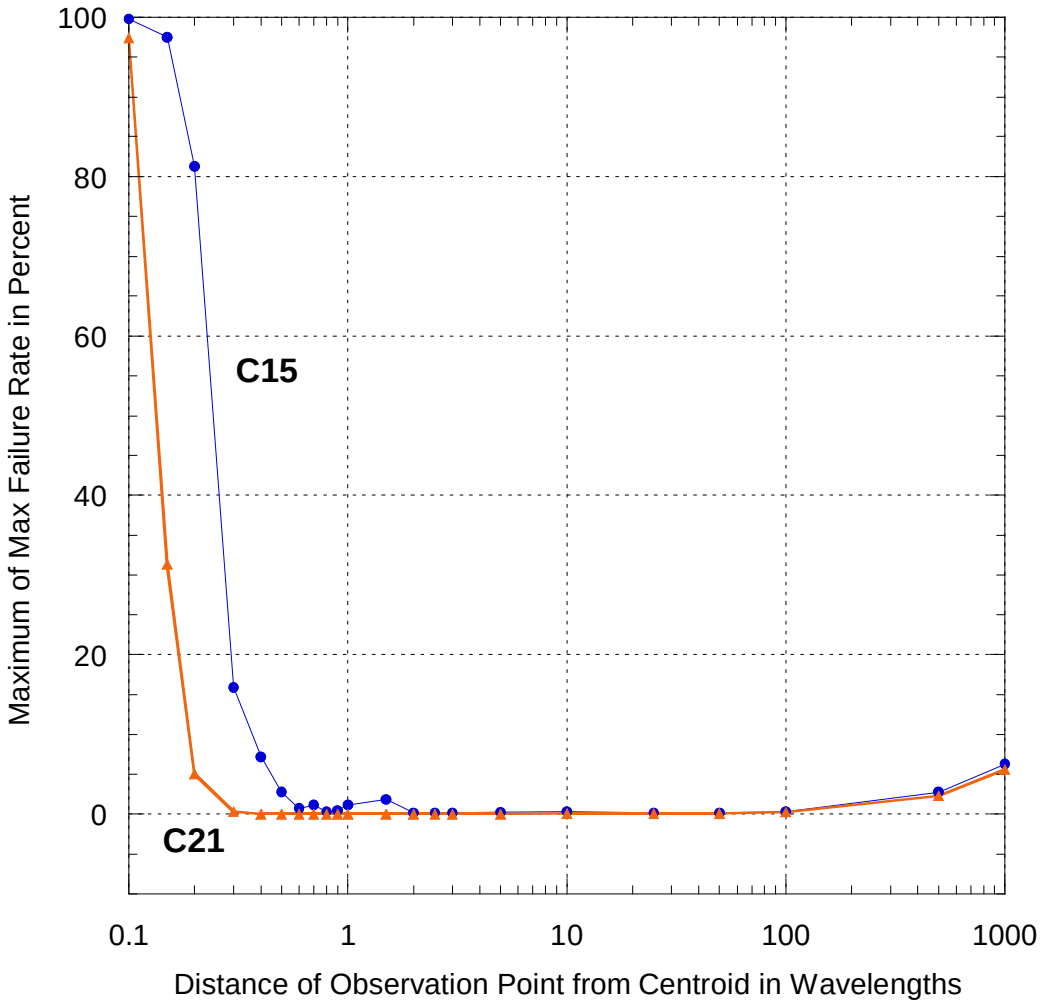

Figure 3.4: Graphical form of right-hand columns of tables 3.6 and 3.7: Maximum MaxAFR as a function of distance of observation point from centroid.

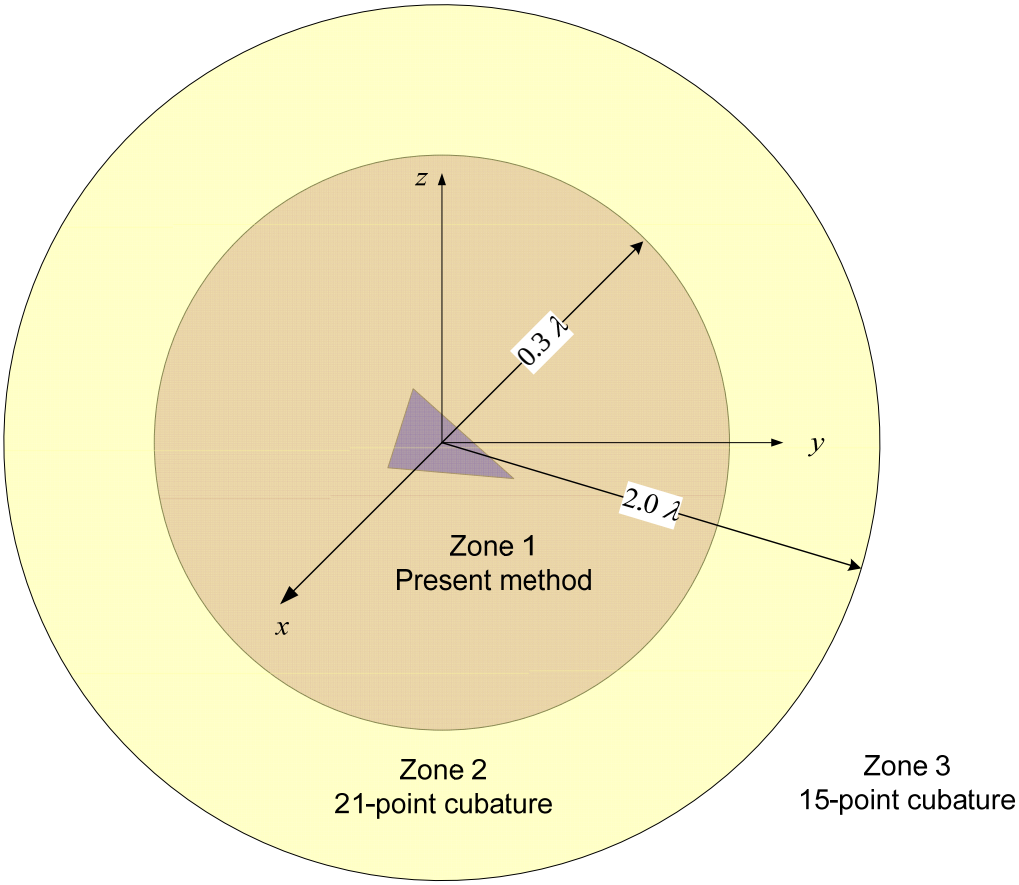

Figure 3.5: A possible zoning strategy for 7 SD based on a less than 1% MaxFR.

This is in brief the strategy for determining the spherical regions where we employ our method (see Part 1 of this report) and the C21 and C15 cubatures. The criteria we used in determining these regions are not unique and can be altered according to the preferences of the user and/or the requirements of the problem. One issue we have not resolved is the rise in the FR for the scalar integral as the observation point tends to infinity. This occurs only in the imaginary part of the integral and reduces the accuracy of that part to 5 SD, on average. It is the result of the subtraction of two numbers that are accurate to 7 SD and whose leading two digits are the same; thus, what remains after subtraction is accurate to 5 SD. This imaginary part is much smaller than the real part, by two or more orders. We do not know how the loss of SD in the considerably smaller part affects the accuracy of the solution of the system of equations, nor do we think that it is easy to analyze.

4. CONCLUSIONS

For the Rao-Wilton-Glisson formulation of the method of moments [5], we have developed a procedure for dividing the observation space into spherical regions when computing the inner surface integrals. This procedure guarantees a prescribed number of SD in the evaluation of these integrals. In the innermost region, we use the method we developed in Part 1 of this report. In the remaining two regions, we use two different size cubatures. The radius of each spherical region and the cubature size depend on the number of SD that we require. The number of spherical regions is not fixed but can be adjusted by the user. In our experience, three spherical regions are sufficient to cover the entire observation space.

We can also express the original integral in terms of line integrals around the triangle's boundary. These integrals can be computed using a Gauss-Legendre quadrature. Convergence to a desired accuracy can be determined in the same way as above by using a sequence of such quadratures. We have not tried this approach but it would be interesting to find out how it compares time wise with the present one.

5. ACKNOWLEDGEMENTS

We thank Dr. Mark Taylor of Sandia National Laboratory for graciously responding to our request for high-precision cubatures and to Prof. Hong Xiao of U. C. Davis for supplying the 175-point cubature.

APPENDIX A
SET OF TEST TRIANGLES

In this appendix we present the set of 25 test triangles we use in Section 3. They appear in figures A.1 – A.4. In figure A.1 we have a right triangle whose hypotenuse is equal to 0.1 wavelengths. The angle θ starts at 10° and is given increments of 5°, up to 45° for a total of eight triangles.

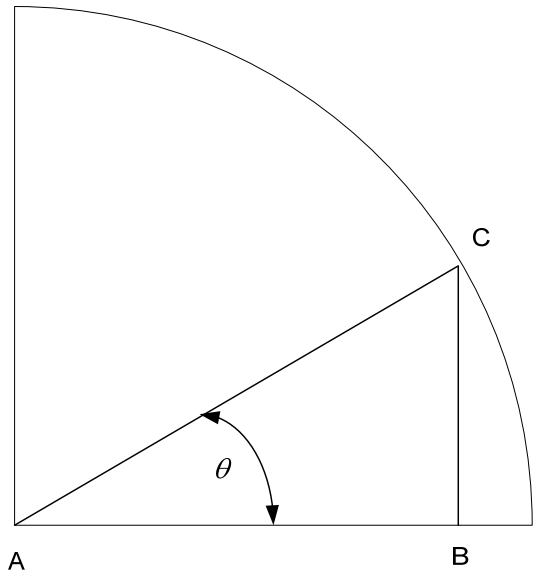

Figure A.1: Set of right triangles. $\overline{AC} = \lambda/10$, $\theta = 10° \left(5°\right) 45°$

In figure A.2 we have a set of obtuse triangles whose maximum side is $\lambda/10$. Again, the angle θ starts at 10° and is given increments of 5°, up to 45° for a total of eight triangles.

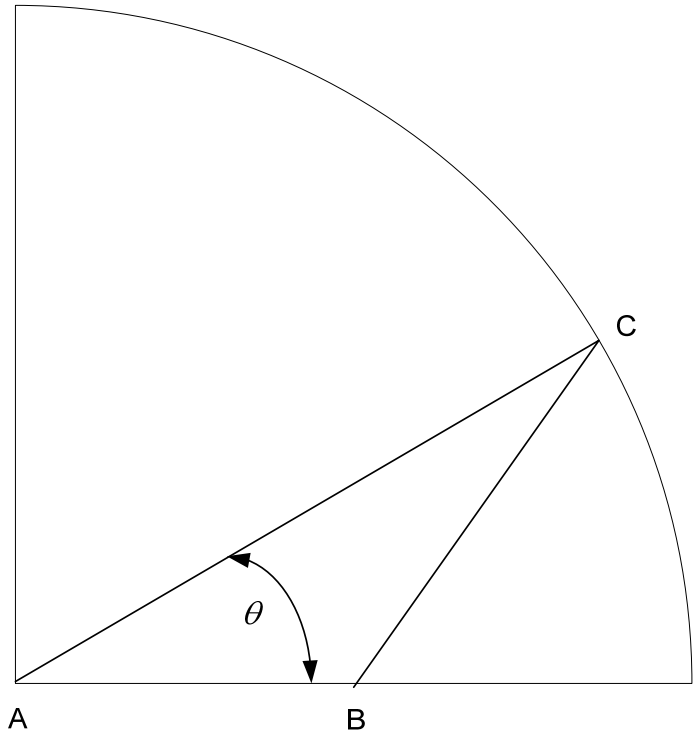

Figure A.2: Set of obtuse triangles. $\overline{AC} = \lambda/10$, $\overline{AB} = \lambda/20$, $\theta = 10° \left(5°\right) 45°$

In figure A.3, we have a set of obtuse isosceles triangles with the equal sides being $\lambda/20$ in length. Again, the angle θ starts at 10° and is given increments of 5°, up to 45° for a total of eight triangles.

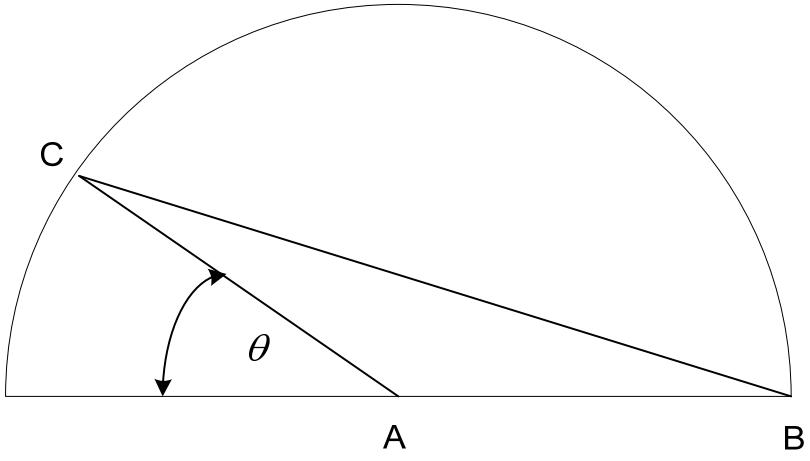

Figure A.3: Set of isosceles triangles. $\overline{AB} = \overline{AC} = \lambda/20$, $\theta = 10° \left(5°\right) 45°$

The last of the 25 triangles is an equilateral triangle whose side is equal to $\lambda/10$. The triangle is rotated clockwise about its centroid, through an angle of $20°$.

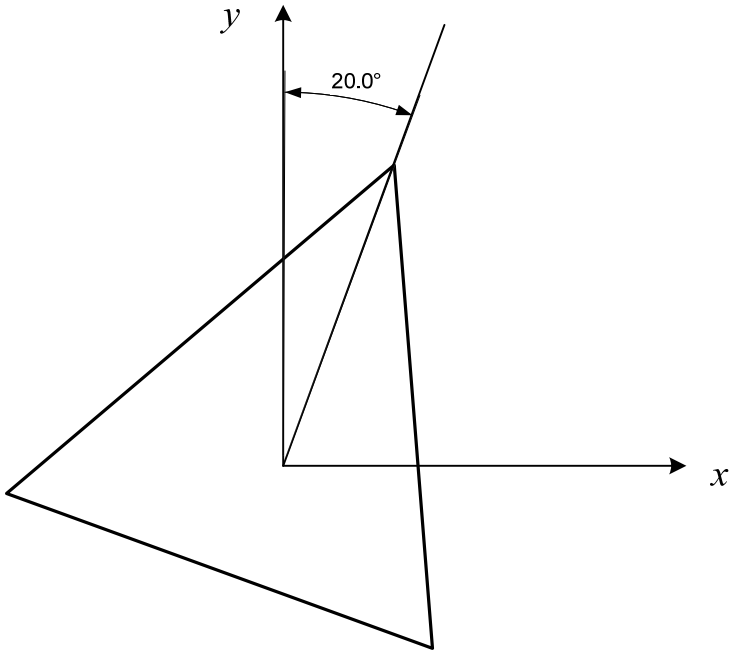

Figure A.4: Single equilateral triangle with side $\lambda/10$, rotated clockwise by $20°$.

APPENDIX B
RAW DATA FOR 10-POINT CUBATURE

Table B.1: AFR for the 10-Point Cubature

r'	Isc_real	Isc_Imag	V1_x_re	V1_x_im	V1_y_re	V1_y_im	V2_x_re	V2_x_im	V2_y_re	V2_y_im	V3_x_re	V3_x_im	V3_y_re	V3_y_im
0.1	99.22	0.00	99.83	13.37	99.83	0.00	99.82	7.33	99.84	0.00	99.78	0.00	99.65	0.00
0.15	96.74	0.00	99.19	16.27	99.07	0.00	99.02	8.84	99.08	0.00	98.66	0.00	98.38	0.00
0.2	87.18	0.00	97.97	18.20	98.45	0.00	98.85	12.66	98.51	0.00	98.62	0.00	96.09	0.00
0.3	21.43	0.00	87.02	22.97	89.95	0.00	91.20	21.60	90.78	0.00	89.19	2.53	74.76	0.00
0.4	0.00	0.00	37.63	36.29	30.33	21.77	40.57	44.70	33.24	25.33	21.02	27.69	7.55	0.85
0.5	0.00	95.72	29.12	99.39	7.17	98.08	27.39	99.49	10.12	98.10	7.10	99.43	0.00	97.94

Table B.2: MinFR for the 10-Point Cubature

r'	Isc_real	Isc_Imag	V1_x_re	V1_x_im	V1_y_re	V1_y_im	V2_x_re	V2_x_im	V2_y_re	V2_y_im	V3_x_re	V3_x_im	V3_y_re	V3_y_im
0.1	97.24	0.00	99.38	0.00	99.64	0.00	99.44	0.00	99.64	0.00	99.52	0.00	98.93	0.00
0.15	91.46	0.00	97.65	0.00	98.24	0.00	96.68	0.00	98.24	0.00	96.72	0.00	96.08	0.00
0.2	63.78	0.00	94.23	0.00	95.96	0.00	96.21	0.00	95.96	0.00	96.25	0.00	91.94	0.00
0.3	0.00	0.00	44.78	0.00	72.40	0.00	66.89	0.00	72.40	0.00	67.11	0.00	40.47	0.00
0.4	0.00	0.00	0.00	0.00	0.00	0.00	0.00	0.00	0.00	0.00	0.00	0.00	0.00	0.00
0.5	0.00	92.10	0.00	96.48	0.00	91.90	0.00	97.90	0.00	91.90	0.00	97.90	0.00	91.82

Table B.3: MaxFR for the 10-Point Cubature

r'	Isc_real	Isc_Imag	V1_x_re	V1_x_im	V1_y_re	V1_y_im	V2_x_re	V2_x_im	V2_y_re	V2_y_im	V3_x_re	V3_x_im	V3_y_re	V3_y_im
0.1	99.88	0.00	100.00	91.52	99.97	0.00	100.00	73.55	99.97	0.00	99.95	0.00	99.94	0.00
0.15	99.10	0.00	99.96	94.19	99.74	0.00	99.96	82.07	99.74	0.00	99.71	0.00	99.63	0.00
0.2	96.87	0.00	99.83	95.41	99.49	0.00	99.96	88.51	99.51	0.00	99.70	0.00	99.13	0.00
0.3	86.51	0.00	99.23	96.65	96.16	0.00	99.41	95.68	97.59	0.00	97.15	63.14	94.11	0.00
0.4	0.00	0.00	99.16	98.90	76.28	66.70	98.77	98.68	87.77	89.07	87.80	80.00	50.30	17.05
0.5	0.00	98.40	98.58	99.99	58.20	99.54	98.66	99.99	73.73	99.54	74.59	99.99	0.00	99.55

APPENDIX C
AVERAGE FAILURE RATE FOR VECTOR INTEGRALS

In tables C.1 – C.3, we present AFR results for the three vector integrals and for the same cubatures as in table 3.3.

Table C.1: First vector integral AFR for four cubatures that are faster than our method. The number we present in each cell is the larger of the AFR for the four real numbers that make up the real and imaginary parts of the two components of the integral.

r' (in wavelengths)	V1 AFR C7	V1 AFR C10	V1 AFR C15	V1 AFR C21
0.1	99.90	99.83	94.28	55.88
0.15	99.42	99.19	47.31	4.26
0.2	98.96	98.45	23.41	0.34
0.3	93.15	89.95	2.62	0.02
0.4	42.50	37.63	0.18	0.00
0.5	99.62	99.39	0.19	0.00
0.6	35.66	33.10	0.05	0.00
0.7	47.05	40.89	0.05	0.00
0.8	40.31	36.34	0.03	0.00
0.9	35.33	31.18	0.02	0.00
1	87.61	81.66	0.05	0.00
1.5	78.03	71.95	0.07	0.00
2	70.69	66.11	0.00	0.00
2.5	66.64	60.82	0.00	0.00
3	64.00	58.70	0.00	0.00
5	57.64	54.42	0.00	0.00
10	55.40	51.62	0.00	0.00
25	57.28	53.95	0.00	0.00
50	55.42	52.91	0.00	0.00
100	55.33	51.40	0.00	0.00
500	55.40	52.92	0.00	0.00
1000	55.32	51.42	0.00	0.00

Table C.2: Second vector integral AFR for four cubatures that are faster than our method. The number we present in each cell is the larger of the AFR for the four real numbers that make up the real and imaginary parts of the two components of the integral.

r' (in wavelengths)	V2 AFR C7	V2 AFR C10	V2 AFR C15	V2 AFR C21
0.1	99.90	99.84	94.24	48.52
0.15	99.41	99.08	50.69	5.32
0.2	99.16	98.85	22.30	0.57
0.3	93.97	91.20	2.53	0.02
0.4	51.43	44.70	0.29	0.00
0.5	99.60	99.49	0.06	0.00
0.6	38.10	34.28	0.04	0.00
0.7	44.82	39.88	0.03	0.00
0.8	44.43	38.96	0.02	0.00
0.9	32.52	27.29	0.02	0.00
1	87.57	81.86	0.03	0.00
1.5	78.21	72.17	0.01	0.00
2	70.70	66.19	0.00	0.00
2.5	66.63	60.85	0.00	0.00
3	64.00	58.70	0.00	0.00
5	57.64	54.41	0.00	0.00
10	55.38	51.62	0.00	0.00
25	57.27	53.94	0.00	0.00
50	55.42	52.91	0.00	0.00
100	55.31	51.40	0.00	0.00
500	55.40	52.92	0.00	0.00
1000	55.32	51.41	0.00	0.00

Table C.3: Third vector integral AFR for four cubatures that are faster than our method. The number we present in each cell is the larger of the AFR for the four real numbers that make up the real and imaginary parts of the two components of the integral.

r' (in wavelengths)	V3 AFR C7	V3 AFR C10	V3 AFR C15	V3 AFR C21
0.1	99.852	99.78	92.41	30.45
0.15	99.094	98.66	27.08	0.01
0.2	98.964	98.62	6.37	0.00
0.3	92.431	89.19	0.00	0.00
0.4	34.798	27.69	0.00	0.00
0.5	99.555	99.43	0.05	0.00
0.6	18.483	14.41	0.00	0.00
0.7	26.936	21.09	0.00	0.00
0.8	24.980	20.04	0.00	0.00
0.9	13.323	10.15	0.00	0.00
1	87.495	81.76	0.03	0.00
1.5	78.102	72.13	0.01	0.00
2	70.724	66.18	0.00	0.00
2.5	66.609	60.87	0.00	0.00
3	64.021	58.55	0.00	0.00
5	57.629	54.39	0.00	0.00
10	55.386	51.66	0.00	0.00
25	57.270	53.93	0.00	0.00
50	55.451	52.91	0.00	0.00
100	55.317	51.41	0.00	0.00
500	55.393	52.90	0.00	0.00
1000	55.320	51.41	0.00	0.00

APPENDIX D
COMPUTATION OF THE FOUR INTEGRALS USING CUBATURES

We show how we computed the integrals (1.1) as well as the scalar integral

$$I_{sc} = \int_T \frac{\mathrm{e}^{-ikR}}{R} dS \,. \tag{D.1}$$

This last integral is computed via a cubature of N points

$$I_{sc} = \sum_{n=1}^{N} w_n \frac{\mathrm{e}^{-ikR_n}}{R_n} \,. \tag{D.2}$$

We compute the integrand at the N points and store the information. The x- components of the integrals in (1.1) are then computed via

$$\mathbf{I}_x^{(l)} = \sum_{n=1}^{N} w_n \left(x_n - x_l\right) \frac{\mathrm{e}^{-ikR_n}}{R_n} \tag{D.3}$$

while the y-components by

$$\mathbf{I}_y^{(l)} = \sum_{n=1}^{N} w_n \left(y_n - y_l\right) \frac{\mathrm{e}^{-ikR_n}}{R_n} \,. \tag{D.4}$$

APPENDIX E
MAXIMUM FAILURE RATE FOR THE FOUR INTEGRALS

In tables E.1 – E.4, we present MaxFR results for the three vector integrals and for the same cubatures as in table 3.3.

Table E.1: Scalar integral MaxFR for four cubatures that are faster than our method. The number we present in each cell is the larger of the MaxFR for the real and imaginary parts of the integral.

r' (in wavelengths)	Isc MaxFR C7	Isc MaxFR C10	Isc MaxFR C15	Isc MaxFR C21
0.1	99.92	99.88	96.40	54.96
0.15	99.31	99.10	26.46	0.00
0.2	98.34	96.87	0.00	0.00
0.3	87.32	86.51	0.00	0.00
0.4	4.40	0.00	0.00	0.00
0.5	98.69	98.40	0.03	0.01
0.6	0.00	0.00	0.00	0.00
0.7	0.00	0.00	0.00	0.00
0.8	0.00	0.00	0.00	0.00
0.9	0.00	0.00	0.00	0.00
1	93.67	92.49	0.22	0.01
1.5	92.21	91.44	0.18	0.01
2	90.35	89.52	0.17	0.01
2.5	87.45	85.66	0.17	0.02
3	90.97	90.11	0.15	0.02
5	91.53	89.52	0.26	0.02
10	94.14	93.98	0.31	0.06
25	85.15	84.98	0.14	0.06
50	90.82	89.71	0.19	0.13
100	86.40	87.97	0.34	0.25
500	84.21	85.47	2.80	2.34
1000	83.33	86.03	6.26	5.62

Table E.2: First vector integral MaxFR for four cubatures that are faster than our method. The number we present in each cell is the larger of the MaxFR for the four real numbers that make up the real and imaginary parts of the two components of the integral.

r' (in wavelengths)	V1 MaxFR C7	V1 MaxFR C10	V1 MaxFR C15	V1 MaxFR C21
0.1	99.99	100.00	99.79	97.44
0.15	99.98	99.96	97.46	18.31
0.2	99.88	99.83	76.93	2.06
0.3	99.47	99.23	15.12	0.11
0.4	99.48	99.16	2.73	0.05
0.5	100.00	99.99	2.78	0.01
0.6	97.43	96.30	0.59	0.01
0.7	97.98	97.11	1.15	0.00
0.8	96.39	93.06	0.28	0.00
0.9	96.19	94.58	0.16	0.00
1	96.25	94.41	1.18	0.00
1.5	94.90	92.85	1.82	0.01
2	88.93	87.21	0.03	0.00
2.5	88.10	85.90	0.01	0.00
3	86.88	84.28	0.02	0.00
5	84.73	82.60	0.04	0.00
10	87.32	85.56	0.04	0.00
25	84.14	82.00	0.02	0.00
50	84.92	82.33	0.01	0.00
100	87.50	85.75	0.03	0.01
500	84.98	82.38	0.01	0.01
1000	87.50	85.77	0.04	0.01

Table E.3: Second vector integral MaxFR for four cubatures that are faster than our method. The number we present in each cell is the larger of the MaxFR for the four real numbers that make up the real and imaginary parts of the two components of the integral.

r' (in wavelengths)	V2 MaxFR C7	V2 MaxFR C10	V2 MaxFR C15	V2 MaxFR C21
0.1	100.00	100.00	99.62	94.77
0.15	99.98	99.96	97.46	31.32
0.2	99.93	99.96	81.28	5.03
0.3	99.50	99.41	15.92	0.30
0.4	99.23	98.77	7.19	0.01
0.5	100.00	99.99	1.45	0.02
0.6	92.61	91.32	0.67	0.00
0.7	97.18	96.09	0.25	0.00
0.8	96.05	94.59	0.34	0.00
0.9	93.45	91.25	0.45	0.00
1	95.87	94.46	0.11	0.00
1.5	92.65	91.83	0.03	0.00
2	88.90	87.22	0.03	0.00
2.5	87.84	85.91	0.01	0.00
3	86.56	84.23	0.02	0.00
5	84.62	82.36	0.07	0.00
10	87.45	85.67	0.09	0.00
25	84.07	81.92	0.04	0.00
50	85.01	82.28	0.08	0.00
100	87.50	85.67	0.09	0.01
500	85.01	82.29	0.04	0.02
1000	87.52	85.71	0.09	0.01

Table E.4: Third vector integral MaxFR for four cubatures that are faster than our method. The number we present in each cell is the larger of the MaxFR for the four real numbers that make up the real and imaginary parts of the two components of the integral.

r' (in wavelengths)	V3 MaxFR C7	V3 MaxFR C10	V3 MaxFR C15	V3 MaxFR C21
0.1	99.95	99.95	97.53	65.99
0.15	99.81	99.71	79.99	0.26
0.2	99.76	99.70	29.22	0.00
0.3	97.30	97.15	0.00	0.00
0.4	88.06	87.80	0.00	0.00
0.5	99.96	99.99	0.14	0.00
0.6	61.53	57.66	0.00	0.00
0.7	74.29	68.55	0.00	0.00
0.8	76.65	68.62	0.00	0.00
0.9	28.76	27.16	0.00	0.00
1	95.60	94.33	0.06	0.01
1.5	92.65	91.83	0.02	0.00
2	88.66	87.15	0.02	0.00
2.5	87.72	85.83	0.01	0.00
3	86.73	84.30	0.02	0.00
5	84.64	82.30	0.02	0.00
10	87.48	85.70	0.02	0.00
25	84.13	81.87	0.01	0.00
50	84.89	82.30	0.01	0.01
100	87.42	85.73	0.04	0.00
500	84.98	82.31	0.01	0.01
1000	87.42	85.76	0.04	0.01

REFERENCES

1. M. A. Taylor, B. A. Wingate and L. P. Bos, “Several new quadrature formulas for polynomial integration in the triangle”, arXiv:math.NA/0501496v2, 8 Feb 2007.

2. S. Wandzura and H. Xiao, “Symmetric quadrature rules on a triangle”, *Comp and Math with Applics*, **45**, pp. 1829-40, 2003.

3. M. Abramowitz and I. A. Stegun, *Handbook of Mathematical Functions*. Washington: National Bureau of Standards, 1964.

4. http://babbage.cs.qc.edu/courses/cs341/IEEE-754references.html

5. S. M. Rao, D. R. Wilton, and A. W. Glisson, “Electromagnetic scattering by surfaces of arbitrary shape”, *IEEE Trans. Antennas Propagat*., vol. AP-30, no. 3, pp. 409-418, 1982.

DISTRIBUTION:

NAVAIRSYSCOM (AIR-4.5.5/Kevin Birney), Bldg. 2187, Room 2184 (1)
48110 Shaw Road, Patuxent River, MD 20670-1906
NAVAIRWARCENACDIV (Dr. Chris Hicks), Bldg. 2187, Room 2172 (1)
48110 Shaw Road, Patuxent River, MD 20670-1906
University of Mississippi (Attn: Prof. Allen W. Glisson), 302 Anderson Hall (1)
P.O. Box 1848, University, MS 38677-1848
Ohio State University (Attn: Prof. John L. Volakis), Electroscience Lab (1)
1320 Kinnear Road, Columbus, OH 43212
University of Houston (Prof. Donald R. Wilton), E.E. Dept. (1)
N 308 Engineering Building 1, Houston, TX 77204-4005
NAVAIRSYSCOM (AIR-5.1), Bldg. 304, Room 100 (1)
22541 Millstone Road, Patuxent River, MD 20670-1606
NAVAIRWARCENACDIV (4.12.6.2), Bldg. 407, Room 116 (1)
22269 Cedar Point Road, Patuxent River, MD 20670-1120
NAVTESTWINGLANT (55TW01A), Bldg. 304, Room 200 (1)
22541 Millstone Road, Patuxent River, MD 20670-1606
DTIC (1)
Suite 0944, 8725 John J. Kingman Road, Ft. Belvoir, VA 22060-6218